CORA Cork Open Research Archive
Cartlann Taighde Oscailte Chorcaí

Title	Optical spectroscopy for biological and biomedical applications: potentially impacting future of healthcare with research, clinical translation and education
Authors	Saito Nogueira, Marcelo
Publication date	2021-11-10
Original Citation	Saito Nogueira, M. 2021. Optical spectroscopy for biological and biomedical applications: potentially impacting future of healthcare with research, clinical translation and education. PhD Thesis, University College Cork.
Type of publication	Doctoral thesis
Rights	© 2021, Marcelo Saito Nogueira. - https://creativecommons.org/licenses/by-nc-sa/4.0/
Download date	2026-11-16 07:36:00
Item downloaded from	https://hdl.handle.net/10468/14150

UCC
University College Cork, Ireland
Coláiste na hOllscoile Corcaigh

Chapter 7

Optical biomarkers of biological tissue and biofluids

Marcelo Saito Nogueira

This chapter is part of the thesis "Optical spectroscopy for biological and biomedical applications: potentially impacting future of healthcare with research, clinical translation and education" by Marcelo Saito Nogueira

The rest of the thesis can be accessed via CORA UCC:

cora.ucc.ie

Please ensure appropriate acknowledgement and referencing when using material and/or ideas outlined in this thesis.

Contents

7. Optical biomarkers of biological tissue and biofluids 229
7.1 Sources of scattering in biological media 229
7.2 Sources of Raman scattering in biological media 233
7.2.1 Sources of Raman scattering in biological tissues 233
7.2.2 Sources of Raman scattering in biofluids 234
7.3 Sources of absorption in biological media 242
7.3.1 Ultraviolet, visible and near-infrared chromophores in biological media 242
7.3.2 Sources of mid- and far-infrared absorption in biological media 248
7.4 Sources of fluorescence in biological media 254
7.5 References 262

7. Optical biomarkers of biological tissue and biofluids

Up to this point of the thesis, the reader should have a good understanding of the device design factors associated with source-detector geometries and specifications. Still, optical device design needs to take into account application-specific biomarkers and how these biomarkers can be detected with sufficient measurement contrast, as these biomarkers determine the medium optical properties. Chapter 7 provides a description of the physical elements generating scattering, absorption, and luminescence (i.e., the sources of these phenomena or photophysical processes).

This description is given by associating a non-exhaustive list of the optical characteristics of physical entities originating elastic scattering, Raman scattering, absorption (from ultraviolet to far-infrared), and fluorescence processes in biological tissues and biofluids and their application-specific characteristics/features extracted by using optical measurements. The extraction of these features involves data preprocessing and analysis methods explained in chapters 9 and 10. The best way of extracting those features is explained in chapter 8.

It is important to note that designing application-specific optical devices and analyzing the data of optical measurements such as those covered in this thesis (Papers 1-4 and chapter 17) require knowledge about the main physical entities generating photophysical processes relevant to their particular application, as microstructural and biochemical information to be extracted from optical measurements are dependent on how these entities affect optical signals. These main physical entities are particular to each application, and the more extensive compilation of optical characteristics and physical entities is provided, the more factors can be taken into consideration when designing optical devices. Hence, the more accurate the design tends to be. Also, an extensive compilation is necessary to explain research results outlined in this thesis, as one should be aware of the complete list of physical entities and their optical characteristics to understand assumptions made for data analysis of optical measurements.

As an example of the importance of knowing the complete list of physical entities and their optical characteristics, we can consider that breast light absorbers (i.e., chromophores) are present at different concentrations compared to those of liver and, thus, designing medical devices for liver applications should not take into account only the specific list of dominant breast chromophores. Providing a short compilation of dominant breast chromophores does not give the necessary list of chromophores required to design liver optical instruments. An extensive compilation containing a complete list of biological chromophores and their absorption characteristics opens up opportunities to design optical devices for multiple applications including the liver ones . Therefore, such extensive compilation can be beneficial to future optical designers and to data analysts searching for the source of unexplained deviations in optical measurements (e.g., measurements displaying absorption at wavelength ranges in which chromophores involved in data analysis models do not absorb light, which is typically an issue of not including chromophores absorbing at those wavelength ranges in the data analysis). To the best of my knowledge, the extensive compilation reported in this thesis is missing in the current literature and is a valuable resource for optical device designers.

7.1 Sources of scattering in biological media

Since scattering is generated from refractive index mismatches with biological media, the major physical entities originating scattering are the micro- or nano-structures which have a refractive index mismatch with the surrounding medium, or tissue layers (with different refractive indexes) which sizes are comparable to the incident (excitation) wavelength λ_{ex}. Evidence of this origin is the typical slope of the wavelength-dependent Mie scattering coefficient (later referred as Mie scattering power or b_{Mie}; Chapters 14 and 15 of this thesis), which ranges between 0.5 and 2 for most tissues. This value of slope indicates scattering particles predominantly range from ~50-200 nm in size. Another evidence

is the dominance of Mie scattering of particles larger than λ_{ex} towards Rayleigh scattering indicated by $1 - f_{Ray}$ for most tissues, as shown in Chapters 14 and 15 (Papers 3 and 4, respectively) and data reviewed by Steven L Jacques in [1]. A summary of these structures and the type of scattering they generate for several wavelength ranges is shown in Appendix 3, Table 7.1.

Macroscopic scattering can be visualized as the Fresnel reflection happening at the surface of a tissue or organ. In this case, the amplitude of such reflection is dependent on the refractive index mismatch between air and the tissue surface as well as on the direction of the incoming light relative to the normal of the tissue surface. Most tissues have refractive indexes (visible light) in the range of 1.315–1.7 [2], as it can be seen in Appendix 4, Table 7.2.

By considering mismatches between refractive indexes of tissues and air with small/intermediate angles of incidence typical from optical measurements, the Fresnel reflection is typically in order of a few percent [3]. However, the difference of a few percent at surfaces of numerous cellular and subcellular structures within tissue generates a significant about of reflections at micro- and nano-scale. The result of these reflections is light scattering, which is mainly dependent on the number of scatterers, size and shape of the scatterer, as well as dependent on the relative refractive index between the scatterer (cell, organelle, molecule, etc) and its surrounding medium.

Essentially, optical scattering is produced by refractive index mismatches throughout the trajectory of light within biological media, which are heterogeneous in micrometer and nanometer scales. Quantifying the influence of refractive index mismatches on sample scattering coefficients has been discussed in section 4.5 Rayleigh and Mie scattering of Chapter 4, where calculations were based on the ratio m between the refractive index of scatterers n_s and that of the ground material n_0 (i.e., $m = \frac{n_s}{n_0}$). The higher the ratio, the higher the scattering coefficient. This proportion can be easily checked with the subcase of Rayleigh scattering shown by equation 4.6 (Chapter 4).

In terms of structures at subcellular level, small differences of refractive indexes between extracellular fluid (1.33 – 1.36) and cell membranes (1.43-1.51), as well as those between intracellular fluid (1.35-1.36) and intracellular structures highly influence measured scattering coefficients, given that cell densities in tissue vary from 1-3 billion cells/ml [4] (i.e., 1-3 million cells per mm^3, considering that the probed volume of light in tissue would be in the order of 0.01-1 mm^3 for reflected light or 1-20 mm^3 for transmitted light depending on the tissue optical properties). These intracellular structures include melanin granules (1.6 – 1.7), cell nucleus (1.38 – 1.41), organelles including mitochondria, lysosomes, peroxisomes and others (1.38 – 1.42). Evidence that even small differences of refractive indexes can generate high scattering coefficients is how scattering objects can be made more transparent to light by inducing refractive index matching between combinations of extracellular and intracellular structures. This is the principle of optical clearing, which allows tissue to be more “transparent” is based on changing the refractive index of the interstitial (extracellular) fluid by using organic agents (dehydration and clearing) and aqueous agents (clearing agents diffusing into the interstitial fluid), or by replacing the cell lipid bilayers by a transparent material (e.g., hydrogel) capable of physically support tissue without lipids causing refractive index mismatches [5].

Optical clearing agents influencing the refractive index and scattering coefficient μ_s due to intra- and extracellular fluids are mainly associated with low-molecular weight solutes (e.g., electrolytes, alcohols and carbohydrates). By making tissue-simulating phantoms with an aqueous suspension of polystyrene spheres, Kohl et al. [6,7] have shown that increasing glucose concentrations raised the total refractive index of the medium (phantom) and decreased in the relative refractive index (compared to the refractive index of polystyrene spheres). The refractive index change resulted in decreased μ_s and increased g-factor [6–8], who have shown that increased concentration of these solutes decreased effective μ_s of in Intralipid phantoms, cell suspensions, and liver tissue.

The simplest model to calculate the effective refractive index $\bar{n}$ takes into account the volume fractions v_{sca} of scattering particles as well as refractive indexes n_{sca} and n_0 of scattering particles and their surrounding medium (ground material), respectively, according to [2]:

$$\bar{n} = v_{sca} n_{sca} + (1 - v_{sca}) n_0. \qquad (7.1)$$

Based on the equation 7.1 above, the estimated refractive index n_{cell} is ~1.3845, as the cell primarily contains the cytoplasm (aqueous solution of electrolytes and proteins with refractive index $n_{cytoplasm} = \mathrm{n}_0 \approx 1.38$), the cell membrane and organelles ($n_{sca} = n_{membrane} = n_{mitochondria} = n_{lysosome} = n_{peroxisome} = n_{organelles} =$ 1.43-1.51) comprised of phospholipid layers and proteins and constituting ~5% of the cell volume fraction ($v_{sca} = 5\%$) [9,10]. In a more sophisticated model by Beuthan et. al. [9], the effective refractive index n_{cell} of cells in general was estimated to be ~1.40. However, note that larger effective refractive indexes $\bar{n}$ do not imply larger μ_s because the equation 7.1 does not consider that higher density of variations of refractive index occur throughout a fixed cell or tissue volume. These variations are more important contributors to the total μ_s than the magnitude of $\bar{n}$.

Although the cell membrane and nucleus have dominant contributions to refractive index in phase microscopy (high refractive indexes) [9], their contribution to the cell scattering coefficient is low due to:

- the thickness of cell membrane (5-10 nm),
- size of nucleus (5-10 μm),
- the small volume fraction of membrane structures in the nucleus ($v_{nuclear\ membrane} =$ 0.2-0.7%) [11,12],
- the low repetition of these structures along the cell volume (only one cellular membrane and cellular nucleus, except from multinucleate cells such as osteoclasts and skeletal muscle cells in mammals).

The small contribution of cell membrane and nucleus to the light scattering of biological tissues can be confirmed by the previously mentioned typical values of b_{Mie}, which suggest that the size of tissue scatterers is in the order 100 nm. With this in mind, the contribution of much smaller or much larger structures appears to be minimal. The main scatterers in tissue include structures with membrane layers repeating multiple times within the cell volume (resulting in a higher density of refractive index mismatches) such as endoplasmic reticulum or Golgi apparatus (high spatial frequency and amplitude of refractive index fluctuations and cell volume fraction of 50-60%), mitochondria (200-800 nm of diameter, 1-5 μm of larger size [13]), other organelles such as lysosomes (250-800 nm of diameter [13], 1-2 μm of larger size [2]), and peroxisomes (200-1000 nm of diameter [13]). Other important cell scatterers melanin granules (1-10 μm of diameter and $n_{melanin} = 1.6 - 1.7$), components of fibrous structures such as collagen and elastin fibers (1.43 - 1.53, depending on the molecular hydration state [14]), and myosin and actin (proteins forming filaments of muscle cells; myosin filaments have ~15 nm of diameter and those of actin ~7 nm of diameter; $n_{myosin} = 1.35$ and $n_{actin} = 1.346$ [15]). Finally, lipid droplets can also constitute a significant scatterer when present in larger quantities such as inside cells of adipose tissue, given their high refractive index ($n_{lipid\ droplets} =$ 1.46-1.53 in the visible wavelength range [16]) and large volume fraction (~88%) in the cell [17]. Finally, Rayleigh scattering may arise from macromolecules such as hemoglobin (red blood cells; RBCs) and albumin (liver cells) within the cytoplasm or interstitial (extracellular) fluid. [18]. As it can be implied from the aforementioned components, the scattering coefficient of each cell and tissue depends on their composition in terms of scatterers. Table 7.3 (Appendix 5) illustrates the dependence of scattering efficiency of cellular components based on their refractive index, size, particle concentration/volume fraction, number of membrane folds.

The contribution of cellular structures to the scattering inside the cells has been studied for mitochondria, cell nucleus, DNA, and lipid droplets. Mitochondria contains many membranes forming many folds within its structure, which increases the spatial density of refractive index mismatches (membrane content between 20-40% [9]). As expected, the mitochondrial content is highly correlated with the tissue reduced scattering coefficient μ_s' [17], as tissues composed by cells with large mitochondrial volume fraction ($v_{mitochrondria}^{hepatocytes} = 22\%$) such as liver tissue exhibit higher μ_s' values [17,19]. Cellular nucleus (or nuclei for multinucleate cells) has a low particle concentration and have a small contribution to the effective scattering despite its refractive index of $n_{nucleus} = 1.38 - 1.41$. The same is valid for the DNA inside the nucleus, which does not have a significant contribution due to its low concentration despite its $n_{DNA} \approx$ 1.44-1.49. On the other hand, contribution of the nuclear size to scattering can be detected in normal, dysplastic and cancer cells. Perelman et. al. [20] showed that normal nuclei have 4–7 μm of diameter, whereas dysplastic nuclei had diameters of up to 20 μm and those of T84 tumor human intestinal cells varied between 7-16 μm.

Contribution of lipid droplets to the total scattering is only substantially upon high concentration of these droplets such as in adipose tissue. However, this contribution varies with the temperature, as the refractive index of lipid droplets changes once lipid changes its "crystalline" structure upon droplet solidification. The refractive index change has been shown to be $\frac{dn}{dT} = -(6.01 \pm 0.29\ x\ 10^{-4}\ °C^{-1}$ by Yanina et. al. [21] for porcine lipid droptlets between 480 to 1550 nm ($\frac{dn}{dT} = -(3.54 \pm 0.15) x\ 10^{-4}\ °C^{-1}$ for all wavelengths), resulting in $\frac{dn}{dT} = -(7.92 \pm 0.74\ \ x\ 10^{-4}\ °C^{-1}$ of the porcine tissue. The resulting increase of reduced scattering coefficient with decreasing temperature was demonstrated by Berg between 37°C to 15°C [22]. While temperature changes lead to small variations in refractive index, one should note that these small variations can potentially vary the tissue scattering coefficient μ_s significantly.

Anisotropy factor g and the scattering cross-section σ_{sca} can change based on the volume and shape of scattering particles [3]. In Mie theory, scatterers smaller than a wavelength exhibit isotropic scattering, whereas scatterers comparable or larger than a wavelength exhibit a more anisotropic scattering. In both cases, g and σ_{sca} increase with the particle volume [23], which happens in biological processes such as osmosis (increased cell size). g and σ_{sca} also increase upon enlargement of cylindrical-shaped particles such as the cylindrical organelles in retinal nerve fibers [10] and collagen fibers during their gestational maturity in neonatal skin [24]. Particularly for layered sphere models taking the Rayleigh-Gans-Debye approximation suggest that, upon constant cell volume, the g-factor (1) increases with the nuclear size (also confirmed by Finite-Difference Time-Domain (FDTD) [25]), (2) decreases with reduction of the refractive index of either the cell nucleus or the cytoplasm [26]. Regarding the shape of the particles, T-matrix calculations [27] indicated that (upon constant cell volume) g and σ_{sca} decrease when the shape of particles with pronounced aspherical shape (e.g., red blood cell) becomes spherical or upon elongation of prolate-shaped particles. Changes of g and σ_{sca} due to alterations in cell morphology are well summarized as per previously reported by Enejder [3] (Appendix 6, Table 7.4).

7.2 Sources of Raman scattering in biological media

Raman scattering originates from molecular vibrations changing the molecular polarizability of the molecule. The simplest case is a triatomic molecule with its two bonds stretched symmetrically. In this case, bonds are easier to polarize and hence, the symmetric stretch is a Raman active mode. On the other hand, neither asymmetric stretch of molecular bonds nor bending these bonds changes molecular polarizability. Therefore, asymmetric stretching and bending are not Raman active and cannot be included as Raman-active vibrational modes of the triatomic molecule. It is worth noting that these Raman inactive modes are infrared (IR) active modes instead, as the molecular dipole moment changes upon asymmetric stretching and bending. The complementarity between IR active and Raman active modes is one reason why both Raman spectroscopy and IR spectroscopy are typically grouped into one category called vibrational spectroscopy. This complementarity is relevant in biological media, which contains complex molecules with 10 to millions of atoms and a large number of both Raman and IR active modes within the same molecule.

Raman spectroscopy (Chapter 8, section 8.2.4) detects the modifications in the conformation and constitutes of cells, tissues, deoxyribonucleic acid (DNA), proteins, and lipids. Complementing infrared spectroscopy, the Raman technique possesses special advantages, including being nondestructive; fast to acquire; capable of providing information at the molecular level and analyzing samples in aqueous solutions since water produces a weak Raman scattering; and important in the biochemical field where researchers study the ionization behavior, pH change, and amino acid configuration. In general, biomolecules with inflexible structures and/or small sizes tend to have vibrational modes with specific wavenumbers and Raman shifts. Within a solution of a particular molecule with strong Raman scattering and at sufficient concentrations for detection of Raman signals, the intensity of Raman spectral peaks associated with these modes is typically expected to have only a slight variation depending on the solvent and/or microenvironment in which this molecule is present. However, Raman spectral analysis can be challenging for large molecules such as proteins.

Proteins contain several smaller intra-molecular structures whose amount and order within a protein molecule can change significantly depending on pH, temperature, and other variables. These structures are called secondary structural elements. Raman bands of secondary structural elements are about 20 cm^{-1} wide in biological media (Appendix 7, Table 7.5) and their intensity changes may alter the protein spectral shape. Since these changes are much smaller scale than those of protein molecules, protein characterization with Raman spectroscopy is typically performed by quantifying the amount of each secondary structural element. Table 7.5 in Appendix 7 shows the Raman-band wavenumber of the amide I group of each [28] secondary structural element. In samples containing many types of proteins and/or proteins with multiple types of secondary structural elements, the amide I band may be broad enough to cover wavenumbers up to 90 cm^{-1}.

7.2.1 Sources of Raman scattering in biological tissues

Raman scattering can be used to characterize and analyze multiple types of biological media. Biomedical applications mainly focus on the analysis of biological tissues and biofluids. In oncological and surgical applications, biological tissues are typically analyzed to speed up the time-consuming histopathological analysis by providing real-time delineation of cancer margins and identifying important structures such as important blood vessels and nerves. In the context of label-free optical spectroscopy (i.e., not using contrast agents), finding nerves or assessing cancer margins can be performed cheaper and faster by relying on Mie scattering information (e.g., nerves are highly scattering and late-stage tumors typically have more mitochondria than normal tissue resulting in a higher reduced scattering coefficient μ_s' than surrounding tissues) or absorption information (e.g., tumors induce angiogenesis and, therefore, exhibit higher absorption coefficient μ_a in wavelengths of blood absorption; section 7.3.1 and Table 7.10 in Appendix 8). However, in some cases, label-free optical spectroscopy information from Mie scattering, absorption and fluorescence information may still not be sufficient to identify tissues (e.g., if a cancer is in a too early stage) and Raman scattering could add prognostic biomarkers

(i.e., biomarkers to predict the patient outcome) to existing applications. Therefore, tissue Raman scattering is useful to provide label-free and non-invasive methods to investigate molecular information complementary to that of Mie scattering, absorption, and fluorescence. This complementarity comes from the molecular specific information that can be retrieved from chemical bonds of molecules composing tissue. An example relevant to Papers 1-3 (Chapters 12-14) and Chapters 16 and 17 of this thesis, Raman scattering allows detection of colorectal cancer (CRC) tissues because they exhibit higher fatty acids and protein content probed by 1134 cm^1, and higher lipid and phospholipid content probed by 1297 cm^1 compared to surrounding normal tissue [29]. Information on protein and phospholipid content is complementary to that of other optical processes when probing endogenous tissue constituents. For imaging applications such as microscopy, well-defined Raman bands enable Raman imaging of structures such as lipid droplets, specific types of proteins and aminoacids, nucleic acids, carbohydrates, and other molecules with only one wavelength excitation and without signal contamination from one molecule type to another. Due to the high molecular specificity resulting from narrow spectral bands between 600-1800 cm^{-1}, this wavenumber range is known as the spectral "fingerprint region" where characteristic Raman bands are found.

When labeling tissues and cells with contrast agents, Raman scattering offers advantages in terms of the width of wavelength-resolved spectral bands, which are much narrower compared with those of fluorescence or phosphorescence. Since detectors are sensitive in specific and limited wavelength ranges, the width of spectral bands determines how many types of structures can be labeled and visualized by using a certain detector (e.g., typical silicon photodetectors are sensitive from 400-1100 nm). This width is narrow (~1 nm in the fingerprint region) for Raman bands because Raman scattering is not broadened by hyperfine structures formed by vibrational and/or rotational states such as processes relying on absorption and radiative emission (e.g., fluorescence or phosphorescence, whose contrast agents exhibit spectral bands of tens of nanometers full-width at half maximum; FWHM). Therefore, Raman scattering allows labeling more cellular and tissue structures to be detected by Raman spectroscopy (Chapter 8, section 8.2.4) upon tagging a larger number of molecule types. Labeling more structures means monitoring more biological processes simultaneously. Combination between Raman and fluorescence imaging modalities, each using their specific contrast agents can considerably increase the number of labeled structures and biological processes investigated.

7.2.2 Sources of Raman scattering in biofluids

In biofluids, given the current higher cost of Raman spectroscopy, Raman scattering provides useful information in similar contexts compared to the those of endogenous tissue constituents and of contrast agents (i.e., labels or exogenous agents). First, Raman spectroscopy can be used to measure biofluids directly for biomarker identification if providing complementary information to cheaper methods based on extracting Mie scattering, absorption and fluorescence information. Biomarkers are different for each biofluid and even within one type of biofluid and sample (e.g., saliva of normal patients), variations in the intensity and positions of Raman peaks can change significantly. Biomarkers for each biofluid are discussed later in this section. Biofluid biomarkers can also change upon sample collection protocols, which may involve the collection of either stimulated or unstimulated saliva, or of either whole blood or one of the blood fractions (plasma, serum, red blood cells, white blood cells, platelets), for instance. Due to currently non-fixed protocols among institutions and lack of multicenter studies using biofluid Raman spectroscopy and other challenges discussed in Chapter 19, biomarker identification in biofluids has been challenging over the last few decades. Therefore, biomarkers have been identified for only a few biofluids such as the cerebrospinal fluid (CSF; Table 7.7 of Appendix 7), in which spectra tends to be reproducible and repeatable over samples. In cases where the Raman spectra of biofluid samples of each study group presents larger intragroup variations, research has mainly focused on identifying biomarkers (corresponding to Raman peaks and bands) leading to the highest difference between two or more study groups (Table 7.8 of Appendix 7). The identified biomarkers are associated with the disease detection for screening and diagnostic applications. To decrease the intragroup variability between normal and diseased groups, populational studies have been proposed to monitor Raman spectra of biofluids until individuals develop a disease. Such variability would potentially be decreased by comparison between Raman spectra before and after each individual develop a certain disease. Thus, the spectral

variation is calculated for each individual separately instead of considering Raman spectra of normal and diseased groups composing of different individuals (approach used by currently available studies in the literature).

Conventional Raman spectroscopy of biofluids has advantages on extracting more reproducible and repeatable biomarkers over studies compared with methods to enhance the Raman signal such as surface-enhanced Raman scattering (SERS) and surface-enhanced resonance Raman spectroscopy (SERRS), which enhance the Raman signal by ~10^8 and up to 10^{11}, respectively. However, one should note that the Raman signal is already weak (discussed further in Chapter 8, section 8.2.4) since 1 in 10^8 photons undergo Raman scattering [30]. Biofluids have a much weaker Raman signal compared with biological tissues because they are less scattering (in general, almost transparent and hence with decreased light pathlength and Raman scattering probability within the medium; Chapter 5, section 5.1) and contain a considerable amount of water, which does not generate Raman signal and while diluting the concentration of Raman active biomolecules. Therefore, using SERS is a good alternative to increase the collected Raman signal to more accurately resolve peaks which can differentiate samples between study groups such as those outlined in Table 7.9 (Appendix 7) for disease diagnosis based on SERS of saliva samples [31].

SERS uses nanoscale roughened metallic surfaces and nanoparticles (typically gold or silver) as substrates to enhance the Raman signal. The clustering, shape, size and materials of nanoparticles are key for this enhancement [32], as they control the number and location of local field hotspots of nanoparticles [32] to optimize the SERS efficiency of molecules of interest [32–37]. For instance, clusters of spherical nanoparticles (nanospheres) enable enhancement at longer wavelengths (which can be seen by the absorbance spectrum of nanoparticles; typically higher at 785 nm the larger the cluster) [38,39] at the cost of having less hotspots in the cluster surface (leading to less signal enhancement) and the irreproducibility of clusters among batches of nanosphere cluster synthesis due to the uncontrollability of the nanosphere aggregation process. In addition, clusters are larger and may have less hotspots, hence leading to less Raman signal enhancement and binding to molecules of specific sizes, as Raman active molecules need to be sufficiently close to hotspots for the Raman signal to be enhanced. Another example is using nanostars (also known as nanourchins), which contain sharper corners and edges than nanospheres, and thus exhibit hybridization of plasmons mainly at the nanoparticle core and tips. This hybridization means that their wavelength dependent SERS efficiency is more tunable and can be changed in their synthesis process by controlling the ratio between metal (e.g., gold; Au) salt concentration and metal seed concentration, as well as colloids obtained at different temperatures [40]. A great number of nanoparticle types can be synthetized for binding to molecules of specific sizes, SER at the desired wavelength ranges, and sufficient SERS efficiency. These types include nanospheres, porous nanospheres, nanocorals, nanostars, nanorods, nanoshells, nanorices, nanotriangles (or nanoprisms), nanocubes, nanododecahedra, nanocages (or nanorattles) of multiple sizes, materials, cluster sizes, etc [41]. It is worth noting that reproducibility and repeatability of nanoparticles is important to compare results across institutions, clinical trials and research studies, especially for high-throughput screening applications.

Finally, it is important to understand the sources of Raman scattering in biofluids (or body fluids) and what applications can be developed based on the characterization of their Raman active compounds. Applications should consider factors discussed in Chapter 3. The most important factors for medical device design involving vibrational spectroscopy applications (i.e., applications involving Raman spectroscopy and FTIR spectroscopy) include biofluid composition, molecular sensitivity of measurement techniques (such as FTIR and ATR-FTIR), technology maturity and adoption aspects, and potential for clinical translation (i.e., how technology can be introduced and adopted in a long-term without disturbing the clinical workflow and/or patients' lives). Therefore, Raman spectroscopy applications for each biofluid have been discussed below based on studies reviewed by [31,42–44] while further explanation on biofluid applications of infrared (IR) spectroscopy is given in section 7.3.2:

- Blood: constitutes about 7% of human body weight and transports substances including hydrogen, oxygen, electrolytes, proteins, sugars, lipids and various cell types, and organic compounds [42,45]. Blood is composed of plasma and specialized cells such as red blood cells (erythrocytes or RBC), platelets and white blood cells (leukocytes or WBC). Blood plasma is the yellowish and semitransparent liquid remaining when clotting is prevented with the addition of an

anticoagulant to a whole blood sample and corresponds to 55% of the blood volume. Blood specialized cells include leukocytes which can be agranulocytes (lymphocytes, monocytes) or granulocytes (eosinophils, basophils and neutrophils). The physiological status of an individual can be determined by the biochemical profile of blood [46]. However, main challenges concerning the determination of individual physiological status through blood analysis rely on (1) detecting and associating specific biomarkers to particular diseases/conditions, (2) cost-effective alternatives for fast and user-friendly blood analysis and (3) current invasiveness of blood collection. If doing SERS analysis of liquid blood, detecting specific biomarkers can potentially be performed by the selectively identifying and restricting the target molecule to specific locations before this molecule conjugate with labels. Despite amplifying Raman signals to potentially increase molecular sensitivity and specificity, it is important to consider that SERS may involve more time-consuming procedures as well as higher costs with professional training, application development and validation compared with conventional Raman spectroscopy [47]. Blood characterization based on vibrational spectroscopy (i.e., Raman spectroscopy and FTIR spectroscopy) has been well documented for disease biomarkers [45,48], and has been used for numerous applications including the diagnosis of adenocarcinoma, oral cancer, HIV/AIDS, diabetes, depression, neurological diseases, and cardiovascular diseases [42,45,47,49–51]. These applications discriminate between the study groups by detecting metabolites mainly associated with inflammation, oxidative stress, peptide/protein expression and lipid metabolism. For instance, the analysis of blood serum (i.e., the liquid remaining after the blood has clotted) has been suggested not to be affected by the drying process, since no statistically significant differences were found between dried and liquid serum samples [50]. Blood serum of depressed patients were shown to have a significant decrease in peak intensity in functional groups associated with phospholipids and proteins [50]. Also, blood plasma of Alzheimer's disease patients exhibited a significant shift of the amide I band to wavenumbers lower than 1643 cm^{-1} and led to patient classification with 85% accuracy, 75% sensitivity and 88% specificity after cross-validation [51]. In general, blood is a promising biofluid for fast analysis using green technologies (no chemical disposal) requiring minimal training from equipment operators once these technologies are automated by using machine learning / artificial intelligence (chapter 10). Blood tests using Raman spectroscopy (or FTIR spectroscopy for complementary information) can be potentially combined with current laboratory biochemical tests which rely on professional training and lead to disposal of chemicals in the environment. A final advantage of using blood analysis with vibrational spectroscopy is the option of enabling healthcare practitioners to use the preferred collection method for each patient, who may have unique diagnostic needs and restrictions due to medical or logistic conditions [42,45,47,49–52].

- Cerebrospinal Fluid (CSF): consists of watery, colorless, clear fluid that flows in and around an individual's brain and spinal cord. CSF is constituted of a unique concentration of potassium, calcium, chloride, magnesium and sodium, sparse cells (cell count typically does not exceed five cells per milliliter), various proteins (including enzymes) and other substances [53]. CSF is produced after passive plasma filtration from choroidal capillaries to the choroidal interstitial compartment according to a pressure gradient [54]. Many enzymes including carbonic anhydrase and membrane ion carrier proteins actively transport the CSF from the interstitial compartment to the ventricular lumen across the choroidal epithelium. These enzymes regulate the CSF composition which can vary with chronobiological cycles such as the Na concentration proposed to be associated with migraine attacks [55]. The CSF composition changes in disease states regulating enzymatic activities and/or the efficiency of membrane filtration of plasma. CSF collection is usually invasive and requires lumbar puncture [53,56]. The value of using CSF relies on the stability and predictability of its expected chemical composition for normal patients, which could be useful to identify disease states upon biochemical changes due to inflammatory conditions, metabolic conditions, infections, and non-infectious diseases compromising the function of brain, meninges, spinal cord and associated parts of the Central Nervous System (CNS) [56,57]. However, it is worth noting that CSF has not been useful in providing exact diagnosis in most studies because of common biomarkers and associated changes in most diseases [53]. In terms of vibrational spectroscopy, CSF analysis can be cheaper and can dramatically decrease the diagnosis time by narrowing down potential conditions an individual may have, while performing an analysis with no contrast agents typically used for brain imaging. It is worth noting that CSF analysis could be used for disease screening, diagnostic and prognostic purposes not requiring knowledge of the disease location (e.g., localizing brain cancer tissues and/or delineate its margins for complete removal). Raman

spectroscopy was shown to be useful for rapid identification of tuberculosis meningitis patients with 91% sensitivity and 82% specificity (comparable to the conventional diagnostic methods) [58]. Also, SERS has been used to detect Neisseria meningitis infection by using a CSF samples deposited onto a Si/ZnO/Au subtrate [59]. This detection can be based on a SERS band at 695 cm^{-1} observed in samples of infected individuals and absent in healthy subjects and corresponding to the C–C vibration and ring modes of neopterin.

- Fecal Material (stool or feces): consists of between 25–54% bacterial biomass, 25% carbohydrate or undigested plant matter, 2–25% protein or nitrogenous substances, and 2–15% fat [60]. Fecal material is also composed of intestinal secretions, calcium and iron phosphates, dried epithelial cells, and mucus [60]. Protein and fat are produced due to secretion in the colon, gut bacterial action and epithelial shedding. Many factors affect fecal material protein-to-fat ratios. In most cases, this ratio is a result diet and body weight [60]. Due to the high personal and situational variability of fecal composition, the analysis of fecal material relies on the standardization of sample collection protocols and appropriate storage to avoid digestion of nutrients (indigestible to humans and/or animals) by the gut microbiota remaining on the sample after collection [61]. Collection of feces is fast and minimally invasive as it expels naturally. This collection is also convenient for the patient who can collect feces privately and does not need to take contrast agents and/or bowel cleansing for endoscopic and radiologic imaging procedures (Chapter 2). Previous vibrational spectroscopy studies have shown that fecal material has been used to diagnose gastrointestinal disorders, *Clostridium difficile* (CD) infections, steatorrhea, and other diseases [61–63]. Still, within vibrational spectroscopy, FTIR spectroscopy is more mature than Raman spectroscopy for the analysis fecal material (section 7.3.2) since feces do not contain a vast amount of water. Raman spectroscopy is still under preliminary development for diagnostic applications mostly due to its poor signal-to-noise ratio and Raman spectroscopy has advantages only in higher limit of detection of particular substances compared to FTIR. In most cases, these advantages do not justify the higher costs compared to FTIR for the analysis of fecal material. Raman spectroscopy was used to determine the accuracy and limit of detection of Clostridium difficile (CD) toxin A and CD toxin B in fecal material compared to conventional CD testing methods such as Cell Culture Cytotoxicity Neutralization Assay (CCNA), which takes 48h, is labor intensive, requires cell culture facility and is not performed as part of the clinical routine in medical facilities [62]. Biologically relevant concentrations range between 1-0.1 ng/mL. Raman spectroscopy could identify CD toxins A and B with between 64%-77% accuracies when testing stool spiked with toxin concentrations of 1 ng/mL, 100 pg/mL, 1 pg/mL, and 0.1 pg/mL [62]. Overall, Raman spectroscopy is promising for some applications involving fecal material and is in preliminary stages of technology development and proof of concept.
- Saliva: originates from the secretion of major (parotid, submandibular and sublingual) and minor (buccal, palatal, lingual and labial) salivary glands in the oral cavity [64]. Human saliva is composed of about 99.5% water, 0.3% proteins (immunoglobulins, antimicrobial peptides and glycoproteins including proline-rich and tyrosine-rich proteins, mucins, sialic acid, lactic acid) and 0.2% inorganic matter (such as thiocyanate) [64–66]. Saliva also contains nasal and bronchial secretions, gingival cervicular fluid, cell debris, flaking cells, dental plaque, blood, bacteria, and exogenous substances [64,67]. Saliva has been widely investigated for biomarker identification and quantification of levels of organic and inorganic substances, given its non-invasiveness, simplicity, low-cost, painless and stress-free collection [68–70]. If done correctly, saliva collection poses minimal risks of exposure to infectious agents, which can be a problem for other disease screening methods (involving biofluids, biosolids and others) [71]. Total human saliva contains over 800 identified metabolites (amino acids, carboxylic acids, steroid derivatives, glucose, etc.) and its metabolome is as chemically complex as human serum metabolome due to the abundance of metabolites which can be detected [64,72]. The diversity of metabolites potentially identifiable in saliva has increased the interest in the development of applications involving proteomics, metabolomics, transcriptomics, or microbiomics, especially for the diagnosis of oral diseases such as oral cancer and periodontitis, as well as systemic diseases including diabetes, breast cancer, and Sjögren's syndrome [64,71]. In vibrational spectroscopy, the highly complex saliva metabolome can pose challenges to identify biomarkers without contrast agents. Even though Raman and IR peaks are specific to the vibration of molecular bonds, the molecular structure of many metabolites contain the same functional groups and hence the same molecular bonds. This can cause the spectra peaks to overlap and the difference between healthy and diseased individuals to be observed only

in peak ratios or shifts with high individual variation. Therefore, it is important to consider the saliva collection method for potential variations due to biochemical differences in stimulated and unstimulated saliva (partially due to significantly different bacterial profiles present in each saliva type [73]. In vibrational spectroscopy, minimal amounts of saliva need to be collected for analysis (typically in the order of microliters) which is much lower than sufficient saliva volumes produced by healthy individuals (estimated to be between 0.5 and 1.5 L of saliva daily) [71]. The ease of salivary collection in addition to the proximity of this biofluid to oral and respiratory tissues has made saliva an attractive candidate for the diagnosis of systemic and autoimmune diseases, hereditary disorders, sickle cell anemia, periodontal disease, cystic fibrosis, oral cancer, dental caries and viral infections including COVID-19 [74–76]. An example of detection of oral squamous cell carcinoma by using SERS is the study of Connolly et. al. who showed that the Raman peaks associated with pyrimidine were 767, 1236, 1330, 1662 and 1688 cm^{-1} in normal patients and differed for cancer patients [52]. Similarly, the peak of mucin was found at 1444 cm^{-1}, whereas peaks at 1158 and 1525 cm^{-1} (associated with carotenoids, according to the authors) were absent in saliva of normal patients. In addition, the amide peak at 1652 cm^{-1} exhibited highest intensity for normal patients followed by malignant patients and last by premalignant patients. Finally, broadening was observed at the hemocyanin band with peak 752 cm^{-1} in saliva of malignant and premalignant patients.

- Semen (or seminal fluid): consists of sperm (reproductive component), proteins, carbohydrates, electrolytes, and other constituents produced by four glands: testes, seminal vesicles, prostate and bulbourethral glands. The 65–75% fraction produced by seminal vesicles contains aminoacids, enzymes, flavins, proteins, phosphorylcholine, vitamin C, citrate, and 2–5 mg of fructose per mL of semen [77] to serve as the main energy source of sperm cells, and prostaglandins (to suppress immune responses by the female against foreign semen). The 25-30% fraction produced by prostate is composed of prostate specific antigen, proteolytic enzymes, fibrinolysin, acid phosphatase, citric acid, and ~135±40 μg/mL of zinc for healthy men [78], used for stabilization of the DNA-containing chromatin in sperm cells (resulting in lowered fertility and spermatogenesis in cases of zinc deficiency). The 2–5% fraction produced by testes (or testicles) contains 200 million to 500 million spermatozoa released per ejaculation, unless vasectomy has been performed. Finally, the 1% fraction produced by the bulbourethral glands contains pre-ejaculate, sialic acid, galactose, and mucus, which increases the mobility of sperm cells in the vagina and cervix. Semen can be collected non-invasively [79–81] and used to diagnose male reproductive disorders [51] and bacterial prostatitis [82,83] upon implementation of next-generation technologies. In the context of vibrational spectroscopy, semen has been investigated mostly with FTIR spectroscopy mainly due to technology maturity, portability, cost-effectiveness and lower measurement times leading to less degradation/deterioration of semen components over time. FTIR spectroscopy typically does not have problems with water absorption in semen because its water volume typically ranges from 0.004-0.15% water (estimated based on mean sperm volume of 20-32 μm^3, water percentage of 50-60% per spermatozoa and 200 million to 500 million spermatozoa released per ejaculation) [84,85]. If tests can be done or samples can be stored in 15-20 minutes after ejaculation, semen can remain coagulated. Otherwise, measurements have to be conducted in semen liquefied form. Still, both FTIR and Raman spectroscopy are used for semen analysis primarily in forensics and urology. Raman spectroscopy is convenient for semen analysis and allows for assessment of its aminoacid, amide, and spermine phosphate hexahydrate content [86,87]. Raman spectroscopy is useful to separate semen samples from saliva, sweat, blood, and vaginal fluid samples [86], which could potentially be confusing in a crime scene but necessary to be separated prior to more labor intensive, expensive and time-consuming analysis. In this context, Raman spectroscopy could decrease the sample pre-analysis time while also providing a biochemical characterization of analyzed samples. In general, lactate, tyrosine, fructose, choline, spermine phosphate hexahydrate, and other metabolites had unique Raman spectral characteristics in semen compared to other biofluids [80]. In addition, Raman spectroscopy has been used for the identification of amino acid peaks in UV damaged semen compared with normal semen [86,87] to assess seminal DNA integrity, and potentially to find diagnostic and prognostic biomarkers of male urological disorders [81,86,87].
- Sweat: is mainly composed of 98-99% water, electrolytes, lactic acid, citric acid, ascorbic acid, fatty acids and nitrogen metabolites including urea, uric acid and ammonia [88–97] produced by the eccrine, apocrine, and apoeccrine glands. Sweat is a cloudy, viscous, oily and originally odorless biofluid [97] which obtains odor upon decomposition by bacteria,

adding a number of volatile compounds with particular olfactory properties to its composition [96,98–100]. Sweat composition also depends on the gland in which it was generated. If it is generated by apocrine glands (i.e., apocrine sweat), sweat is mixed with a fraction of the sebum produced by the sebaceous glands open into the hair follicle. Since sebum is composed of ~41% triglycerides, ~26% wax esters, ~16% free fatty acids and ~12% squalene [101,102], apocrine sweat would have a varying fraction of this mixture depending on the amount of sebum close the sweat, its contact time with sebum and at which temperature (i.e., factors which control the solvation of sebum components in sweat). Currently, the clinical use of sweat analysis is still being evaluated [103], despite the recent advancements enabling its rapid and reliable collection, as well as potentially fast and accurate analysis of its metabolites [104–106]. Sweat analysis can be useful to diagnose cystic fibrosis and it has been proposed that it can also be used to diagnose diseases including Addison's disease, Parkinson's disease, and schizophrenia has been inferred [104,105,107]. One of the main candidates for sweat analysis is vibrational spectroscopy because small sample volumes can be quickly analyzed with no labor-intensive techniques. Small sample volumes can be useful to select small areas to collect the sweat from (for instance, at which part of the skin and/or close or further from sebaceous glands). In addition, rapid identification of sweat metabolites could improve early disease detection [104–106]. Raman spectroscopy has been shown to have sufficient sensitivity to detect amino acids, proteins, and metabolites in sweat samples [108], and is capable to identify small concentrations of biomolecules when Surface enhanced Raman spectroscopy (SERS) is used. SERS using silver nanoparticles (AgNPs) could detect sweat left by a fingerprint on surfaces of objects [109–111], which can be useful for forensic, diagnostic and prognostic purposes. Clinically, further validation of vibrational spectroscopy techniques can potentially lead to development of schizophrenia biomarker proteins based on eccrine sweat [111], not only helping patients with bedside instruments, but also expanding the number of diseases to be detected. In this context, Raman and FTIR spectroscopy have potential to still be uncovered by future proof of concept studies and are currently considered promising techniques for next-generation devices.

- Tears: are composed of a complex molecular mixture containing ~98% water and ~2% of lipids, urea, and mixture of about 500 proteins such as mucins and lysozyme [112]. Human tear is produced in the lacrimal glands and its components play a key role in the ocular health including lubrication, cleansing the ocular surface of particles, eye protection against disease and infections, and oxygen supply to corneal cells [113,114]. Tears can be collected non-invasively or minimally-invasively from the conjunctival sac, to investigate the pathophysiology of ocular diseases and infections [115–117], as well as to diagnose renal diseases by using SERS to monitor its urea concentration [118]. It is worth noting that tear collection may be induced by eyeball irritation to increase lacrimal flow by using onion vapor or ammonia solution, in which case tears are collected by using a basal capillary tube [119]. In addition, collecting tears from the right or left eye of an individual lead to significant differences in detected phosphate esters, phospholipids and phosphoproteins, according to biochemical differences identified by FTIR analysis [119]. Currently, the analysis of lacrimal proteins is challenging due to limitations of analytical technologies, which require larger sample volumes (typically not easily available), are not capable of analyzing tears while keeping the high alkalinity of tear proteins and their natural high (and highly variable) ion concentrations [114,120]. One type of tear analysis is based on fluctuations in protein concentration in its aqueous layer representing an individual's immune response. Such immune response causes changes in tear metabolites which can be targeted for detection of virus or fungi infections such as in keratitis cases [121]. Currently, vibrational spectroscopy usually requires drying the sample to concentrate metabolites (and increase signal amplitudes) and, in FTIR, suppress water absorption from measured signals. Raman spectroscopy is used to identify tear metabolites at the edge of dried tear patterns. These metabolites include bicarbonate and urea found at concentrations of ~2 and ~0.3 $mg \cdot mL^{-1}$, respectively [122]. Also protein groups can be detected upon mass separation by using Drop Coating Deposition Raman Spectroscopy (DCDRS) [122,123]. The diagnostic and prognostic value of tears is still under discussion and further studies involving non-specific and specific analyses are required for the first steps of clinical translation.
- Urine: in healthy individuals, urine is composed of ~95% water, ~2% urea, ~0.1% creatinine, ~0.03% uric acid and other components including ammonium, sulphate, bicarbonate, phosphate, potassium, sodium, chloride, magnesium and other ions [124–126]. Urinalysis is integral part of laboratory routine exams for identification of microbial infections and mineral accumulation (leading to mineral crystallization during the formation of kidney or bladder stones) by analyzing

urine sediments in the physical analysis. Urianalysis can also quantify a wide range of substances such as urea, creatinine, cysteine C, and can be used to diagnose conditions associated excess excretion of proteins, microalbumin, inulin, iohexol and iotalamate. In addition, urinalysis biochemical markers can be combined with glomerular filtration rate (GFR) which is typically evaluated for renal function. Since urine composition depends on blood filtration, kidney and bladder function (especially on waste storage and disposal/clearing), the main predictors of renal dysfunction are 24-h protein dosage, urea, and creatinine content partly due to their association with the concentration of protein, urea and creatinine in blood [127,128]. The possibility of detecting blood biomarkers in urine tests makes urinanalysis an attractive option for non-invasive assessment of conditions. Furthermore, urine can be used to diagnose multiple diseases early [129], including kidneys and glomerulus diseases [129] as well as type 2 diabetes, prostate cancer, and bladder cancer [45,129–131]. When using Raman spectroscopy, Jaychandran et. al. [45] showed that key urine metabolites can be rapidly identified with no contrast agent and non-destructively. These metabolites included uric acid (567 cm^{-1}), FAD (606 cm^{-1}), ethanol (890 cm^{-1}), urea (1002 cm^{-1}), glucose (1046 cm^{-1}), creatinine, tryptophan and indoxylsulphate. The Raman peaks for creatinine, tryptophan and indoxylsulphate differed between normal, premalignant and malignant patients. The creatinine peak was found at 692 cm^{-1} for samples of normal patients, and 1336 and 1427 cm^{-1} for samples of malignant patients. Similarly, the tryptophan peak occurred at 1417 cm^{-1} in normal and at 1547 cm^{-1} in premalignant and malignant patients, whereas the indoxylsulphate peak was found at 1615 cm^{-1} in normal and at 1351 cm^{-1} in malignant patients [45]. Given that vibrational spectroscopy can provide a rapid, molecular specific and/or selective, and non-invasive sample characterization, applications for real-time medical checks using smart toilets have been proposed [132].

- Vaginal Fluid (or vaginal discharge): is a naturally produced liquid mixture of proteins, carbohydrates, cells, fungi and bacteria with the function of lubricating and protecting the vagina [133]. Vaginal fluid contains 3.1 g/L of total low molecular weight organic constituents [134], 1.035-1.95 g/L sodium, 0.547-0.900 g/L potassium, ~2.94 g/L chloride [135,136], 0.015-0.026 g/L protein content during the follicular phase and 0.053 g/L protein content during the luteal phase [137,138], 1-5 g/L of lactic acid content [134,139,140], 0.20-0.52 g/L acetic acid [134,139], 0.16 g/L glycerol (with a significant concentration increase after sexual stimulation) [134], 0.3-0.4 g/L urea [139,141], glycogen concentrations of about 4.4-15 g/L [135,142], 5.0-6.2 g/L glucose [142–144], and between 0-4% of total concentration of reducing substances [143]. Because of the composition of vaginal fluid, it can appear like a mucus or secretion (i.e., vaginal fluid may have a thick, sticky consistency or a thin, watery consistency, while its color may be either white or clear). Vaginal fluid can be generated as normal or abnormal discharges including infectious cases (such as vaginal thrush and bacterial vaginosis) or inflammatory cases (vaginitis) [145,146]. Since abnormal discharges change the biochemistry of vaginal fluid, it has been used to diagnose inflammatory diseases such as endometriosis [147], as well as vaginitis [145] and bacterial infections [145–148]. Vaginal fluid is already collected as part of the speculum exam for a number of clinical routine tests such as Pap smear tests and/or a test for human papillomavirus (HPV) in cervical cancer screening. In general, the speculum exam can be used to assess the vagina, the cervix, and the vaginal fluid. The sample of vaginal fluid is usually collected by using a cotton-swab prior to pH tests and microscopy examination. Since the composition of vaginal fluid changes as vaginal diseases progress, vibrational spectroscopy could add value to routine clinical tests as a rapid and green technology for early disease detection. Currently, little progress has been made towards proof-of-concept studies for clinical application of vibrational spectroscopy. Previous studies focused mostly in forensic applications while identifying vibrational modes and corresponding biochemical structures potentially associated with cancer, HPV and/or bacterial infections for next-generation superabsorbent pad technologies [149]. The relationship with cervical cancer can be associated with HPV because about 10% of women with cervical HPV infection develop long-lasting infections that includes them into the high-risk category for cervical cancer [150]. Raman spectroscopy has only been proposed/hypothesized to identify endometriosis biomarkers due to its capability of reliably detect interleukin-6 as a detect cytokine [151] and that Interleukin-1α (IL) has been suggested as a potential biomarker for endometriosis with 100% specificity and 100% sensitivity [148]. Hence, there is an indirect inference that Raman spectroscopy could be used for early endometriosis detection which needs to be confirmed by proof of concept studies. If confirmed, Raman spectroscopy could be an alternative to eliminate the need for reagents, expensive machines and associated costs [42]. Currently, it is only known

that Raman spectroscopy can identify urea, acetic acid, lactate and other metabolites of vaginal fluid to differentiate it from other biofluids including semen, sweat, saliva, and blood. [133,145]. Similar as forensic applications for other biofluids, Raman spectroscopy can offer a rapid, non-destructive, and simple biofluid identification before more detailed and labor-intensive tests.

7.3 Sources of absorption in biological media

As discussed in previous chapters, absorption attenuates light traveling in biological media. This attenuation is caused by absorbing molecules which are called chromophores if they purely convert the absorbed light into molecular vibrations via non-radiative pathways (chapter 4, section 4. Light-tissue interactions and light propagation in biological media, figure 4.1) or luminophores if part of the absorbed light is converted into another type of light via radiative pathways (chapter 4, section 4. Light-tissue interactions and light propagation in biological media, figure 4.1). In this section we discuss the main chromophores found in tissues and biofluids.

7.3.1 Ultraviolet, visible and near-infrared chromophores in biological media

In this section, we describe the main endogenous tissue and biofluid chromophores. A complete list of their characteristics can be found in Table 7.10 (Appendix 8):

- Hemoglobin (Hb) is the oxygen- and carbon-dioxide- transport metalloprotein of red blood cells of nearly every vertebrate and some invertebrate tissues. Blood hemoglobin delivers oxygen from the lungs or gills to all parts of the organisms' body, as well as collects carbon dioxide from these parts to be released in the lungs or gills. By monitoring Hb oxygenated or deoxygenated states, Hb has been widely used to evaluate tissue oxygenation, which provides valuable information for many applications including assessment of organ function and viability, cancer detection and margin delineation, prediction treatment outcomes, monitoring of sports performance, sleep quality to name a few. Hemoglobin can assume many states including
    - Deoxyhemoglobin (Hb or deoxyHb): Hb form in which Hb is not bound with O_2 and typically formed by decreasing the Hb oxygen binding capacity by increasing the concentration of CO_2 in an organisms' body (or *in vitro* by nitrogen or CO_2 purging). Formation of Hb is physiologically induced by the Bohr effect.
    - Oxyhemoglobin (HbO_2; oxyHb or ferrous Hb): Hb form in which Hb is bound to O_2 due to the decrease of CO_2 binding capacity to Hb via rising of O_2 concentration. O_2 binds to Hb until its four binding sites are bound with O_2. The more O_2 is bound to Hb, the quicker other O_2 molecules will bind to other sites (cooperative binding). Hb and HbO_2 can be combined into total hemoglobin concentration (THb = HbO_2 + Hb) and the oxygenation level (or oxygen saturation; StO_2) for calculation of more relevant parameters associated with clinical, medical, and home- or sports-healthcare applications.
    - MetHb (ferric Hb or ferriHb),
    - Ferryl Hb,
    - Carboxyhemoglobin (COHb; carboxyHb),
    - Carbaminohemoglobin ($HbCO_2$; carbaminoHb),
    - Sulfhemoglobin (SHb)
    - Glycated hemoglobin (HbA1c; glycated Hb): a form of Hb when it is chemically linked to a sugar (monosaccharides, disaccharides, etc). Most monosaccharides (such as glucose, galactose and fructose) non-enzymatically/spontaneously bond with Hb when both are present in the bloodstream. The formation of glycated hemoglobin indicates the excessive sugar in one's bloodstream and, therefore, is often used as diabetes biomarker.
    - Sickle cell hemoglobin (HbS; sickle cell Hb): abnormal form of Hb which causes red blood cells to become misshapen, rigid, and sticky. HbS has a recessive genetic origin of sickle cell anemia (found on a recessive allele of the hemoglobin gene) which is translates into a defective form of Hb as a protein derived from RNA translation to proteins.

Redox states happen due to hemoglobin oxidation via reactions between $O_2^{\cdot-}$ superoxide anions and hydrogen peroxide (H_2O_2) with its iron center [152] in a catalytic cycle forming ferrousHb ($HbFe^{2+}$) into ferric Hb (MetHb; $HbFe^{3+}$), ferryl Hb ($HbFe^{4+}$), and the ferryl radical (·HbFe4+):

$$HbFe^{2+}O_2 + H_2O_2 \rightarrow HbFe^{4+} = O + H_2O + O_2 \quad (1)$$

$$HbFe^{4+} = O + e - + 2H^+ \rightarrow HbFe^{3+} + H_2O \quad (2)$$

$$HbFe^{3+} + H_2O_2 \rightarrow \cdot HbFe^{4+} = O + H_2O \quad (3)$$

Despite the well-documented research on the contribution of Hb redox reactivity to cellular/subcellular oxidative alterations, the role of Hb redox forms still remain ambiguous in tissue and organ toxicities [152]. Hemoglobin types absorb primarily in the visible and ultraviolet wavelength ranges (table 7.10).

- Myoglobin is an iron- and oxygen-binding protein present in the cardiac and skeletal muscles of vertebrates. Myoglobin traps oxygen within muscle cells in order to enable production of sufficient energy for muscle contraction. Heart or skeletal muscle damage cause myoglobin release into the blood. Large quantities of myoglobin are toxic to the kidneys, as they filter myoglobin from the blood to release it into the urine. If substantial concentrations of myoglobin are released into the bloodstream (such as after severe traumas or muscle injuries), its excess may cause kidney damage and eventually failure. Myoglobin can be detected in urine or tissues. In tissues, oxymyoglobin (oxyMb) and deoxymyoglobin (deoxyMb) have similar absorption features as HbO_2 and Hb, respectively (table 7.10).
- Water is the most abundant substances in soft tissues. A human body is composed of between 60-80% of water in total body weight [153]. The water composition of soft and hard tissues varies between 10-90%, where highest water percentages can be found in fetal muscle tissues and lowest percentages in adult cortical bone and adipose tissues [154,155]. As the universal solvent in biological media, water is present in any biological medium at liquid and solid states where biochemical reactions need to happen at faster rates (e.g., biological tissues with significant metabolic rates). Water absorption is significant at ultraviolet and shorter wavelengths, as well as infrared and longer wavelengths, whereas absorption is negligible (below 0.01 cm^{-1}) in visible wavelength ranges. Water absorption coefficients exhibit substantial changes at different temperatures [156] including the shift of absorption peak of 972 nm to lower wavelengths and increase of ~5% absorption per 10 °C of water temperature increase from 30 °C to 45 °C, and decreasing absorption at 1192 nm with no significant wavelength shift [156]. Therefore, water temperature may influence measurements of *ex vivo* or *in vivo* tissues.
- Lipids/fat composition of body tissues varies between 1-91%, where highest lipid content can be found in adipose tissues (composed of ~60-91% of lipids in adults and 23-47% in infants [154] and located at tissues such as visceral and subcutaneous fat) and lowest content in fetal muscle tissue [154,155]. Human body lipid mainly consists of saturated, monounsaturated and polyunsaturated fat, including subcutaneous fat which is composed of ~21%, ~46%, and ~33% of saturated, monounsaturated, and polyunsaturated fat, respectively [157]. Lipids are the primary component of cell membranes and energy reserve of animal bodies. This reserve is stored in adipose tissues in form of triacylglycerols for long-term storage purposes, whereas most eukaryotic cells temporarily store lipids in form of triglycerides and sterol esters at cytosolic fat storage organelles known as lipid droplets. Lipid droplets handle the management of endoplasmic reticulum and oxidative stress, as well as the storage of hydrophobic vitamin and signaling precursors [158]. Early lipid absorption measurements started with Conway et al. [159], Van Veen et al. [160] and Nachabé et al [156], who made available the absorption spectra of pork lard between 800-1080 nm, 440-1100 nm and 900-1600 nm, respectively. The re-measured lipid spectrum from 400-2200 nm has been shown at [157,161]. As mentioned before lipid scattering changes with temperature. A similar effect happens for lipid absorption due to the molecular arrangements and binding states of solid (more “crystalline”) and liquid (more “amorphous”) phases [162,163]. Lipid absorption also changes with the degree of saturation of lipid bonds, as differences at the 1170-nm absorption peak were observed between animal fat constituted of 42%, 46%, and 12%

of saturated, monounsaturated and polyunsaturated, respectively, and oil composed of 10% saturated, 30% monounsaturated, and 60% polyunsaturated fat [156].

- Carotenoids such as α-Carotene, β-carotene, β-cryptoxanthin, lutein, zeaxanthin, and lycopene can be found in the blood stream, skin, liver, and adipose cells. Carotenoids are naturally-occurring yellow, orange and red lipofilic pigments synthesized by plants, algae, and photosynthetic bacteria. They are present in fruits and vegetables, whose consumption by humans makes them to accumulate in skin and adipose tissues. Carotenoids have the capability to scavenge free radicals therefore interrupting their harmful oxidation of potentially important cell molecules [164], which suggest that carotenoids have anti-carcinogenic effects in multiple epidemiological studies while others indicate pro-oxidation effects in oxidative stress conditions [165].
    - β-carotene can be found in the skin, blood stream, liver, and adipose tissues. Adipose cells are believed to contain more than 80% of β-carotene reserves [166]. Under normal conditions, β-carotene and retinol uptake happens in the intestines, circulate in the blood, and are delivered to the liver, adipose cells, and gradually distributed to other parts of the body [166–168]. In skin, β-carotene accumulates in subcutaneous fat and stratum corneum tissues, giving a distinct yellow color, especially in regions like the palm of the hand and the sole of the foot where the stratum corneum is more pronounced [169–171]. β-carotene was considered an important absorber in studies of oral cancer [172], vessel plaque detection [173], and adipose tissue of human breast [174–180]. Previous studies suggest that β-carotene may exhibit limited antioxidant protection or to act as a pro-oxidant under oxidative stress conditions [165]. β-carotene has characteristic absorption peaks at 450 and 480 nm when diluted in hexane [169,181] (table 7.10). Still, the β-carotene absorption depends on its solvent and, thus, can be different between *in vitro* and intracellular molecular environments, as illustrated by Bydlon et. al. [157] in the 25-nm broadening of the 480 nm absorption peak and pronounced decrease on absorption in the 450 nm peaks for β-carotene dissolved in lipid/adipose cells compared to that dissolved in hexane.
    - Lycopene as tomato byproduct has been suggested to have antioxidant, hypolipidemic, and anticarcinogenic effects based on *in vitro* and *in vivo* studies [182,183]. In general, lycopene is distributed to fatty tissues, testes, adrenal glands, liver prostate and other organs after ingestion. Lycopene absorption peaks can be found at 443 nm, 471 nm, and 502 nm when dissolved in hexane [157].
- Bilirubin is a yellowish pigment mainly found in spleen and liver fluids. Bilirubin is formed as a result of the breakdown of red blood cells and is excreted out of the body via bile under normal conditions. Bilirubin can accumulate in skin and other organs due to liver or bile duct problems, as liver has excessive bilirubin secretion which causes it to flow into the blood stream. This accumulation (hyperbilirubinemia) results in a yellow skin appearance and is associated with diseases such as Hemolytic jaundice, Gilbert's disease, physiological jaundice and Crigler-Najjar syndrome, Dubin-Johnson syndrome, and biliary obstruction. Hyperbilirubinemia affects 60-70% of term infants and nearly all premature infants [184]. Bilirubin is toxic and its high concentrations may cause brain damage (reason newborns receive therapy for jaundice via light therapy or blood transfusion in severe cases [185,186]. In addition, bilirubin is the responsible for the yellow color of old bruises, as hemoglobin is broken down by macrophages recruited to the wounded area by chemicals released upon local trauma. Macrophages phagocytize both whole erythrocytes and hemoglobin molecules and catabolize the hemoglobin using the heme oxygenase system [187–190].
- Bile is a dark-green-to-yellowish-brown fluid produced by the liver and stored in the gallbladder. Bile has a number of functions including:
    - Digestion: complete digestion of fats, and, indirectly, proteins and carbohydrates via bile salts which reduce fat surface tension via their emulsification, activate lipases, promote action of lipases by offering one solvent for both lipids and lipases, i.e., lipid-splitting enzymes)
    - Absorption: increasing the solubility of hydrophobic substances and reducing the surface tension of lipids and epithelium membranes enables larger permeability of lipids through the absorbing epithelium
    - Excretion of bile, bacteria, toxins, copper, zinc, mercury, and other substances

- Peristalsis stimulation
- Cholagogue Action: Bile contains its own production stimulant, i.e., cholagogues in bile salts, which are absorbed in the intestines, transported to the liver and stimulate bile secretion.
- Maintenance of suitable pH of duodenal contents
- Lubricant: bile contains mucin which acts as a lubricant and buffer.
- Neutralization of gastric acidity via regurgitation into the stomach which may prevent damage on the gastric mucosa

Since bile is abundant in bile ducts, it is an important absorber in liver and intestinal tissues. It may also be a biomarker for liver metastasis [191]. Bile consists of a mixture of several components including other chromophores. Its composition includes about 95% water, bilirubin phospholipid, cholesterol, porphyrins, vitamins, steroids, bile salts, amino acids, enzymes, heavy metals, exogenous drugs, xenobiotics and environmental toxins [192,193]. It is worth noting that bile scatters light. When using spectral fitting to extract tissue chromophore concentrations and scattering properties, bile scattering would be considered as part of the tissue scattering. Using bile absorption spectra with scattering included should not change the estimation of its concentration, tissue scattering properties such as the fraction of Rayleigh scattering, and the Mie scattering power estimated by spectral fitting may vary if these properties are different between bile and tissue.

- Biliverdin is a green pigment of bile and is produced during the heme catabolism. Biliverdin gives the green color of some bruises. Heme oxygenase generates biliverdin, which produces bilirubin after conversion by biliverdin reductase so that bilirubin can be removed by the lymphatic system (in case of injured sites) and excretion into the bile.
- Hemosiderin is an iron-storage brown pigment produced from breakdown of heme within macrophages, which form hemosiderin by partially digesting ferritin and lysosomes. Upon accumulation of this pigment, tissues may appear to have yellow, brown, or black stains, which usually appear on the lower leg. Hemosiderin may be found in tissue- resident macrophages for months after traumas [187–190,194].
- Collagen is a structural protein found in connective tissues, skin, eye and various organs of the cardiovascular system. *Collagen* is a major component of the extracellular matrix (ECM) which holds cells together in organs and holds different organs in place. The ECM also provides cellular communication through a structural lattice to send chemical signals between cells and tissues, especially during biological processes such as neoplasia and angiogenesis. A number of collagen types exist. Collagen type I is the most abundant and one of the main components of the interstitial matrix. Type I collagen exhibits both optical scattering and endogenous fluorescence properties used for noninvasive estimation of changes in the ECM [195]. The mechanical stability of tissues and tissue-engineered models is typically enabled by collagen fibrils and elastin stabilized by covalent cross-links based on aldehyde formation [196]. Measuring fibrous collagen absorption spectrum (as it would mostly be found *in vivo*) is hindered by its inhomogeneous structure due to gaps exist between fibers, whereas denaturing the collagen may change its absorption spectrum. Taroni et al. measured the absorption coefficient of collagen between 600-1100 nm and to spectrally fit dense breast tissue measurements [197–199]. Nachabé et al. collected the collagen absorption spectrum from 500-1600 nm and investigated its concentration in brest tumor [200].
- Elastin a key tissue constituent of the extracellular matrix of connective tissues, highly elastic tissues and organs such as skin, arteries, ligaments, tendons, cartilage and lungs [201]. Elastin gives elasticity to tissues, which changes under pathological conditions such as breast cancer [202–205]. Also, the ratio between collagen and elastin is often used as a measurement of skin aging and early pathologies, especially with ultrasound, elastography, supersonic shear wave imaging and magnetic resonance imaging techniques detecting tissue differences due to larger tissue rigidity when collagen is predominant and elasticity when elastin is predominant [206].
- Cytochrome C is a mitochondrial protein which is essential for the electron transport chain, and, therefore, in the energy production and storage processes within cells. Cytochrome C is a biomarker of mitochondrial content, which could potentially be useful to investigate a bigger picture of tissue metabolism together with parameters

of aerobic and anaerobic cell respiration (such as redox ratios, concentrations of bound and free NADH or FAD provided by fluorescence measurements). Accurately estimating cytochrome C can be challenging due to its strong overlap with HbO_2 absorption spectrum, as HbO_2 tends to be a predominant absorber in *in vivo* tissues (whose metabolism is interesting to uncover, as opposed to metabolism of *ex vivo* tissues or cells *in vitro*). Still, an example of inclusion of cytochrome C in a spectral fitting model is illustrated by Lindbergh et al. [207] for diffuse reflectance spectroscopy (DRS) measurements of calves' myocardium during heart surgery. According to the authors, the spectral fitting was improved from 540-620 nm compared to a model without cytochrome c.

- Melanin refers to a group of natural pigments found in most organisms. It is one of the most versatile biological pigments and exhibits a variety of chemical functions which result in a broad set of physiological properties and responses [208]. Melanin chemical functions include radiation protection [209], thermoregulation [210], metal chelation [211,212], and structural coloration [213]). Melanin is produced by melanocytes through melanogenesis, which consists of oxidation of the tyrosine aminoacid followed by polymerization to result protein-polymer complexes acting as pigments of different colors. Melanin types include:
    - Black-to-brown eumelanin typically alkali insoluble and found in human skin and hair [214,215].
    - Red-to-yellow pheomelanin typically alkali soluble and also found in human skin and hair. Pheomelanin is a cysteine-derivative containing polybenzothiazine portions [214,215].
    - Black-to-brown Neuromelanin found in brain. Neuromelanin has been investigated to understand the molecular origin of neurodegenerative disorders, as well as its functions in neuron disruption, dopamine sequestration and release for chemical memory, and induction of Parkinson's disease [216].
    - Black-to-dark-brown allomelanin generally found in fungi. Allomelanin is a nitrogen-free melanin.
    - Red-to-brown pyomelanin (also known as alkaptomelanin) commonly produced by several fungal and bacterial species. Pyomelanin is a nitrogen-free melanin.

  In skin, melanin is found within epidermal melanosomes [217] typically in form of granules. Melanin absorbs over 99.9% of ultraviolet (UV) radiation and its broad absorption band ranges from the UV to near-infrared (NIR) wavelengths [215]. This absorption and melanin concentration determines the apparent skin color and melanin-related properties. Melanin absorption rapidly decreases as a function of wavelength, leading to a number of researchers modeling its absorption as a power function and typically proportional to $\lambda^{-3.46}$ [218]. For instance, by considering that the melanin absorption coefficient is $\mu_{a,m} = 225\, m^{-1}$ at 694 nm for fair, sun protected Caucasian skin, the absorption spectrum of such skin could be calculated by [219,220]:

$$\mu_{a,m} = 225\, m^{-1} \left(\frac{694nm}{\lambda}\right)^{3.46}$$

- Thyroglobulin is an iodo-glycoprotein of ~70 tyrosine residues produced by follicular cells of thyroid gland to synthetize the thyroid hormones T3 (triiodothyronine) and T4 (thyroxine), which regulate cell/tissue metabolism, body temperature, and heart rate. Iodination of tyrosine residues of thyroglobulin happens once it is transported from thyrocytes to the follicular lumen of the thyroid gland through secretion. This iodination forms mono-iodotyrosine (MIT) and/or di-iodotyrosine (DIT) which lead to preferential formation of T4 synthesized via oxidative coupling between two DIT side chains primarily at a conserved site near the amino terminus, and synthesis of T3 via coupling between one MIT donor and one DIT acceptor at conserved sites at the carboxy terminus. Thyroglobulin concentration varies between 3-40 nanograms/milliliter in healthy patients. High thyroglobulin concentrations can be associated with thyroid cancer, especially if such concentration increases after complete removal of the thyroid gland [221]. Thyroglobulin is one of the main constituents of thyroid tissue and account for 10-20% of its concentration in rat thyroid [222–224].
- Iodine is a trace element present in some foods and an essential component of the thyroid hormones T3 and T4 through the formation of MIT and DIT, as described above. Iodine has also been used to assess the average chain length of glucans such as glycogen and amylose, as this length is proportional to the wavelength of maximum absorption at the iodine spectrum [225]. Lower than average iodination may indicate glycogen-branching enzyme

deficiency in cats [226]], glycogenosis/amylopectinosis and associated diseases in humans [226–228] and amylose/amylopectin ratio in plant tissues [229].

- Tyrosine is a nonessential aminoacid which can be obtained by the body through the metabolism of the aminoacid phenylalanine. Tyrosine is involved in a number of functions including hormone regulation in thyroid (as previously discussed), adrenal, and pituitary glands, as well as production of neurotransmitters in brain (such as epinephrine, norepinephrine, and dopamine) and melanin in hair and skin. L-tyrosine (biologically/enzymatically tyrosine produced in our body) is also present in the structure of nearly every protein and, for this reason, tyrosine is used as a chromophore to study the structure of proteins with techniques involving UV–Vis spectroscopy, fluorescence spectroscopy, resonance Raman spectroscopy, and circular dichroism [230,231].
- Other chromophores include pyrimidines and pyrines of nucleic acids, which absorb light primarily at UV wavelengths (typically shorter than 300 nm), as well as flavins, vitamins and porphyrins, which are weak absorbers in UV and visible wavelengths and/or or are present in very low concentrations in tissues to have significantly accountable absorption. When investigating biofluids directly or measuring signals within blood vessels or internal body structures, chromophores such as cholestherol, cholesteryl oleate, cholesteryl linoleate, glucose, lactate, sucrose, urea to name a few may be of relevant to biological research.

In addition to the description of biological chromophores, the change in chromophore concentrations is shown in Table 7.11 to shown evidence on application-specific changes expected for differentiation between benign and malignant tissues such as those covered in subsequent chapters of this thesis and which may be covered by future applications of developed optical systems (as a result of the thesis work). It is worth noting that chromophore concentration increases and decreases due to tissue malignancy are not consistent across the literature (even for the same tissue types). Therefore, detecting and diagnosing cancer by using one chromophore-associated parameter is not accurate, and multivariate analysis is suggested to be a better approach for cancer detection and delineation, as it will be shown in Chapters 12-14 (Papers 1-3).

7.3.2 Sources of mid- and far-infrared absorption in biological media

Mid- and far-infrared absorption is primarily associated with transitions between vibrational states instead of transitions between electronic states induced by ultraviolet, visible and near-infrared light. In biological media, absorption at mid- and far-infrared wavelengths is associated with vibrational modes of molecular bonds of biomolecules. The association between energy levels of vibrational states and such absorption makes it complementary to information obtained from Raman scattering, which is also related to molecular vibrational modes. The main difference is that infrared (IR) active modes only occur when the vibration changes the molecular dipole moment, whereas Raman active modes occur when the vibration alters the molecular polarizability. Especially for small molecules, mathematical group theory can used to theoretically predict the number of vibrational bands, qualitative description of normal modes associated with these bands, their polarization and shape [232]. Such theory is based on the symmetry element of molecular structures for classification by a point group, which relate to a set of compactible symmetry operations (and thus to symmetric/asymmetric vibrations and polarizability). In general, IR active modes could be most easily recorded for polar groups, and out-of-phase or asymmetric vibrations, while Raman active modes could be most conveniently probed for nonpolar groups, in-phase or symmetric vibrations [233]. Still, calculating IR and Raman active modes for biomolecules can be complex when they are long and can exhibit numerous constitutional Isomers, tautomers, stereoisomers, diastereomers and enantiomers. This complexity is further increased by the dynamic molecular environment of biological media, which can change rapidly over time and originate multiple biomolecules interlinked by numerous metabolic pathways.

With the above in mind, the only way to narrow down biomolecules which could be associated with wavenumber ranges is identifying common functional organic groups and inorganic compounds associated with IR and Raman bands as well as their strength and broadness [234]. By matching characteristics of those bands with those of specific organic groups found in biomolecules [233], it is possible to assign wavenumbers [235] (Tables 7.12 and 7.13) and bands [67] (figure 7.1) to molecules such as lipids, proteins, carbohydrates, and nucleic acids. A more detailed description of the correspondence between IR absorption wavenumbers and secondary structural elements of proteins is given in Table 7.13. In addition, Table 7.14 indicates the infrared band/wavenumbers which intensities can be used for calculation of ratios of lipid-to-protein, protein-to-lipid, DNA-to-protein, nucleic-acid-to-protein, and mineral-to-protein in biological samples.

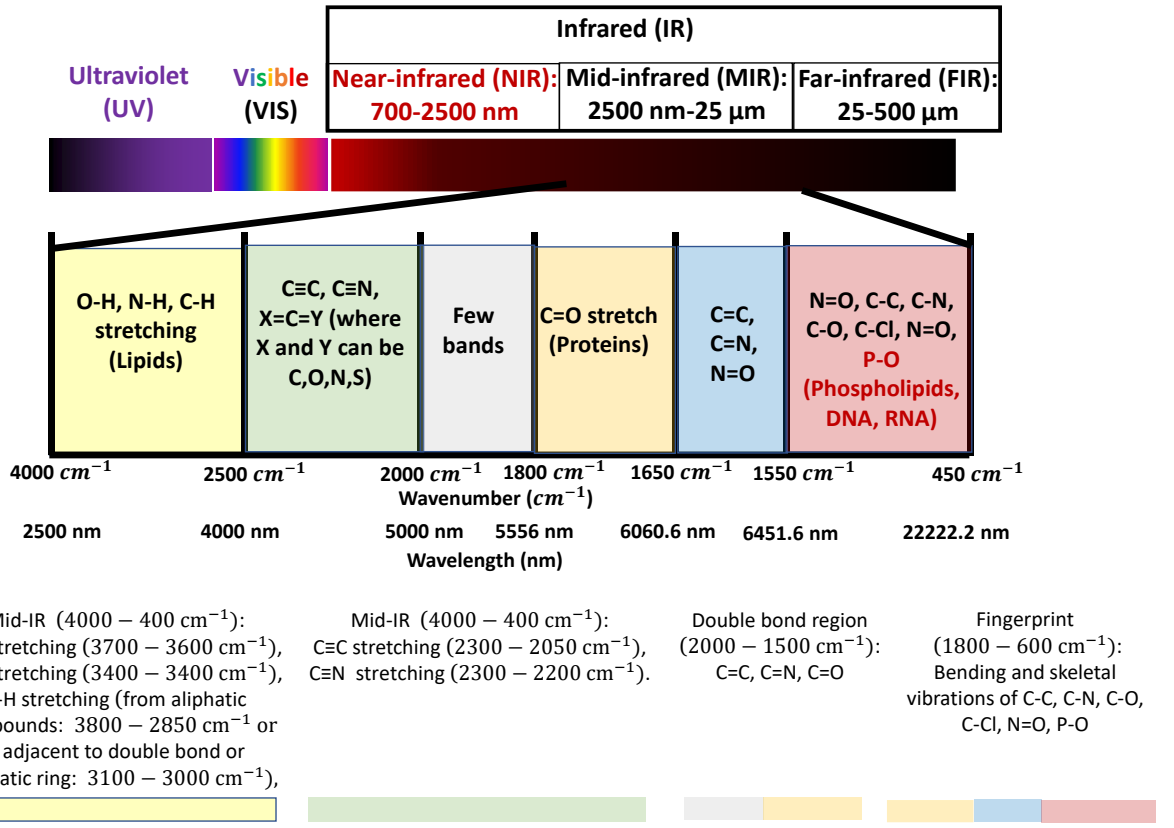


Figure 7.1: Infrared wavelength/wavenumber range options available for spectroscopy of biological media and main vibrational modes of chemical bonds with absorption in the mid-infrared range.

Finally, it is worth noting that information on IR bands and their measurements via transmission Fourier-transform infrared (FTIR) spectroscopy or Attenuated Total Reflection (ATR) FTIR, as well as information on Raman bands (data collected via Raman spectroscopy; to be discussed in chapter 18) are registered in multiple commercial reference spectra databases. These databases contain data collected from respected institutions or companies for high confidence results and include spectra of thousands of compounds separated by applications such as biomedical (biochemical category), forensics, pharmaceuticals, solvents, aldehydes and ketones, polymer and polymer additives, alcohols and phenols, etc. Searches can be particular to sample preparation, instrument accessories, analysis conditions and other factors. Examples of databases include the [67]:

- SDBS FTIR Transmission databases (more than 21,140 spectra)
- Aldrich Database (18,513 ATR FTIR spectra)
- IChem database (12,706 ATR FTIR spectra)
- Elsevier FT-Raman and FTIR polymer database
- National Institute of Standards and Technology (NIST) IR database
- Others

7.3.2.1 Mid- and far-infrared absorption in biological tissues

General IR absorption bands for tissues (especially brain tissues) have been reviewed by Caine at al. [236], who attributed the 3050 − 2800 cm^{-1} range to symmetric and antisymmetric C–H stretches of lipid and proteins, the ester

carbonyl band between 1745 − 1725 cm^{-1} to lipids, absorption bands between 1700 − 1500 cm^{-1} to amide I and II groups of peptide bonds in proteins, a minor band of amide III from 1350-1200 cm^{-1} to proteins, the symmetric and antisymmetric C−O and P−O vibrations between 1235 − 1080 cm^{-1} to phospholipids, deoxyribonucleic acid (DNA), ribonucleic acid (RNA), and vibrational bands between 1150 -1025 cm^{-1} to carbohydrate such as glucose, fructose and glycogen. The accuracy of band assignment depends on the accuracy of peaks and bands of the previously mentioned international databases. Pathological conditions cause intensity, ratiometric, wavenumber translational changes in these peaks/bands due to molecular alterations in biological tissues.

Mid-IR and far-IR absorption is often obtained by using Fourier Transform Infrared (FTIR) spectroscopy (i.e., the most used modality of IR spectroscopy). Similar to Raman spectroscopy (Chapter 8, section 8.2.4) discussed in section 7.2, FTIR spectroscopy is often used to compare FTIR signals between positive controls and diseased tissues, i.e., compare FTIR signals of diseased tissues with either signals of normal tissues surrounding such diseased tissues or normal tissues on the contralateral (anatomical) side from the same diseased patients, if anatomical symmetry and access to the contralateral side is possible. However, studies rarely compare FTIR signals of normal tissues from healthy patients (i.e., negative control measurements) with diseased tissues of diseased patients, and rarely perform populational studies comparing samples of the same patients before and after these patients become diseased. Negative control measurements are required to develop technologies targeting multiple applications including screening, monitoring tissue/organ function and viability, delineating diseased regions (e.g., delineating cancer margins; Chapters 12-17), and robust diagnosis (i.e., diagnostic applications based on robust pattern finding on a large variety of patients with data analysis methods such as machine learning, discussed in Chapter 10).

In populational studies focusing on monitoring individual health status, it is important to monitor features of absorption bands corresponding to the healthy status of a certain individual and look for spectral changes corresponding to a diseased state. If changes indicating diagnostic or prognostic biomarkers are constant for each individual (i.e., if individual relative changes in IR absorption follow a particular trend), patient stratification would be possible by monitoring changes in individual IR absorption spectra. If changes in data analysis metrics (Chapter 10) such as absolute IR absorption (or IR absorption spectra normalized by the IR absorption value at a fixed wavenumber) are sufficient large to differentiate the entire population of healthy from the entire population of diseased individuals and/or to find all individuals with a better prognosis after specific treatment, these changes can be used to identify diagnostic or prognostic biomarkers without need to prior monitoring individual changes in FTIR spectra. A similar rationale can be applied to biofluids. In addition, biofluid analysis can be used for disease screening purposes.

It is important to note that decreasing the variability of FTIR spectroscopic signals with negative controls and populational studies is essential to increase the detection accuracy in every targeted application compared to Raman spectroscopy. Decreasing FTIR signal variability by external factors helps identifying biomarkers more specifically, given that FTIR signals (generated by the absorption by IR active molecular vibrational modes) are broadened by multiple molecular rotational states, and given that FTIR signals are heavily contaminated by water absorption. For instance, populational studies avoid taking the variability generated by neglecting the intraindividual differences when comparing two study groups, i.e., by comparing normal samples of group A and diseased samples of group B into data analysis methods to predict normal and diseased states. Instead, populational studies compare between normal and diseased samples of the same individual before and after becoming diseased, and hence corresponding measurements are taken for groups A and B. By considering only intraindividual variations, the measurement specificity increases. This specificity facilitates identifying IR active vibrational modes and biomolecules involved in the transition between normal and diseased states. Still, one should note that performing populational studies requires laborious work of collecting data from patients who might or might not develop diseases, who might have a worse or a better prognosis after a specific treatment, who might or might not have organ rejections and others. The uncertainty of collecting useful data for every study volunteer slows the data collection process and, hence populational studies are more suitable for more mature and cost-effective technologies such as FTIR spectroscopy instead of Raman spectroscopy. Also, populational studies require collecting data from a larger population compared to other study settings, which makes them more suitable when biofluid

applications are involved rather than tissue applications (typically limited by the number of patients in need for clinical intervention).

7.3.2.2 Mid- and far-infrared absorption in biofluids

With the above in mind, the maturity and cost-effectiveness of FTIR spectroscopy facilitates the measurement of biofluids in numerous scenarios. Easier measurements also imply that more data is available for mid-IR and far-IR absorption of biofluids, including IR band assignments (to vibrational modes and corresponding molecules) of typical absorption bands of plasma samples (Table 7.16, Appendix 10.2) [237], saliva samples (Table 7.17, Appendix 10.2) [43], blood samples (Table 7.19, Appendix 10.2) [43], urine samples (Table 7.20, Appendix 10.2) [43], and normal human cerebrospinal fluid samples (Table 7.21, Appendix 10.2) [238]. In addition, Table 7.18 (Appendix 10.2) shows the IR vibrational mode assignments and molecular signatures using FTIR spectroscopy for saliva-based disease diagnosis of diabetes [31,239]. Finally, data collected in the tables reproduced from previous studies has been collected by using attenuated total reflection FTIR (i.e., ATR-FTIR) spectroscopy, which quantifies the attenuation of an internally-reflected IR beam, once this beam comes into contact with a sample deposited on the top of a high refractive index crystal (such as diamond, zinc selenide (ZnSe), and germanium (Ge) crystals). By focusing the IR beam onto the crystal at a set angle on one side of the crystal, the resulting internal reflections produce a transient wave reaching beyond the outer surface of the crystal (i.e., reaching approximately between 0.5-5 µm within the sample). The wavelength-resolved (or wavenumber-resolved) spectrum is a result of the attenuated energy from transition waves as a function of wavelength, which can be measured as each wave is guided back to the original IR beam that leaves on the other side of the crystal and is sent to a spectrometer.

In addition to making measurements more specific by performing populational studies (section 7.3.2.1), FTIR data collection of biofluids has an advantage compared with data collection on biological tissues. Despite the FTIR signal contamination by water, obtaining sharper peaks in the fingerprint region (from 600-1800 cm^{-1}) is possible by concentrating biofluid components and eliminating non-bound water (i.e., water molecules bound to biofluid proteins, carbohydrates, and other components) by letting the biofluid droplets to dry on the ATR-FTIR crystal prior to measurements. However, one should note that the drying process introduces physical and chemical inhomogeneity to analyzed samples, as drying follows the coffee ring effect, generate gelation and cracking patterns [119,240]. Sample inhomogeneity may make sample measurement protocols irreproducible and non-repeatable without proper validation studies [241]. With this in mind, building drying substrates with specific shapes to deposit biofluid droplets and/or controlling the drying process based on ambient humidity, temperature and other variables may help increasing the measurement reproducibility.

Another sample preparation step which may help in ATR-FTIR signal analysis is separating biofluid components prior to analysis. A simple separation method is biofluid fractionation by centrifugation, which has been shown to improve the quantification of low molecular weight biomarkers [242] such as glucose and glycine in whole human serum [241].

Finally, we can use liquid based cytology to find biofluid biomarkers based on cell ratios and cellular composition together with biofluid analysis, since cells can be separated from biofluids by using centrifugation. Liquid based cytology (also known as *ex vivo* spectroscopic cytology) is commonly used to analyze exfoliated oral cell samples, which can be easily collected non-invasively and without disturbing the clinical workflow [241]. In this case, the analysis of cell pellets could potentially be conducted similar to biofluid ATR-FTIR analysis, whereas FTIR microspectroscopy focuses on understanding changes in cell biochemistry in normal, benign and/or diseased states by monitoring biological processes within cells. Information from these biological processes may provide information about the molecular origin of diseases.

Similar to using Raman spectroscopy to investigate biofluid biomarkers (section 7.2.2), applications involving mid- and far-infrared absorption should consider biofluid composition, molecular sensitivity of measurement techniques (such as FTIR and ATR-FTIR), technology maturity and adoption aspects, and potential for clinical translation (i.e., how

technology can be introduced and adopted in a long-term without disturbing the clinical workflow and/or patients' lives). While most of the necessary information has already been discussed in section 7.2.2, applications below have been discussed based on studies reviewed by [31,42,43] and separated for each biofluid:

- Blood: FTIR spectroscopy has been used to detect a wide variety of diseases including infectious diseases [243 244 245 246 247 248 249], cancer [250 251 252], brain disorders [253 254], renal failure, jaundice and rheumatoid arthritis [255–257], while having potential to be used to monitor the risk to develop diseases associated with Very-low-density lipoprotein (VLDL), cholesterol, glucose, and triglycerides [258,259], and being useful to assess individual nutritional status and hydration state [260 261]. Detecting infectious diseases is an especially important application with the increased global burden during pandemics and epidemics in which infectious agents emerge rapidly. In this context, FTIR spectroscopy is a candidate for disease real-time, cost-effective and non-invasive diagnostics, with potential for high-throughput analysis. Attenuated total reflection (ATR) FTIR spectroscopy (or ATR-FTIR) has been used to determine the stages of malarial infection by using PLSR chemometrics of FTIR spectra [243] with a 0.00001% limit of detection of parasetemia for ring staged parasites. In 2018, Wood et. al. patented the use of FTIR spectroscopy for detection of malarial parasites based on their lipid signals [244]. By using mid-infrared spectroscopy combined with logistic regression, malarial parasites could be detected in blood spots dried in filter papers with 92% accuracy for *Plasmodium falciparum* infections and 85% accuracy for *Plasmodium ovale* infections [245]. In terms of disease screening and diagnostic applications, ATR-FTIR of blood serum was used to classify healthy patients, HIV patients and patients with AIDS or HIV/HCV co-infections with 97.67% accuracy [246], as well as to discriminate healthy control samples from HIV-infected untreated samples and HIV-infected treatment-experienced by using PLS-DA and OPLS-DA [247]. Discrimination between control and infected samples was based on spectral bands with peaks around 3010 cm^{-1}, 1600–1652 cm^{-1} and 1299–1498 cm^{-1} corresponding to lipids, protein and carbohydrates, respectively. By using ATR-FTIR combined with PCA-LDA, GA-LDA and SPALDA classification, zika, chikungunya and dengue viruses (which have been causing emerging arbovirus infections globally) can be detected with ~100% specificity and sensitivity when separating healthy from dengue and chikungunya infected samples, and ~90% specificity and sensitivity when separating healthy from zika infected samples [248]. In addition, FTIR spectroscopy of frozen dried blood sera combined with PCA-LDA could classify dengue infected from healthy control samples with 85% sensitivity and 95% specificity [249]. In terms of cancer detection, ATR-FTIR of blood serum has been combined with RBF-SVM to detect gliomas (a type of brain tumor) with 93.75% sensitivity and 96.53% [250]. In addition, colorectal cancer patients could be classified based on their blood plasma samples with 100% precision and accuracy by using FTIR and PLS-DA [251], whereas basal cell carcinoma patients could be classified with 97.6% accuracy by analyzing whole blood samples with ATR-FTIR spectroscopy [252]. In terms of brain disorders, ATR-FTIR spectroscopy has been used to assess schizophrenia, dementia, and bipolar disorders. Evaluation of spectral characteristics of blood plasma using PLS-DA could generate models to classify schizophrenic, bipolar and control samples with up to 100% sensitivity and 100% specificity when using the full wavenumber range from 500-4000 cm^{-1} [253]. By extracting and analyzing white blood cells and plasma from isolated blood samples, FTIR spectroscopy combined with PCA-LDA could classify Alzheimer patients and healthy subjects with 67-82% sensitivity, 79-90% specificity and 75-85% accuracy [254] Quantification of blood cholesterol, VLDL, glucose and triglycerides was also reported by using ATR-FTIR combined with PLS, PCA and LDA [258,259]. In addition to quantifying blood substances, ATR-FTIR spectroscopy could also evaluate individual hydration state, nutritional status and associated illnesses by quantifying proteins in human whole blood and/or blood serum in which immunoglobulin G (IgG), globulin and albumin were spiked [260 261]. More specifically, ATR-FTIR spectroscopy estimated total immunoglobulin, albumin, globulin concentrations, and the albumin/globulin ratio in blood sera samples to have results compared with capillary electrophoresis results as ground truth for accuracy determination and assessment of potential for point-of-care diagnostics [260 261].
- Cerebrospinal Fluid (CSF): FTIR spectroscopy of CSF suggested that healthy subjects and Alzheimer's disease (AD) patients could be differentiated based on signals associated with decreased levels of beta-Amyloid protein and increased levels of tau protein in AD patients (compared with healthy subjects) with high sensitivity and specificity [56,57]. Other abnormalities associated with neurodegenerative disorders could potentially be identified by monitoring albumin and lactate as biomarkers [262] due to their characteristic spectral bands.

- Fecal Material (stool or feces): FTIR spectroscopy can be used to rapidly analyze fecal material in clinical routine tests with little influence of water absorption in the signal. Monitoring IR absorption of fecal material components has been shown with both FTIR spectroscopy and Near-Infrared Reflectance Spectroscopy (NIRS) [63]. In particular, FTIR spectroscopy can be used to diagnose and monitor steatorrhea with precision comparable to the conventional methods [62]. Hence, FTIR spectroscopy and NIRS could potentially identify diagnostic and/or prognostic biomarkers of interest as rapid, cost-effective methods for analysis of fecal material samples. It is worth noting that validation with clinical studies is required, especially to identify biomarkers with less personal and situational variation responsible for biochemical changes of fecal material. Personal variation could be mitigated with monitoring intrapatient variation periodically, while situational variation in fecal composition would require long-term clinical studies.
- Saliva: ATR-FTIR spectroscopy studies have found spectral characteristics corresponding to lipids, aminoacids, proteins, carbohydrates, and nucleic acids changing due to diseases including SARS-CoV-2, cancer, psoriasis, diabetes mellitus, chronic kidney disease (CKD), systemic diseases, as well as potential cofounding factors associated with gender, age and behavioral factors (such as tobacco smoking and periodontitis) [66,75,76,239,263–272]. However, as per section 7.2, saliva composition depends on its collection and processing methods, which can affect the sensitivity and specificity achieved by clinical studies using vibrational spectroscopy. For instance, FTIR microscopy coupled with PLS-DA showed that lipids, proteins, aminoacids, nucleic acids, and carbohydrates in saliva change (1) between stimulated and non-stimulated saliva samples, (2) between centrifugated and non-centrifugated samples, and (3) between drying passively or by vacuum centrifugating samples [273] supernatant collection by cotton after centrifugation could be lead to more reproducibility for carbohydrate-based analyses/assays, whereas not collecting supernatant by cotton saturation could be more reproducible for aminoacid-based assays[273]. In addition, lipids and proteins in the 2800–3000 cm^{-1} wavenumbers have been considered saliva biomarkers for periodontitis diagnosis using ATR-FTIR spectroscopy [66,263] To identify tobacco smoking, thiocyanates have been identified as saliva biomarkers [66,263], whereas FTIR spectral bands between 950–1180 cm^{-1} (assigned to glycogen and glucose) and at 1546 cm^{-1} and 1655 cm^{-1} (assigned to amide I and II) were considered saliva biomarkers for diabetes [239,264].
- Semen (or seminal fluid): Compared with Raman spectroscopy, FTIR spectroscopy is a less expensive alternative involving shorter measurement times and a more mature technology (i.e., with more portable and user-friendly instruments). Combined with the non-invasiveness offered by vibrational spectroscopy, FTIR spectroscopy of semen could be clinically translated in shorter times. Semen has characteristic lipid, protein and phosphate spectral peaks that can differentiate semen from other biofluids [83,86,274] while allowing for FTIR analysis of cells, aminoacids, citrate, enzymes, seminal plasma and other components [274].
- Tears: FTIR spectroscopy has been used to identify meibum and tear lipids to enable addressing dry eye issues associated with the presence of these substances [48].
- Urine: ATR-FTIR has been used to find diagnostic biomarkers of ovarian cancer, cystinuria and renal disease [275–277]. Preliminary studies showed that spectra regions corresponding to protein and nucleic acid bands could discriminate between healthy individuals and ovarian cancer patients [277].
- Vaginal fluid (or vaginal discharge): Similar to Raman spectroscopy, FTIR spectroscopy has been used to find characteristic spectral peaks of vaginal fluid for preliminary evaluation for biofluids in forensic applications (prior to labor-intensive and more detailed analyses) and to propose clinical applications benefitting from FTIR molecular sensitivity, rapid, and non-destructive analysis. By identifying characteristic spectral peaks corresponding to vaginal fluid amides, carbohydrates and epithelia [149], FTIR spectroscopy is capable of differentiating vaginal fluid from menstrual blood and seminal fluid. This identification is based on amide groups, methyl groups and phosphoric acid [149]. In addition, automated FTIR analysis of vaginal fluid cells could enable early detection of HPV, cervical cancer and bacterial infections [149].

7.4 Sources of fluorescence in biological media

Fluorescence has been widely exploited in terms of its wavelength- and time-dependent properties of biological tissues and biofluids. Wavelength-resolved fluorescence spectra (WRFS or FS) has been extensively used to obtain information mainly on tissue biochemistry and occurrence of chemical reactions (e.g., redox ratios) based on relative peak intensities, spectral shape, Stokes shift, fluorescence quenching, photobleaching, estimation of fluorophore concentrations via spectral fitting with fractions of pure fluorophore spectra or multi-Gaussian fittings. On the other hand, time-resolved fluorescence spectroscopy (TRFS) has been used to determine tissue biochemical changes which could not be determined with wavelength-dependent measurements such as the discrimination between chemical species with similar wavelength-dependent spectra (e.g., free and bound NADH, free and bound FAD) and determination of the local tissue microenvironment (e.g., pH, $[O_2]$, $[Ca^{2+}]$) [278]. The challenge of TRFS measurements relies on the accurate extraction of fluorescence lifetime of more than 3 fluorophores given that the fluorescence decay of fluorophores is exponential and typically overlaps significantly with fluorescence emission of other fluorophores over time. This overlap hinders the accurate determination of the concentration and lifetime of multiple fluorophores if TRFS measurements do not have sufficiently high signal-to-noise ratio, were not acquired for sufficiently long times (to fit for long lifetime molecules) and/or the instrument response function cannot be measured accurately. Despite this limitation, extraction of concentrations and fluorescence lifetime of multiple fluorophores have been researched with a wide range of algorithms including multiexponential fittings, Legendre- and Laguerre-deconvolution methods, phasor analysis, phase-modulation analysis of frequency-domain data, to name a few.

Determination of tissue biochemistry for a wide range of applications using FS and TRFS is possible via non-invasive extraction of characteristics of multiple endogenous tissue fluorophores such as

- structural proteins (e.g., collagen, elastin and keratin)
- metabolites and coenzymes (e.g., nicotinamide adenine dinucleotide (NADH), nicotinamide adenine dinucleotide phosphate (NADPH), flavins coenzymes such as flavin adenine dinucleotide (FAD) and flavin mononucleotide (FMN))
- lipids, lipopigments and lipid sources (e.g., lipofuscin, ceroids, advanced glycation end-products (AGE)
- porphyrins
- pigments (e.g., melanin, neuromelanin and mucin)
- vitamins (e.g., Vitamin B12, Vitamin K, Vitamin D, Vitamin C, Vitamin B6 or Pyridoxine (PN)), vitamin precursors and co-factors (e.g., 4-Pyridoxic acid, pyridoxal, pyridoxamine, pyridoxal 5'-phosphate, 4-Pyridoxic acid, pterins (xantoperins), biopterins, neopterins, 6-carboxypterins (used for folic acid assay), β-Carotene)
- aminoacids (e.g., tryptophan, phenylalanine, histidine, tyrosine, tetraglycine, triglycine, glycyl-aspartic acid, glycyl-serine, histidyl-histidine, glycyl-asparagine, hydroxylysine, glycyl-asparagine, glycyl-proline)

whereas specific applications involving local accumulation of biomarkers (such as determination of the monitoring treatment efficacy, delineation of cancer margins, finding remaining pathological features after surgical/clinical procedures, and surface/liquid decontamination) can be exploited by applying and detecting the fluorescence of exogenous fluorophores such as:

- fluorescent proteins (e.g., genetically engineered fluorescent protein reporters including cyan-, green-, yellow-, orange-, red- and far-red fluorescent proteins)
- near-infrared probes (e.g., indocyanine green and biodegradable nanoparticles)
- fluorescent dyes/photosensitizing agents (e.g., σ-aminolevulinic acid (ALA), protoporphyrin IX, chlorins, bacteriochlorophylls, benzoporphyrins, purpurins, phthalocyanines, naphthalocyanines, texaphyrins, meso-tetra(hydroxyphenyl)chlorin (mTHPC, Foscan®))
- phospholipid markers including cell-membrane-specific probes such as 1,6-diphenyl-1,3,5-hexatriene or DPH
- organelle, membrane, or ion-sensitive probes

- probes for pH, temperature, glucose, oxygen, reactive-nitrogen or reactive-oxygen-species sensing
- metal-based nanoparticles (typically used for theranostics due to combined properties allowing for photothermal therapy or photodynamic therapy along with diagnostics).
- upconverting nanoparticles

In terms of endogeneous fluorophores, NAD(P)H and FAD are some of the most known metabolic biomarkers in cancer diagnostics. NADH is the reduced form of the coenzyme nicotinamide adenine dinucleotide, NADPH is the reduced nicotinamide adenine dinucleotide phosphate, and FAD is the oxidized form of flavin adenine dinucleotide. NADH and NADPH contribute to most of the UV-excited fluorescence in biological tissues and play a key role in numerous biological processes involving oxidative phosphorylation (in mitochondria [279]), cell signaling, aging and apoptosis.

NADH is an electron carrier in oxidative phosphorylation, whereas NADPH acts as an electron carrier in antioxidant processes and anabolic reactions (e.g., the Calvin cycle and lipid / nucleic acid syntheses). Metabolic differences due to NAD(P)H are indicated by the ratio between reduced NADPH and NADH, which is five times lower in healthy cells compared with cells under oxidative stress (e.g., cancer cells) in brain and liver. [280,281]. If quantifying this ratio in mitochondria, one should consider that the contribution of NADPH to NAD(P)H fluorescence is much lower than the contribution of NADH, since the NADH quantum yield is about 1.25-2.5 higher than the quantum yield of NADPH [282]. In overall tissue, the contribution of NADPH is typically negligible. However, this is not true for NADH, which has an increased quantum yield of 4 times for its bound state (bound NADH) compared to its free NADH [283], despite the quantum yield of free NADH being lower than the quantum yield of riboflavin (vitamin B2) [284].

Another biomarker for oxidative stress and metabolic changes is the ratio between free NAD(P)H and bound NAD(P)H. Since the wavelength-resolved fluorescence spectra (Chapter 8, sections 8.1.1 and 8.2.5) of free and bound NAD(P)H are similar and their fluorescence lifetimes differ (Table 7.22, Appendix 11.1), this ratio is typically quantified by comparing the amplitude of biexponential components of time-resolved fluorescence (Chapter 8, section 8.1.4 and 8.2.5) of NAD(P)H. In cell studies, the free-to-bound NAD(P)H ratio has been proposed to refer to NADH/NAD+ reduction/oxidation pair [285,286] and a biomarker to estimate metabolic oxidative state through metabolic redox imaging targeting time-resolved NAD(P)H fluorescence. is widely studied for estimation of metabolic oxidative state and thus for metabolic redox imaging. An additional way of detecting the free/bound ratio of NAD(P)H is potentially monitoring the spectral shift of the NADH absorption spectrum, which has been reported to happen when lactic dehydrogenase binds to NADH, possibly altering the structure of NADH [287–289]. Finally, the free/bound ratio of NAD(P)H can also be measured by using fluorescence anisotropy [290], as NADH binding to proteins increases the fluorescence anisotropy decay time [291].

The FAD coenzyme is part of a category of compounds called flavins (also known as isoalloxazines), which are ubiquitous redox carriers in mammal metabolism. This category includes the flavin mononucleotide (FMN). Both FAD and FMN are derivates of vitamin B2 (riboflavin). Most biological system flavins are bound to proteins and act as their cofactors. Hence, flavins are often referred to as flavoenzymes and flavoproteins. FAD is involved with oxidoreductases which require FAD as a prosthetic group for electron transport. The NADH/FAD ratio changes in cancer due to the Warburg effect [292–295], which describes the higher rates of glycolysis (involving energy production with NAD+/NADH reduction/oxidation pairs only) than oxidative phosphorylation rates (involving both NAD+/NADH and FAD/$FADH_2$ pairs in energy production) in cancer cells compared with normal (healthy) cells. Glycolysis rates tends to be higher the more aggressive cancers are, since uncontrolled accelerated tumor growth requires producing energy quicker than rates enabled by oxidative phosphorylation. NADH/FAD ratio are known as the optical reduction-oxidation (redox) ratio and are typically measured by the ratio between fluorescence intensities of NADH and FAD, or by the amplitude contribution of NADH and FAD to the fluorescence decay in time-resolved fluorescence spectroscopy (Chapter 8, section 8.1.4). Ratios of free/bound FAD may isolate the contribution of oxidative phosphorylation in the total cell energy production, which is not possible to measure with free/bound NADH ratios due to the NADH involvement in both glycolysis and oxidative phosphorylation. Isolating this contribution can be useful to monitor the mammal cell status (which tends to have higher oxidative phosphorylation rates when closer to the healthy status). Since the free/bound FAD contribution is particular to mammals, comparison with free/bound NADH can be useful as an assessment of recovering rates of infection and/or wound healing by monitoring the ratio between mammal and other types of cells (e.g., bacteria and fungi). The ratio between free/bound FAD can be measured by the reduction of fluorescence lifetime of FAD+ upon protein binding (from 2.8 ns to less than 0.4 ns, respectively) [296–300], which has been attributed to the presence of aromatic residues close to the protein binding group, including tyrosine and tryptophan [301].

The formation of FAD depends on the enzymatic conversion of riboflavin into FMN (by riboflavin kinase), and the conversion of FMN into FAD (by flavin mononucleotide adenylyltransferase) [302]. The association between FAD and FMN with flavoproteins controls cellular processes including energy production, DNA repair, protein folding, chromatin remodeling, light emission, detoxification, neural development, and apoptosis. FAD is about 10 times less fluorescent compared to riboflavin and FMN, which are the most intensely fluorescent flavins [303]. Even though the fluorescence quantum yield and lifetime of riboflavin varies with the pH, solvent and presence of nearby amino acids [304], in general flavins absorption maximum occurs around 450 nm and maximal fluorescence emission falls between 520–530 nm (Table 7.22, Appendix 11.1). Deviations from expected emission (e.g., wavelength shifts, fluorescence lifetime changes, etc) could be biomarkers of intracellular pH increase, if other factors causing potential deviations remain constant over the investigation time (e.g., experiment duration, time monitoring tissues, and times between patient visits in case changes are monitored over time for the same patient).

In addition to riboflavin (vitamin B2), other vitamins can provide information on tissues health status or prediction of long-term organ function, since they act as both catalysts and participants in biochemical reactions. Vitamins are essential for cell function, growth, and development. In case of local or systemic vitamin deficiency (potentially measured either in tissues or in biofluids, respectively), vitamins can be replenished through normal diet or dietary supplements mainly to prevent long-term effects of such deficiency. Most vitamins have aromatic ring structures with delocalized electrons and thus exhibit endogenous fluorescence (Table 7.22, Appendix 11.1). Vitamin A is fluorescent in both retinol (vitamin A alcohol) and retinol palmitate (vitamin A palmitate) forms [305]. Retinol palmitate excitation band occurs between 325–330 nm, its emission ranges from 505–510 nm, and it has a fluorescence lifetime of 2.17 ns [280]. Similar to B2 being precursor of FAD and FMN, B3 vitamins can be found as nicotinamide (niacinamid) and niacin, which are precursors to NADH and NADP. Also, niacin is a precursor to NAD+/NADH and NADP+/NADPH, and therefore plays an indirect role in previously mentioned cell metabolic rates.

Another fluorescent vitamin with a major role in metabolism is vitamin B6. The active form of vitamin B6 (i.e., pyridoxal 5'-phosphate) is a coenzyme in more than 140 enzymatic reactions of glucose, aminoacid and lipid metabolism (with majority of reactions involving aminoacid biosynthesis and catabolism, as well as fatty acid biosynthesis). It is worth noting that this active form is dependent on FMN (and hence on riboflavin or vitamin B2 indirectly). Despite vitamin B6 deficiency being rare, genetic defects can cause epileptic seizures in infants. In adults, symptoms of vitamin B6 deficiency vary from drownsiness, peripheral neuropathy, and inflammation with or without rash around mouth and eyes. The excess of vitamin B6 is degraded in the liver and eliminated as 4-pyridoxic acid in urine. Therefore, biofluid analysis can potentially be used to detect this excess. Detection can be performed by using excitation at ~315 nm and monitor the emission around 425 nm (Table 7.22, Appendix 11.1). The relevance of vitamin B6 excess detection is not only due to its potential long-term metabolic effects, but also due to the induction of UVA phototoxicity [306] by vitamin B6 compounds, since these compounds are skin photosensitizers [307]. These compounds have been hypothesized to induce DNA damage by photoinduced electron transfer reaction to DNA bases and amino acids [308]. Finally, diseases such as cirrhosis, renal disease, and cancer are associated with vitamin B6 metabolism defects [280]. Vitamin B6 (pyridoxine) and its constituents (i.e., pyridoxinic compounds) have excitation peaks between 315-350 nm, emission maxima between 380-425 nm [309], and fluorescence lifetimes between 0.6-8.4 ns [308] (Table 7.22, Appendix 11.1). Among these constituents, pyridoxamine and 4-pyridoxic acid exhibit the highest quantum yield and longer lifetime. At 25°C in neutral aqueous solution, the quantum yields for pyridoxal, pyridoxamine, and pyridoxamine-5-phosphate are 0.048, 0.11, and 0.14, respectively [310]. It is important to note that the fluorescence spectral properties of vitamin B6 (pyridoxinic) compounds are sensitive to their molecular microenvironment, including pH, temperature and other factors. Further investigation is needed to understand the changes in these properties and evaluate whether vitamin B6 levels could be monitored by optical techniques potentially adaptable to real-time and high-throughput screening and diagnostic tests.

Vitamin B9 (also known as folate, folic acid, pteroylglutamate and pteroyl-L-glutamic acid) is involved in the biosynthesis, repair and methylation of nucleic acids and aminoacid metabolism in cell division. Accurate intake of vitamin B9 is important to reduce the risk of many diseases and defects. First, low vitamin B9 levels are a major cause of neural tube defects (NTDs) in babies, as NTD rates have decreased by 28% since mandatory vitamin B9 supplementation began

in the United States in 1998 [311]. Currently, either mandatory or voluntary fortification of certain foods with vitamin B9 is used in more than 80 countries to decrease NTD rates [312]. However, guidelines of when to vitamin B9 are not adequate because vitamin B9 supplementation is advised "during the periconceptional period before a woman might be aware that she is pregnant" when a large portion of pregnancies are unplanned (~50% in the United States and similar statistics are followed for many countries around the globe). Excess of vitamin B9 is not ideal, since long-term supplementation with reasonably large amounts of vitamin B9 can mask vitamin B12 deficiency. For men, this excess increases the risk of prostate cancer [313]. On the other hand, vitamin B9 deficiency may result in anemia, shortness of breath, heart palpitations, fatigue, changes in the color of the skin or hair, and open sores on the tongue. Therefore, timely management of vitamin B9 can potentially reduce NTDs and long-term excess or deficiency symptoms in adults and children. Since vitamin B9 contains is pterin group in its molecular structure (consisting of para-aminobenzoic acid (PABA), a pteridine attached to PABA amino end, and a carboxyl group in the α-amino group of glutamic acid), one can monitor the fluorescence emission of 6-carboxypterin to determine the concentration of vitamin B9 [314]. Even though monitoring pterin fluorescence is an indirect measurement, it allows for more cost-effective instrumentation aiming for lower limit of detection (LOD) requirements, given that vitamin B9 has a much lower quantum yield compared with pterins [315,316]. It is important to note that the molecular specificity of pterin detection, either by separating specific pterin types through analytical chemistry techniques or by ensuring fluorescence emission is captured from the particular pterin types, is essential to associate pterin concentrations with those of vitamin B9. This is because pterins participate in biochemical reactions of multiple biological processes, including generation of natural pigments, activation of the cell-mediated immune system, and others. Pterin excitation and emission occur at 350 nm and 450 nm, respectively. Biopterin fluorescence lifetimes are dependent on the phosphate concentration [317].

Vitamin B12 (also known as cobalamin) is an essential cofactor in methylation reactions metabolized in liver and liver extract [318], a cofactor in fatty acid and amino acid metabolism, as well as DNA synthesis. Symptoms of vitamin B12 deficiency include limb neuropathy, and pernicious anemia, which causes fatigue, headache, lightheadedness, breathlessness, pins and needles sensations, loss of appetite, muscle weakness, severe joint pain, changes in mobility, decreased level of consciousness, memory problems, brain fog, and many others.[319]. In infants, untreated vitamin B12 deficiency may lead to anemia and neurological damage and anemia. [320]. In developed countries, vitamin B12 deficiency is most commonly caused by impaired absorption due to loss of a glycoprotein (also known as the gastric intrinsic factor or GIF) which must be bound to vitamin B12 for absorption to occur. [321]. The second most common cause is the age-related or therapy-related decrease of acid production in stomach (achlorhydria), which is necessary to free the protein-bound vitamin [322]. Therapy-related decrease is associated with medicines for proton-pump inhibition, H2 blockage and other antacids. [323] Also, appropriate vitamin B12 intake is typically not provided by vegetarian and vegan diet, which may need to be followed by dietary supplementation. Monitoring vitamin B12 levels is essential to prevent long-term effects of its deficiency. Among fluorescent vitamins, vitamin B12 has the shortest excitation and emission wavelength maxima, i.e., 275 nm and 305 nm, respectively (Table 7.22, Appendix 11.1).

The endogenous fluorescence of other vitamins such as A (also known as retinol or β-carotene), C (ascorbic acid), D, K have been characterized (Table 7.22, Appendix 11.1) but less deeply investigated up to date. A quantitative antioxidant assay has been proposed by Ohara et. al. [324] based on a preliminary assessment of fluorescence-based detection of synthetized vitamin K and dilution in ethanol. Finally, vitamin A fluorescence is expected to be similar to those of carotenoids, which exhibit emission at ~538 nm upon 325 nm excitation [309].

Another main category of endogenous fluorophores is structural proteins. These proteins form a 3D molecular network known as extracellular matrix (ECM) in biological tissues and organs, and are responsible for cell morphology and behavior such as migration efficiency. The ECM provide biochemical and structural support to the surrounding cells, helping them to communicate with and attach to nearby cells, and influencing cell growth, movement, and others. Since ECM is involved in many biological processes, it is usually changed during pathological conditions such as those involving angiogenesis and neoplasia. These changes can be detected by label-free fluorescence spectroscopy and imaging measurements [309] of major ECM constituents, i.e., collagen and elastin (which have been discussed in section 7.3.1). Elastin and collagen fibrils are stabilized by covalent cross-links based on aldehyde formation [196]. Mature collagen cross-links

occur connective tissues after biochemical linkage induced by advanced glycation end products (AGE) [325,326] such as pentosidine (i.e., an AGE which forms cross-links between lysine and arginine residues of collagen). AGE accumulation is a result of extended exposure to monosaccharides leading to spontaneous nonenzymatic protein glycation (i.e., binding between a protein residue and a reducing sugar). AGEs endogenous fluorescence may change spectral characteristics of AGE induced collagen cross-linking. The tyrosine and dityrosine of collagen cause its blue fluorescence emission, whereas its yellow-green fluorescence has been attributed to pentosidine [301,327]. Normal collagen and elastin cross-links exhibit fluorescence from either hydroxylysyl pyridinoline (HP) or lysyl pyridinoline (LP) and have excitation maxima ~325 nm, and emission maxima ~400 nm (Table 7.22, Appendix 11.1). Fluorescence detection of pathological conditions is feasible because collagen cross-linking is:

- reduced in photodamaged skin, which decreases collagen synthesis and the collagen fluorescence lifetime *in vitro* [328]
- increased in diabetic corneas upon induction by AGEs (confirmed by increased pentosidine content) [329]
- increased aging of human skeletal muscle upon induction by AGEs [326]
- increased skin pepsin digestable collagen cross-links (340 nm excitation) upon aging and no difference on skin collagenase digestable collagen cross-links (360 nm excitation) on chronically aged and UVB exposed photoaged mice 34–38 week old [330]. Collagen was measured in the epidermal and dermal skin layers.
- increased skin collagen upon aging (monitored by wavelength-resolved fluorescence emission at 385 nm and 440 nm following 335 nm and 370 nm excitation, respectively), and no correlation with body weight, sex or type of vascular pathology on 26 human subjects between 42 to 78 years old [331].

Also, collagen content increases in breast tumors (detected with second harmonic generation; SHG) [332], whereas it decreases in skin melanoma [333]. It is worth noting that the elastin/collagen ratio determines the ECM functional properties and can be used to assess the quality of engineered replacement tissues in terms of expected mechanical properties close to native tissue [334]. To differentiate collagen and elastin fluorescence while still monitoring their cross-linking (e.g., in tissues/organs with different collagen/elastin ratios), one typically separates them by fluorescence lifetime, since they have similar excitation and emission wavelength-resolved characteristics (Table 7.22, Appendix 11.1).

Keratin is another fluorescent structural protein. Numerous skin diseases change the keratin expression (and hence keratin concentration) [335], which is associated with reduced migration of cancer and epithelial cells [336]. This change led keratin profiling to be used as a diagnostic, prognostic and risk stratification biomarker for epithelial-based tumors [337]. Changes in keratin post-translational modifications (i.e., adding chemical functional groups immediately after producing the keratin protein from translating genetic codons from mRNA to a sequence of aminoacids) can be related to regulation of cell growth, cell migration and regulation of cell architecture [336]. These modifications occur in different types of keratin separated by either type I (more acidic with isoelectric point (pI) between 4.5–6.0 and smaller protein size of 40–65 kDa) and type II (more basic/neutral with pI between 6.5–8.5 and larger protein size of between 50–70 kDa), or by their protein folding into predominantly α-helix or β-sheet structures [338]. Therefore, if diseases and/or tissue and organ function impairment involve changes in keratin chemical functional groups, protein folding or ratios between keratin types, alterations in tissue composition and/or molecular microenvironment may potentially change the fluorescence intensity, fluorescence lifetime or cause a spectral shift on fluorescence excitation or emission spectra. Skin epithelial cell plasticity is changed by the phosphorylation of keratins K4, K5 and K6 [339]. Cell growth in epithelial wound healing is stimulated by interaction between keratin K17 and 14-3-3 [336]. Glycosylation of the head domain (Ser30, Ser31,and Ser49) of keratin K18 prevents injury of epithelial cells [340]. Keratin phosphorylation processes which affect cell motility are believed to be associated with cancer cell migration and metastasis [341,342]. Depending on cell stimulus and cell type, Keratin K8 phosphorylation can inhibit or promote of cell migration, [343], decreasing the migration of oral squamous carcinoma cells but increasing that of pancreatic and gastric cells. Furthermore, time-resolved fluorescence spectroscopy (Chapter 8, section 8.1.4) can identify endogenous melanin and keratin to evaluate accumulation of intrahair dye, and to monitor intratissue diffusion of cosmetic and pharmaceutical formulations along hair shafts [344]. Also, Wu, Y. and Qu, J. Y [345]

described autofluorescence changes during keratinization of oral epithelial tissues, as well as esophageal and cervical tissues. In hair and skin, keratin has shown to exhibit fluorescent lifetime of 1.4 ns [344]

For each endogenous fluorophore, properties may vary due to the molecular bonds, states and microenvironment, which can be associated to diseases, organ function and viability, systematic or local metabolic changes, etc. Examples of that are the change of proportions and states of NADH and FAD components in cancer compared to normal tissues, which gives a meaning to redox ratio and/or wavelength-band shifts calculated from the NADH and FAD intensity of FS and TRFS measurements, bound/free ratios obtained from TRFS measurements, among other tissue parameters. A similar rationale can be applied collagen and elastin cross-links, predominance of certain aminoacids or aminoacids at proteins with specific structures (due to different protein folding), presence of excess/lack of lipopigments, vitamins, and vitamin precursors.

A more detailed description of the above can be found below and a review of fluorescent characteristics is shown in Tables 7.22 and 7.23 (Appendix 11.1 and Appendix 11.2, respectively).

Fluorescent probes administered externally to the tissue are known as exogenous fluorophores. These fluorophores are typically used to target specific molecules, cells and tissues (i.e., "labeling" them) to detect them with much higher sensitivity compared to conventional medical methods or those involving only sensing of endogenous fluorophores (label-free detection methods). Advantages of exogenous fluorophores include:

- Higher fluorescence intensity upon systemic/local distribution the fluorophore and before its excretion out of the body.
- More accurate location via intensity-based point or imaging measurements (microscopic and macroscopic).
- Can be combined with therapeutic drugs for photothermal, photodynamic, sonodynamic and other therapies as well as synergic treatments.
- Higher limit of detection compared to molecular-sensitive methods.
- Detection sensitivity is not limited by the tissue composition and biophotonics application: decreases the requirement of sophisticated equipment typically used to compensate for low sensitivity of biomolecules found at low concentrations. Sensitivity can be increased to the extent that background fluorescence does not hinder the detection of the targeted fluorophore, the fluorophore concentration is administered within FDA requirements, below cytotoxicity, and within the biological uptake limit of the fluorophore. It is important to note that enhanced sensitivity does not enable single molecule measurements in biological tissues and biofluids by using conventional methods.
- Potentially more molecular specificity.
- May be used to monitor treatment efficacy based on fluorophore photobleaching upon tissue/biofluid/sample illumination.

whereas limitations involve:

- More invasive compared to label-free detection methods (administration through injection or topical application)
- Pre-operative preparation may be required
- Large number of studies are required to establish an optimized protocol
- Any fluorophore parameter is based on its concentration and molecular specificity, which may vary from patient to patient due to fluorophore distribution, diffusion, microenvironment, and other factors.
- Detection, monitoring, guidance of procedures and other applications are limited by the time the drug is systemic/local distributed and reached the site of detection.
- Inhomogeneous distribution hinders the prediction of the tissue depth where signals are collected from.
- If photosensitizers are used the sensitive of the patient's organs to light may increase for some time after photodynamic therapy (PDT).
- Involves larger costs for ordering and disposing chemicals.
- Living cells cannot handle the reactive potential of a number of fluorophores (except by fluorescent proteins, fluorophores used for light-induced therapy, or histology and cytometry kits) by prolonged periods of time, limiting clinical diagnostics applications [280].
- Significantly change cell homeostasis and typically exhibit various major physiological alterations [280].
- Might lead to post-operative side effects (even though a tremendous effort has been made into designing non-invasive/minimally-invasive probes to justify it administration to patients).
- Clinical approval for medical procedures humans was obtained for only a limited number of exogenous fluorophores.

Exogenous fluorophores can be divided into (1) non-targeting probes, (2) molecular-targeting probes, (3) event-targeting / activable probes, (4) genetically-produced probes (i.e., fluorescent proteins), (5) theranostics probes (i.e.,

photosensitizers), (6) quantum dots, and (7) nanoparticles. Some examples of these fluorophores are included in Table 7.24.

Take home messages

- Chapter 7 provides a guide on the physical elements generating scattering, absorption, and luminescence. A list of these elements is shown in Appendices 3 to 11. If the amount of scatterers, their proportions, refractive indexes and particle sizes (shown in Tables 7.1 to 7.4, from Appendices 3 to 6) are known for biological media one would like to simulate, and these media can be considered approximately homogeneous, one could estimate the scattering of such media by using Mie theory (Chapter 4, section 4.5 Rayleigh and Mie scattering). The reduced scattering coefficient μ_s' could be estimated by taking into account the anisotropy factor g of the medium in question, since $\mu_s' = (1 - g) * \mu_s$. Similarly, one could calculate absorption and luminescence properties of a medium based on $\mu_a, \epsilon, \phi_{lum}\ and\ \tau_{Lum}$ of each chromophore or luminophore, and their proportions in the medium. Chromophore absorption, and fluorophore absorption, excitation and emission characteristics are listed in Tables 7.10 to 7.24 from Appendices 8 to 11. Main components of scattering, absorption, and fluorescence are used for modeling expected experimental measurements through forward Monte Carlo simulations of light propagation in tissues to build reflectance or fluorescence emission databases (Papers 3 and 4, and Chapters 14 and 15) and extracting tissue scattering properties, chromophore and fluorophore concentrations based on diffuse reflectance spectroscopy (DRS) and fluorescence spectroscopy (FS) measurements.
- If tissue constituents in terms of chromophores and scatterers are known by methods (e.g., invasive and time-consuming biochemical methods such as High-performance liquid chromatography; HPLC) other than optical methods, expected DRS signals can be simulated to check the feasibility of measuring the concentration of certain biomolecules and scattering properties non-invasively before building an optical instrument. Similarly, by knowing such biomolecular concentration and scattering properties, one could estimate signals to be obtained by biochemical methods. Also, biochemical methods may measure concentrations of different biomolecules compared with optical methods. Therefore, optical methods with the aim of structural and biochemical characterization of tissues (such as those of Papers 3 and 4) could complement biochemical methods.
- The variation between tissue structural and biochemical characteristics upon the development of diseases is still scarcely studied. Then, comparison of these characteristics between studies using similar experimental conditions including sample preparation (e.g., drying time, transport, storage), time between specimen devascularization and measurements, optical instrument parameters and data analysis is also scarce in the literature. Currently, one could guess what the expected tissue structural and biochemical variation would be only if experimental conditions are similar compared with previous studies. Increasing the number of measurements taken at each experimental conditions will enable building a database for future optical instrument design based on expected development of tissue responses for each disease, treatment progression, and other conditions [44,162,163,294,295,346–431].

7.5 References

[1] Jacques, S. L., “Optical properties of biological tissues: a review,” Phys. Med. Biol. **58**(11), R37 (2013).

[2] Tuchin, V. V., “Tissue optics and photonics: light-tissue interaction,” J. Biomed. Photonics \& Eng. **1**(2) (2015).

[3] Enejder, A. M. K., [Light scattering and absorption in tissue-models and measurements], Lund University (1997).

[4] Enderle, J., [Introduction to biomedical engineering], Academic press (2012).

[5] Costantini, I., Cicchi, R., Silvestri, L., Vanzi, F. and Pavone, F. S., “In-vivo and ex-vivo optical clearing methods for biological tissues,” Biomed. Opt. Express **10**(10), 5251–5267 (2019).

[6] Kohl, M., Essenpreis, M. and Cope, M., “The influence of glucose concentration upon the transport of light in tissue-simulating phantoms,” Phys. Med. \& Biol. **40**(7), 1267 (1995).

[7] Kohl, M., Cope, M., Essenpreis, M. and Böcker, D., “Influence of glucose concentration on light scattering in tissue-simulating phantoms,” Opt. Lett. **19**(24), 2170–2172 (1994).

[8] Qu, J. Y. and Wilson, B. C., “Monte Carlo modeling studies of the effect of physiological factors andother analytes on the determination of glucose concentration in vivoby near infrared optical absorption and scattering measurements,” J. Biomed. Opt. **2**(3), 319–325 (1997).

[9] Beuthan, J., Minet, O., Helfmann, J., Herrig, M. and Müller, G., “The spatial variation of the refractive index in biological cells,” Phys. Med. \& Biol. **41**(3), 369 (1996).

[10] Zhou, Q. and Knighton, R. W., “Light scattering and form birefringence of parallel cylindrical arrays that represent cellular organelles of the retinal nerve fiber layer,” Appl. Opt. **36**(10), 2273–2285 (1997).

[11] Lin, J. C. and Guy, A. W., “A note on the optical scattering characteristics of whole blood,” IEEE Trans. Biomed. Eng.(1), 43–45 (1974).

[12] Meyer, R. A., “Light scattering from red blood cell ghosts: sensitivity of angular dependent structure to membrane thickness and refractive index,” Appl. Opt. **16**(8), 2036–2038 (1977).

[13] Turzhitsky, V., Qiu, L., Itzkan, I., Novikov, A. A., Kotelev, M. S., Getmanskiy, M., Vinokurov, V. A., Muradov, A. V and Perelman, L. T., “Spectroscopy of scattered light for the characterization of micro and nanoscale objects in biology and medicine,” Appl. Spectrosc. **68**(2), 133–154 (2014).

[14] Wang, X., Milner, T. E., Chang, M. C. and Nelson, J. S., “Group refractive index measurement of dry and hydrated type I collagen films using optical low-coherence reflectometry,” J. Biomed. Opt. **1**(2), 212–216 (1996).

[15] Young, K. W., Radic, S., Myslivets, E., O’Connor, S. M. and Lieber, R. L., “Resonant reflection spectroscopy of biomolecular arrays in muscle,” Biophys. J. **107**(10), 2352–2360 (2014).

[16] Tiffany, J. M., “Refractive index of meibomian and other lipids,” Curr. Eye Res. **5**(11), 887–889 (1986).

[17] Beauvoit, B., Evans, S. M., Jenkins, T. W., Miller, E. E. and Chance, B., “Correlation between the light scattering and the mitochondrial content of normal tissues and transplantable rodent tumors,” Anal. Biochem. **226**(1), 167–174 (1995).

[18] Daley, M. L., Watzke, R. C. and Riddle, M. C., “A model for the apparent decrease in optical transmittance of the diabetic eye,” IEEE Trans. Biomed. Eng. **39**(1), 88–94 (1992).

[19] Beauvoit, B., Kitai, T. and Chance, B., “Contribution of the mitochondrial compartment to the optical properties of the rat liver: a theoretical and practical approach,” Biophys. J. **67**(6), 2501–2510 (1994).

[20] Perelman, L. T., Backman, V., Wallace, M., Zonios, G., Manoharan, R., Nusrat, A., Shields, S., Seiler, M., Lima, C., Hamano, T. and others., “Observation of periodic fine structure in reflectance from biological tissue: a new technique for measuring nuclear size distribution,” Phys. Rev. Lett. **80**(3), 627 (1998).

[21] Yanina, I. Y., Lazareva, E. N. and Tuchin, V. V., "Refractive index of adipose tissue and lipid droplet measured in wide spectral and temperature ranges," Appl. Opt. **57**(17), 4839–4848 (2018).

[22] Berg, R. O., "Laser-based cancer diagnostics and therapy: Tissue optics considerations." (1997).

[23] Nilsson, A. M. K., Sturesson, C., Liu, D. L. and Andersson-Engels, S., "Changes in spectral shape of tissue optical properties in conjunction with laser-induced thermotherapy," Appl. Opt. **37**(7), 1256–1267 (1998).

[24] Saidi, I. S., Jacques, S. L. and Tittel, F. K., "Mie and Rayleigh modeling of visible-light scattering in neonatal skin," Appl. Opt. **34**(31), 7410–7418 (1995).

[25] Dunn, A. K., Smithpeter, C. L., Welch, A. J. and Richards-Kortum, R. R., "Finite-difference time-domain simulation of light scattering from single cells," J. Biomed. Opt. **2**(3), 262–266 (1997).

[26] Sloot, P. M. A., Hoekstra, A. G. and Figdor, C. G., "Osmotic response of lymphocytes measured by means of forward light scattering: theoretical considerations," Cytom. J. Int. Soc. Anal. Cytol. **9**(6), 636–641 (1988).

[27] Nilsson, A. M. K., Alsholm, P., Karlsson, A. and Andersson-Engels, S., "T-matrix computations of light scattering by red blood cells," Appl. Opt. **37**(13), 2735–2748 (1998).

[28] Tantipolphan, R., Rades, T. and Medlicott, N. J., "Insights into the structure of protein by vibrational spectroscopy," Curr. Pharm. Anal. **4**(2), 53–68 (2008).

[29] Liu, W., Sun, Z., Chen, J. and Jing, C., "Raman spectroscopy in colorectal cancer diagnostics: Comparison of PCA-LDA and PLS-DA models," J. Spectrosc. **2016** (2016).

[30] Jones, R. R., Hooper, D. C., Zhang, L., Wolverson, D. and Valev, V. K., "Raman techniques: fundamentals and frontiers," Nanoscale Res. Lett. **14**(1), 1–34 (2019).

[31] Derruau, S., Robinet, J., Untereiner, V., Piot, O., Sockalingum, G. D. and Lorimier, S., "Vibrational spectroscopy saliva profiling as biometric tool for disease diagnostics: A systematic literature review," Molecules **25**(18), 4142 (2020).

[32] Tian, F., Bonnier, F., Casey, A., Shanahan, A. E. and Byrne, H. J., "Surface enhanced Raman scattering with gold nanoparticles: Effect of particle shape," Anal. Methods **6**(22), 9116–9123 (2014).

[33] Butler, H. J., Fogarty, S. W., Kerns, J. G., Martin-Hirsch, P. L., Fullwood, N. J. and Martin, F. L., "Gold nanoparticles as a substrate in bio-analytical near-infrared surface-enhanced Raman spectroscopy," Analyst **140**(9), 3090–3097 (2015).

[34] Gebauer, J. S., Malissek, M., Simon, S., Knauer, S. K., Maskos, M., Stauber, R. H., Peukert, W. and Treuel, L., "Impact of the nanoparticle--protein corona on colloidal stability and protein structure," Langmuir **28**(25), 9673–9679 (2012).

[35] Bonifacio, A., Dalla Marta, S., Spizzo, R., Cervo, S., Steffan, A., Colombatti, A. and Sergo, V., "Surface-enhanced Raman spectroscopy of blood plasma and serum using Ag and Au nanoparticles: A systematic study," Anal. Bioanal. Chem. **406**(9–10), 2355–2365 (2014).

[36] Seo, J.-H., Park, H. S., Yoo, Y., Seong, T.-Y., Li, J., Ahn, J.-P., Kim, B. and Choi, I.-S., "Origin of size dependency in coherent-twin-propagation-mediated tensile deformation of noble metal nanowires," Nano Lett. **13**(11), 5112–5116 (2013).

[37] Bonifacio, A., Cervo, S. and Sergo, V., "Label-free surface-enhanced Raman spectroscopy of biofluids: Fundamental aspects and diagnostic applications," Anal. Bioanal. Chem. **407**(27), 8265–8277 (2015).

[38] Rodr\'\iguez-Fernández, J., Pastoriza-Santos, I., Perez-Juste, J., de Abajo, F. J. and Liz-Marzán, L. M., "The effect of silica coating on the optical response of sub-micrometer gold spheres," J. Phys. Chem. C **111**(36), 13361–13366 (2007).

[39] Wei, A., Kim, B., Sadtler, B. and Tripp, S. L., “Tunable surface-enhanced Raman scattering from large gold nanoparticle arrays,” ChemPhysChem **2**(12), 743–745 (2001).

[40] Barbosa, S., Agrawal, A., Rodr\’\iguez-Lorenzo, L., Pastoriza-Santos, I., Alvarez-Puebla, R. A., Kornowski, A., Weller, H. and Liz-Marzán, L. M., “Tuning size and sensing properties in colloidal gold nanostars,” Langmuir **26**(18), 14943–14950 (2010).

[41] Amendola, V., Pilot, R., Frasconi, M., Maragò, O. M. and Iat\`\i, M. A., “Surface plasmon resonance in gold nanoparticles: a review,” J. Phys. Condens. Matter **29**(20), 203002 (2017).

[42] Hackshaw, K. V, Miller, J. S., Aykas, D. P. and Rodriguez-Saona, L., “Vibrational spectroscopy for identification of metabolites in biologic samples,” Molecules **25**(20), 4725 (2020).

[43] Naseer, K., Ali, S. and Qazi, J., “ATR-FTIR spectroscopy as the future of diagnostics: a systematic review of the approach using bio-fluids,” Appl. Spectrosc. Rev. **56**(2), 85–97 (2021).

[44] Leal, L. B., Nogueira, M. S., Canevari, R. A. and Carvalho, L., “Vibration spectroscopy and body biofluids: Literature review for clinical applications,” Photodiagnosis Photodyn. Ther. (2018).

[45] Jaychandran, S., Meenapriya, P. K. and Ganesan, S., “Raman spectroscopic analysis of blood, urine, saliva and tissue of oral potentially malignant disorders and malignancy-A diagnostic study,” Int. J. Oral Craniofacial Sci. **2**(1), 11–14 (2016).

[46] Johnson, K. P., “Cerebrospinal fluid and blood assays of diagnostic usefulness in multiple sclerosis,” Neurology **30**(7 Part 2), 106–109 (1980).

[47] Alamdari, D. H., Ghayour-Mobarhan, M., Tavallaie, S., Parizadeh, M. R., Moohebati, M., Ghafoori, F., Kazemi-Bajestani, S. M. R., Paletas, K., Pegiou, T. and Koliakos, G., “Prooxidant--antioxidant balance as a new risk factor in patients with angiographically defined coronary artery disease,” Clin. Biochem. **41**(6), 375–380 (2008).

[48] Mantsch, H. H., “The road to medical vibrational spectroscopy--a history,” Analyst **138**(14), 3863–3870 (2013).

[49] Bonifacio, A., Cervo, S. and Sergo, V., “Label-free surface-enhanced Raman spectroscopy of biofluids: fundamental aspects and diagnostic applications,” Anal. Bioanal. Chem. **407**(27), 8265–8277 (2015).

[50] Depciuch, J. and Parlinska-Wojtan, M., “Comparing dried and liquid blood serum samples of depressed patients: An analysis by Raman and infrared spectroscopy methods,” J. Pharm. Biomed. Anal. **150**, 80–86 (2018).

[51] Hrubešová, K., Fousková, M., Habartová, L., Fišar, Z., Jirák, R., Raboch, J. and SETNIČKA, V., “Search for biomarkers of Alzheimer‘s disease: Recent insights, current challenges and future prospects,” Clin. Biochem. **72**, 39–51 (2019).

[52] Connolly, J. M., Davies, K., Kazakeviciute, A., Wheatley, A. M., Dockery, P., Keogh, I. and Olivo, M., “Non-invasive and label-free detection of oral squamous cell carcinoma using saliva surface-enhanced Raman spectroscopy and multivariate analysis,” Nanomedicine Nanotechnology, Biol. Med. **12**(6), 1593–1601 (2016).

[53] Di Terlizzi, R. and Platt, S., “The function, composition and analysis of cerebrospinal fluid in companion animals: Part I--Function and composition,” Vet. J. **172**(3), 422–431 (2006).

[54] Sakka, L., Coll, G. and Chazal, J., “Anatomy and physiology of cerebrospinal fluid,” Eur. Ann. Otorhinolaryngol. Head Neck Dis. **128**(6), 309–316 (2011).

[55] Harrington, M. G., Salomon, R. M., Pogoda, J. M., Oborina, E., Okey, N., Johnson, B., Schmidt, D., Fonteh, A. N. and Dalleska, N. F., “Cerebrospinal fluid sodium rhythms,” Cerebrospinal Fluid Res. **7**(1), 1–9 (2010).

[56] Conly, J. M. and Ronald, A. R., “Cerebrospinal fluid as a diagnostic body fluid,” Am. J. Med. **75**(1), 102–108 (1983).

[57] Teunissen, C. E., Petzold, A., Bennett, J. L., Berven, F. S., Brundin, L., Comabella, M., Franciotta, D., Frederiksen, J. L., Fleming, J. O., Furlan, R. and others., “A consensus protocol for the standardization of cerebrospinal fluid

collection and biobanking," Neurology **73**(22), 1914–1922 (2009).

[58] Sathyavathi, R., Dingari, N. C., Barman, I., Prasad, P. S. R., Prabhakar, S., Narayana Rao, D., Dasari, R. R. and Undamatla, J., "Raman spectroscopy provides a powerful, rapid diagnostic tool for the detection of tuberculous meningitis in ex vivo cerebrospinal fluid samples," J. Biophotonics **6**(8), 567–572 (2013).

[59] Kamińska, A., Witkowska, E., Kowalska, A., Skoczyńska, A., Gawryszewska, I., Guziewicz, E., Snigurenko, D. and Waluk, J., "Highly efficient SERS-based detection of cerebrospinal fluid neopterin as a diagnostic marker of bacterial infection," Anal. Bioanal. Chem. **408**(16), 4319–4327 (2016).

[60] Rose, C., Parker, A., Jefferson, B. and Cartmell, E., "The characterization of feces and urine: a review of the literature to inform advanced treatment technology," Crit. Rev. Environ. Sci. Technol. **45**(17), 1827–1879 (2015).

[61] Jakobs, B. S., Volmer, M., Swinkels, D. W., Hofs, M. T. W., Donkervoort, S., Joosting, M. M. J., Wolthers, B. G., De Peinder, P. and Voorbij, H. A. M., "New method for faecal fat determination by mid-infrared spectroscopy, using a transmission cell: an improvement in standardization," Ann. Clin. Biochem. **37**(3), 343–349 (2000).

[62] Koya, S. K., Yurgelevic, S., Brusatori, M., Huang, C., Diebel, L. N. and Auner, G. W., "Rapid detection of Clostridium difficile toxins in stool by Raman spectroscopy," J. Surg. Res. **244**, 111–116 (2019).

[63] Nirea, K. G., de Nanclares, M., Skugor, A., Afseth, N. K., Meuwissen, T. H. E., Hansen Jon Øand Mydland, L. T. and Øverland, M., "Assessment of fecal near-infrared spectroscopy to predict feces chemical composition and apparent total-tract digestibility of nutrients in pigs," J. Anim. Sci. **96**(7), 2826–2837 (2018).

[64] Kaczor-Urbanowicz, K. E., Martin Carreras-Presas, C., Aro, K., Tu, M., Garcia-Godoy, F. and Wong, D. T. W., "Saliva diagnostics--Current views and directions," Exp. Biol. Med. **242**(5), 459–472 (2017).

[65] Schafer, C. A., Schafer, J. J., Yakob, M., Lima, P., Camargo, P. and Wong, D. T. W., "Saliva diagnostics: utilizing oral fluids to determine health status," Saliva Secret. Funct. **24**, 88–98 (2014).

[66] Derruau, S., Gobinet, C., Mateu, A., Untereiner, V., Lorimier, S. and Piot, O., "Shedding light on confounding factors likely to affect salivary infrared biosignatures," Anal. Bioanal. Chem. **411**(11), 2283–2290 (2019).

[67] Balan, V., Mihai, C.-T., Cojocaru, F.-D., Uritu, C.-M., Dodi, G., Botezat, D. and Gardikiotis, I., "Vibrational spectroscopy fingerprinting in medicine: from molecular to clinical practice," Materials (Basel). **12**(18), 2884 (2019).

[68] Nunes, L. A. S., Brenzikofer, R. and Macedo, D. V., "Reference intervals for saliva analytes collected by a standardized method in a physically active population," Clin. Biochem. **44**(17–18), 1440–1444 (2011).

[69] Marinho, C. C., da Silva Campos, M. J., Silveira, C., Ferreira, A. P. and Vitral, R. W. F., "Avaliação da influência do dispositivo de coleta de saliva na análise de imunoglobulina A secretora e alfa-amilase," Rev. Interdiscip. Estud. Exp. e Humanos Interdiscip. J. Exp. Stud. **2**(4) (2010).

[70] da Costa, F. R. H., de Moura, S. A. B., de Medeiros, A. M. C., de MORAES, P. H. and de Oliveira Filho, S. A., "Valor diagnóstico da saliva em doenças orais e sistêmicas: uma revisão de literatura," Pesqui. Bras. em Odontopediatria e Cl{\'\i}nica Integr. **7**(2), 187–194 (2007).

[71] Wang, A., Wang, C. P., Tu, M. and Wong, D. T. W., "Oral biofluid biomarker research: current status and emerging frontiers," Diagnostics **6**(4), 45 (2016).

[72] Streckfus, C. F., [Advances in salivary diagnostics], Springer (2015).

[73] Gomar-Vercher, S., Simón-Soro, A., Montiel-Company, J. M., Almerich-Silla, J. M. and Mira, A., "Stimulated and unstimulated saliva samples have significantly different bacterial profiles," PLoS One **13**(6), e0198021 (2018).

[74] Greabu, M., Battino, M., Mohora, M., Totan, A., Didilescu, A., Spinu, T., Totan, C., Miricescu, D. and Radulescu, R., "Saliva--a diagnostic window to the body, both in health and in disease.," J. Med. Life **2**(2), 124–132 (2009).

[75] Khaustova, S. A., Shkurnikov, M. U., Grebenyuk, E. S., Artyushenko, V. G. and Tonevitsky, A. G., "Assessment of biochemical characteristics of the saliva using Fourier transform mid-infrared spectroscopy," Bull. Exp. Biol. Med. **148**(5), 841–844 (2009).

[76] Azzi, L., Carcano, G., Gianfagna, F., Grossi, P., Dalla Gasperina, D., Genoni, A., Fasano, M., Sessa, F., Tettamanti, L., Carinci, F. and others., "Saliva is a reliable tool to detect SARS-CoV-2," J. Infect. **81**(1), e45--e50 (2020).

[77] Harvey, C., "Relation between the volume and fructose content of human semen," Nature **162**(4125), 812–813 (1948).

[78] Canale, D., Bartelloni, M., Negroni, A., Meschini, P., Izzo, P. L., Bianchi, B. and Menchini-Fabris, G. F., "Zinc in human semen," Int. J. Androl. **9**(6), 477–480 (1986).

[79] Wood, B. R., Quinn, M. A., Tait, B., Ashdown, M., Hislop, T., Romeo, M. and McNaughton, D., "FTIR microspectroscopic study of cell types and potential confounding variables in screening for cervical malignancies," Biospectroscopy **4**(2), 75–91 (1998).

[80] Virkler, K. and Lednev, I. K., "Raman spectroscopic signature of semen and its potential application to forensic body fluid identification," Forensic Sci. Int. **193**(1–3), 56–62 (2009).

[81] Drabovich, A. P., Saraon, P., Jarvi, K. and Diamandis, E. P., "Seminal plasma as a diagnostic fluid for male reproductive system disorders," Nat. Rev. Urol. **11**(5), 278–288 (2014).

[82] Kline, E. E., Treat, E. G., Averna, T. A., Davis, M. S., Smith, A. Y. and Sillerud, L. O., "Citrate concentrations in human seminal fluid and expressed prostatic fluid determined via 1H nuclear magnetic resonance spectroscopy outperform prostate specific antigen in prostate cancer detection," J. Urol. **176**(5), 2274–2279 (2006).

[83] Mobley, D. F., "Semen cultures in the diagnosis of bacterial prostatitis," J. Urol. **114**(1), 83–85 (1975).

[84] Curry, M. R., Millar, J. D., Tamuli, S. M. and Watson, P. F., "Surface area and volume measurements for ram and human spermatozoa," Biol. Reprod. **55**(6), 1325–1332 (1996).

[85] Kleinhans, F. W., Travis, V. S., Du, J., Villines, P. M., Colvin, K. E. and Critser, J. K., "Measurement of human sperm intracellular water volume by electron spin resonance," J. Androl. **13**(6), 498–506 (1992).

[86] Virkler, K. and Lednev, I. K., "Raman spectroscopy offers great potential for the nondestructive confirmatory identification of body fluids," Forensic Sci. Int. **181**(1–3), e1--e5 (2008).

[87] Agarwal, A., Majzoub, A., Esteves, S. C., Ko, E., Ramasamy, R. and Zini, A., "Clinical utility of sperm DNA fragmentation testing: practice recommendations based on clinical scenarios," Transl. Androl. Urol. **5**(6), 935 (2016).

[88] Emrich, H. M. and Oelert, H., "pH value and total ammonia in human sweat," Pflugers Arch. Gesamte Physiol. Menschen Tiere **290**(4), 311–314 (1966).

[89] Peter, G., Schröpl, F., Feisel, H. G. and Thürauf, W., "Gaschromatographic investigations of free and esterified fatty acids in human eccrine sweat," Arch. Klin. Exp. Dermatol. **238**(2), 154–159 (1970).

[90] Takemura, T., Wertz, P. W. and Sato, K., "Free fatty acids and sterols in human eccrine sweat," Br. J. Dermatol. **120**(1), 43–47 (1989).

[91] Zeng, X.-N., Leyden, J. J., Lawley, H. J., Sawano, K., Nohara, I. and Preti, G., "Analysis of characteristic odors from human male axillae," J. Chem. Ecol. **17**(7), 1469–1492 (1991).

[92] Bernier, U. R., Booth, M. M. and Yost, R. A., "Analysis of human skin emanations by gas chromatography/mass spectrometry. 1. Thermal desorption of attractants for the yellow fever mosquito (Aedes a egypti) from handled glass beads," Anal. Chem. **71**(1), 1–7 (1999).

[93] Haze, S., Gozu, Y., Nakamura, S., Kohno, Y., Sawano, K., Ohta, H. and Yamazaki, K., "2-Nonenal newly found in human body odor tends to increase with aging," J. Invest. Dermatol. **116**(4), 520–524 (2001).

[94] Huang, C.-T., Chen, M.-L., Huang, L.-L. and Mao, I.-F., "Uric acid and urea in human sweat," Chin. J. Physiol. **45**(3), 109–116 (2002).

[95] Curran, A. M., Rabin, S. I., Prada, P. A. and Furton, K. G., "Comparison of the volatile organic compounds present in human odor using SPME-GC/MS," J. Chem. Ecol. **31**(7), 1607–1619 (2005).

[96] Zernecke, R., Kleemann, A. M., Haegler, K., Albrecht, J., Vollmer, B., Linn, J., Brückmann, H. and Wiesmann, M., "Chemosensory properties of human sweat," Chem. Senses **35**(2), 101–108 (2010).

[97] Draelos, Z. D., "Prevention of cosmetic problems," [Preventive Dermatology], Springer, 173–186 (2011).

[98] Schneider, R. A. and Schmidt, C. E., "Dependency of olfactory localization on non-olfactory cues," Physiol. \& Behav. **2**(3), 305–309 (1967).

[99] Doty, R. L., Brugger, W. E., Jurs, P. C., Orndorff, M. A., Snyder, P. J. and Lowry, L. D., "Intranasal trigeminal stimulation from odorous volatiles: psychometric responses from anosmic and normal humans," Physiol. \& Behav. **20**(2), 175–185 (1978).

[100] Doty, R. L., "Intranasal trigeminal detection of chemical vapors by humans," Physiol. \& Behav. **14**(6), 855–859 (1975).

[101] Thody, A. J. and Shuster, S., "Control and function of sebaceous glands," Physiol. Rev. **69**(2), 383–416 (1989).

[102] Cheng, J. B. and Russell, D. W., "Mammalian wax biosynthesis: II. Expression cloning of wax synthase cDNAs encoding a member of the acyltransferase enzyme family," J. Biol. Chem. **279**(36), 37798–37807 (2004).

[103] Sato, K., Kang, W., Saga, K. and Sato, T., "Biology of the eccrine sweat gland. I. Mechanism of sweat secretion," J Am Acad Dermatol **20**, 537–563 (1989).

[104] Sato, K., Kang, W. H., Saga, K. and Sato, K. T., "Biology of sweat glands and their disorders. I. Normal sweat gland function," J. Am. Acad. Dermatol. **20**(4), 537–563 (1989).

[105] Sato, K., Kang, W. H., Saga, K. and Sato, K. T., "Biology of sweat glands and their disorders. II. Disorders of sweat gland function," J. Am. Acad. Dermatol. **20**(5), 713–726 (1989).

[106] Jadoon, S., Karim, S., Akram, M. R., Kalsoom Khan, A., Zia, M. A., Siddiqi, A. R. and Murtaza, G., "Recent developments in sweat analysis and its applications," Int. J. Anal. Chem. **2015** (2015).

[107] Blanco-Formoso, M. and Alvarez-Puebla, R. A., "Cancer diagnosis through SERS and other related techniques," Int. J. Mol. Sci. **21**(6), 2253 (2020).

[108] Gonçalves, A. C., Marson, F. A. L., Mendonça, R. M. H., Bertuzzo, C. S., Paschoal, I. A., Ribeiro, J. D., Ribeiro, A. F. and Levy, C. E., "Chloride and sodium ion concentrations in saliva and sweat as a method to diagnose cystic fibrosis," J. Pediatr. (Rio. J). **95**, 443–450 (2019).

[109] Sikirzhytski, V., Sikirzhytskaya, A. and Lednev, I. K., "Multidimensional Raman spectroscopic signature of sweat and its potential application to forensic body fluid identification," Anal. Chim. Acta **718**, 78–83 (2012).

[110] Song, W., Mao, Z., Liu, X., Lu, Y., Li, Z., Zhao, B. and Lu, L., "Detection of protein deposition within latent fingerprints by surface-enhanced Raman spectroscopy imaging," Nanoscale **4**(7), 2333–2338 (2012).

[111] Raiszadeh, M. M., Ross, M. M., Russo, P. S., Schaepper, M. A., Zhou, W., Deng, J., Ng, D., Dickson, A., Dickson, C., Strom, M. and others., "Proteomic analysis of eccrine sweat: implications for the discovery of schizophrenia biomarker proteins," J. Proteome Res. **11**(4), 2127–2139 (2012).

[112] Marks, H., Schechinger, M., Garza, J., Locke, A. and Coté, G., "Surface enhanced Raman spectroscopy (SERS) for in

vitro diagnostic testing at the point of care," Nanophotonics **6**(4), 681–701 (2017).

[113] Tong, L., Zhou, X. Y., Jylha, A., Aapola, U., Liu, D. N., Koh, S. K., Tian, D., Quah, J., Uusitalo, H., Beuerman, R. W. and others., "Quantitation of 47 human tear proteins using high resolution multiple reaction monitoring (HR-MRM) based-mass spectrometry," J. Proteomics **115**, 36–48 (2015).

[114] Posa, A., Bräuer, L., Schicht, M., Garreis, F., Beileke, S. and Paulsen, F., "Schirmer strip vs. capillary tube method: non-invasive methods of obtaining proteins from tear fluid," Ann. Anatomy-Anatomischer Anzeiger **195**(2), 137–142 (2013).

[115] Sharma, S., Chophi, R. and Singh, R., "Forensic discrimination of menstrual blood and peripheral blood using attenuated total reflectance (ATR)-Fourier transform infrared (FT-IR) spectroscopy and chemometrics," Int. J. Legal Med. **134**(1), 63–77 (2020).

[116] Travo, A., Paya, C., Déléris, G., Colin, J., Mortemousque, B. and Forfar, I., "Potential of FTIR spectroscopy for analysis of tears for diagnosis purposes," Anal. Bioanal. Chem. **406**(9), 2367–2376 (2014).

[117] Borchman, D., Foulks, G. N., Yappert, M. C., Tang, D. and Ho, D. V., "Spectroscopic evaluation of human tear lipids," Chem. Phys. Lipids **147**(2), 87–102 (2007).

[118] Elkins, K. M., "Rapid presumptive 'fingerprinting' of body fluids and materials by ATR FT-IR spectroscopy," J. Forensic Sci. **56**(6), 1580–1587 (2011).

[119] Filik, J. and Stone, N., "Analysis of human tear fluid by Raman spectroscopy," Anal. Chim. Acta **616**(2), 177–184 (2008).

[120] Li, S., Sack, R., Vijmasi, T., Sathe, S., Beaton, A., Quigley, D., Gallup, M. and Mcnamara, N. A., "Antibody protein array analysis of the tear film cytokines," Optom. Vis. Sci. **85**(8), E653--E660 (2008).

[121] Choi, S., Moon, S. W., Shin, J.-H., Park, H.-K. and Jin, K.-H., "Label-free biochemical analytic method for the early detection of adenoviral conjunctivitis using human tear biofluids," Anal. Chem. **86**(22), 11093–11099 (2014).

[122] Filik, J. and Stone, N., "Investigation into the protein composition of human tear fluid using centrifugal filters and drop coating deposition Raman spectroscopy," J. Raman Spectrosc. An Int. J. Orig. Work all Asp. Raman Spectrosc. Incl. High. Order Process. also Brillouin Rayleigh Scatt. **40**(2), 218–224 (2009).

[123] Nagase, Y., Yoshida, S. and Kamiyama, K., "Analysis of human tear fluid by Fourier transform infrared spectroscopy," Biopolym. Orig. Res. Biomol. **79**(1), 18–27 (2005).

[124] Sodré, F. L., Costa, J. C. B. and Lima, J. C. C., "Avaliação da função e da lesão renal: um desafio laboratorial," J. Bras. Patol. e Med. Lab. **43**, 329–337 (2007).

[125] Sarigul, N., Korkmaz, F. and Kurultak, \.Ilhan., "A new artificial urine protocol to better imitate human urine," Sci. Rep. **9**(1), 1–11 (2019).

[126] Putnam, D. F., "Composition and concentrative properties of human urine" (1971).

[127] Peixoto, E. F. and da Costa Lamounier, T. A., "Métodos laboratoriais para a identificação da insuficiência renal crônica," Acta ciências e saúde **1**(1), 1–15 (2016).

[128] Pookaiyaudom, P., Seelanan, P., Lidgey, F. J., Hayatleh, K. and Toumazou, C., "Measurement of urea, creatinine and urea to creatinine ratio using enzyme based chemical current conveyor (CCCII+)," Sensors Actuators B Chem. **153**(2), 453–459 (2011).

[129] Jing, J. and Gao, Y., "Urine biomarkers in the early stages of diseases: current status and perspective.," Discov. Med. **25**(136), 57–65 (2018).

[130] Jia, L., Li, X., Shao, C., Wei, L., Li, M., Guo, Z., Liu, Z. and Gao, Y., "Using an isolated rat kidney model to identify

kidney origin proteins in urine," PLoS One **8**(6), e66911 (2013).

[131] Alqaraleh, M., Kasabri, V., Farha, R. A., Naffa, R. G., Yousef, I. and Aljaafreh, A., "Branched amino acids as potential biomarkers in metabolic syndrome patients and as hypolipidemic compounds," EurAsian J. Biosci. **13**(2), 2233–2241 (2019).

[132] Leordean, C., Canpean, V. and Astilean, S., "Surface-enhanced Raman scattering (SERS) analysis of urea trace in urine, fingerprint, and tear samples," Spectrosc. Lett. **45**(8), 550–555 (2012).

[133] Sikirzhytskaya, A., Sikirzhytski, V. and Lednev, I. K., "Raman spectroscopic signature of vaginal fluid and its potential application in forensic body fluid identification," Forensic Sci. Int. **216**(1–3), 44–48 (2012).

[134] Preti, G., Huggins, G. R. and Silverberg, G. D., "Alterations in the organic compounds of vaginal secretions caused by sexual arousal," Fertil. Steril. **32**(1), 47–54 (1979).

[135] Stamey, T. A. and Timothy, M. M., "Studies of introital colonization in women with recurrent urinary infections. I. The role of vaginal pH," J. Urol. **114**(2), 261–263 (1975).

[136] Levin, R. J. and Wagner, G., "Human vaginal fluid-ionic composition and modification by sexual arousal [proceedings].," J. Physiol. **266**(1), 62P--63P (1977).

[137] Abdallah, M. A. and de Vargas-Linares, R., "Polyacrylamide gel electrophoresis of normal human vaginal fluid," Acta Physiol. Lat. Am. **20**(4), 445–446 (1971).

[138] Raffi, R. O., Moghissi, K. S. and Sacco, A. G., "Proteins of human vaginal fluid," Fertil. Steril. **28**(12), 1345–1348 (1977).

[139] Huggins, G. R. and Preti, G., "Volatile constituents of human vaginal secretions," Am. J. Obstet. Gynecol. **126**(1), 129–136 (1976).

[140] Oberst, F. W. and Plass, E. D., "The hydrogen ion concentration of human vaginal discharge," Am. J. Obstet. Gynecol. **32**(1), 22–35 (1936).

[141] Wagner, G. and Levin, R. J., "Vaginal fluid," Hum. vagina **2**, 121–137 (1978).

[142] Lapan, B. and Friedman, M. M., "Glycogen and reducing substances in vaginal mucus: Gestational and cyclical variations," Am. J. Obstet. Gynecol. **59**(4), 921–923 (1950).

[143] Rakoff, A. E., Feo, L. G. and Goldstein, L., "The biologic characteristics of the normal vagina," Am. J. Obstet. Gynecol. **47**(4), 467–494 (1944).

[144] Owen, D. H. and Katz, D. F., "A vaginal fluid simulant," Contraception **59**(2), 91–95 (1999).

[145] Thinkhamrop, J., Lumbiganon, P., Thongkrajai, P., Chongsomchai, C. and Pakarasang, M., "Vaginal fluid pH as a screening test for vaginitis," Int. J. Gynecol. \& Obstet. **66**(2), 143–148 (1999).

[146] Powell, A. M. and Nyirjesy, P., "New perspectives on the normal vagina and noninfectious causes of discharge," Clin. Obstet. Gynecol. **58**(3), 453–463 (2015).

[147] Grande, G., Vincenzoni, F., Milardi, D., Pompa, G., Ricciardi, D., Fruscella, E., Mancini, F., Pontecorvi, A., Castagnola, M. and Marana, R., "Cervical mucus proteome in endometriosis," Clin. Proteomics **14**(1), 1–11 (2017).

[148] Mardanian, F. and Sheikh-Soleimani, Z., "The diagnostic role of cervico-vaginal fluid interleukins-1$α$ in endometriosis: A case-control study," J. Res. Med. Sci. Off. J. Isfahan Univ. Med. Sci. **19**(12), 1145 (2014).

[149] Gregório, I., Zapata, F. and Garc\'\ia-Ruiz, C., "Analysis of human bodily fluids on superabsorbent pads by ATR-FTIR," Talanta **162**, 634–640 (2017).

[150] Sheet, C. D. C. F., "Genital HPV" (2007).

[151] de la O-Cuevas, E., Badillo-Ram\'\irez, I., Islas, S. R., Araujo-Andrade, C. and Saniger, J. M., "Sensitive Raman detection of human recombinant interleukin-6 mediated by DCDR/GERS hybrid platforms," RSC Adv. **9**(22), 12269–12275 (2019).

[152] Meng, F. and Alayash, A. I., "Determination of extinction coefficients of human hemoglobin in various redox states," Anal. Biochem. **521**, 11–19 (2017).

[153] Marieb, E. N., "Human anatomy and physiology,(1995)," Redw. City, Calif. Benjamin/Cummings (1995).

[154] Woodard, H. Q. and White, D. R., "The composition of body tissues," Br. J. Radiol. **59**(708), 1209–1218 (1986).

[155] White, D. R., Widdowson, E. M., Woodard, H. Q. and Dickerson, J. W. T., "The composition of body tissues.(II) Fetus to young adult," Br. J. Radiol. **64**(758), 149–159 (1991).

[156] Nachabe, R., Hendriks, B. H. W., Desjardins, A. E., Van Der Voort, M., Van Der Mark, M. B. and Sterenborg, H. J. C. M., "Estimation of lipid and water concentrations in scattering media with diffuse optical spectroscopy from 900 to 1600 nm," J. Biomed. Opt. **15**(3), 37015 (2010).

[157] Bydlon, T. M., Nachabé, R., Ramanujam, N., Sterenborg, H. J. C. M. and Hendriks, B. H. W., "Chromophore based analyses of steady-state diffuse reflectance spectroscopy: current status and perspectives for clinical adoption," J. Biophotonics **8**(1–2), 9–24 (2015).

[158] Welte, M. A. and Gould, A. P., "Lipid droplet functions beyond energy storage," Biochim. Biophys. Acta (BBA)-Molecular Cell Biol. Lipids **1862**(10), 1260–1272 (2017).

[159] Conway, J. M., Norris, K. H. and Bodwell, C. E., "A new approach for the estimation of body composition: infrared interactance," Am. J. Clin. Nutr. **40**(6), 1123–1130 (1984).

[160] Van Veen, R. L. P., Sterenborg, H. J. C. M., Pifferi, A., Torricelli, A., Chikoidze, E. and Cubeddu, R., "Determination of visible near-IR absorption coefficients of mammalian fat using time-and spatially resolved diffuse reflectance and transmission spectroscopy," J. Biomed. Opt. **10**(5), 54004 (2005).

[161] Nachabé, R., van der Hoorn, J. W. A., van de Molengraaf, R., Lamerichs, R., Pikkemaat, J., Sio, C. F., Hendriks, B. H. W. and Sterenborg, H. J. C. M., "Validation of interventional fiber optic spectroscopy with MR spectroscopy, MAS-NMR spectroscopy, high-performance thin-layer chromatography, and histopathology for accurate hepatic fat quantification," Invest. Radiol. **47**(4), 209–216 (2012).

[162] Nogueira, M. S., Raju, M., Komolibus, K., Grygoryev, K. and Andersson-Engels, S., "Assessment of tissue biochemical and optical scattering changes due to hypothermic organ preservation: a preliminary study in mouse organs," J. Phys. D. Appl. Phys. (2021).

[163] Nogueira, M. S., Raju, M., Gunther, J., Grygoryev, K., Komolibus, K., Lu, H. and Andersson-Engels, S., "Diffuse reflectance spectroscopy for determination of optical properties and chromophore concentrations of mice internal organs in the range of 350 nm to 1860 nm," Proc. SPIE 10685 Biophotonics Photonic Solut. Better Heal. Care VI **10685**, 106853G (2018).

[164] Woodall, A. A., Lee, S. W.-M., Weesie, R. J., Jackson, M. J. and Britton, G., "Oxidation of carotenoids by free radicals: relationship between structure and reactivity," Biochim. Biophys. Acta (BBA)-general Subj. **1336**(1), 33–42 (1997).

[165] Black, H. S., Boehm, F., Edge, R. and Truscott, T. G., "The benefits and risks of certain dietary carotenoids that exhibit both anti-and pro-oxidative mechanisms—a comprehensive review," Antioxidants **9**(3), 264 (2020).

[166] Lunetta, J. M., Zulim, R. A., Dueker, S. R., Lin, Y., Flaig, V., Schneider, P. D., Wolfe, B. M. and Clifford, A. J., "Method for the simultaneous determination of retinol and $β$-carotene concentrations in human tissues and plasma," Anal. Biochem. **304**(1), 100–109 (2002).

[167] Yeum, K.-J., Ahn, S.-H., de Paiva, S. A., Lee-Kim, Y. C., Krinsky, N. I. and Russell, R. M., "Correlation between carotenoid concentrations in serum and normal breast adipose tissue of women with benign breast tumor or breast

cancer," J. Nutr. **128**(11), 1920–1926 (1998).

[168] El-Sohemy, A., Baylin, A., Kabagambe, E., Ascherio, A., Spiegelman, D. and Campos, H., "Individual carotenoid concentrations in adipose tissue and plasma as biomarkers of dietary intake," Am. J. Clin. Nutr. **76**(1), 172–179 (2002).

[169] Du, H., Fuh, R.-C. A., Li, J., Corkan, L. A. and Lindsey, J. S., "PhotochemCAD‡: a computer-aided design and research tool in photochemistry," Photochem. Photobiol. **68**(2), 141–142 (1998).

[170] Piérard, G. E., "EEMCO guidance for the assessment of skin colour," J. Eur. Acad. Dermatology Venereol. **10**(1), 1–11 (1998).

[171] Biesalski, H. K. and Obermueller-Jevic, U. C., "UV light, beta-carotene and human skin—beneficial and potentially harmful effects," Arch. Biochem. Biophys. **389**(1), 1–6 (2001).

[172] McGee, S., Mardirossian, V., Elackattu, A., Mirkovic, J., Pistey, R., Gallagher, G., Kabani, S., Yu, C.-C., Wang, Z., Badizadegan, K. and others., "Anatomy-based algorithms for detecting oral cancer using reflectance and fluorescence spectroscopy," Ann. Otol. Rhinol. \& Laryngol. **118**(11), 817–826 (2009).

[173] Scepanovic, O. R., Fitzmaurice, M., Gardecki, J., Angheloiu, G. O., Awasthi, S., Motz, J. T., Kramer Jr, J. R., Dasari, R. R. and Feld, M. S., "Detection of morphological markers of vulnerable atherosclerotic plaque using multimodal spectroscopy," J. Biomed. Opt. **11**(2), 21007 (2006).

[174] Brown, J. Q., Bydlon, T. M., Kennedy, S. A., Caldwell, M. L., Gallagher, J. E., Junker, M., Wilke, L. G., Barry, W. T., Geradts, J. and Ramanujam, N., "Optical spectral surveillance of breast tissue landscapes for detection of residual disease in breast tumor margins," PLoS One **8**(7), e69906 (2013).

[175] Kennedy, S., Geradts, J., Bydlon, T., Brown, J. Q., Gallagher, J., Junker, M., Barry, W., Ramanujam, N. and Wilke, L., "Optical breast cancer margin assessment: an observational study of the effects of tissue heterogeneity on optical contrast," Breast Cancer Res. **12**(6), 1–13 (2010).

[176] Wilke, L. G., Brown, J. Q., Bydlon, T. M., Kennedy, S. A., Richards, L. M., Junker, M. K., Gallagher, J., Barry, W. T., Geradts, J. and Ramanujam, N., "Rapid noninvasive optical imaging of tissue composition in breast tumor margins," Am. J. Surg. **198**(4), 566–574 (2009).

[177] Zhu, C., Palmer, G. M., Breslin, T. M., Harter, J. M. and Ramanujam, N., "Diagnosis of breast cancer using fluorescence and diffuse reflectance spectroscopy: a Monte-Carlo-model-based approach," J. Biomed. Opt. **13**(3), 34015 (2008).

[178] Zhu, C., Palmer, G. M., Breslin, T. M., Harter, J. and Ramanujam, N., "Diagnosis of breast cancer using diffuse reflectance spectroscopy: Comparison of a Monte Carlo versus partial least squares analysis based feature extraction technique," Lasers Surg. Med. Off. J. Am. Soc. Laser Med. Surg. **38**(7), 714–724 (2006).

[179] Volynskaya, Z. I., Haka, A. S., Bechtel, K. L., Fitzmaurice, M., Shenk, R., Wang, N., Nazemi, J., Dasari, R. R. and Feld, M. S., "Diagnosing breast cancer using diffuse reflectance spectroscopy and intrinsic fluorescence spectroscopy," J. Biomed. Opt. **13**(2), 24012 (2008).

[180] van Veen, R. L. P., Amelink, A., Menke-Pluymers, M., van der Pol, C. and Sterenborg, H. J. C. M., "Optical biopsy of breast tissue using differential path-length spectroscopy," Phys. Med. \& Biol. **50**(11), 2573 (2005).

[181] Stahl, W., Heinrich, U., Jungmann, H., von Laar, J., Schietzel, M., Sies, H. and Tronnier, H., "Increased dermal carotenoid levels assessed by noninvasive reflection spectrophotometry correlate with serum levels in women ingesting Betatene," J. Nutr. **128**(5), 903–907 (1998).

[182] Viuda-Martos, M., Sanchez-Zapata, E., Sayas-Barberá, E., Sendra, E., Pérez-Álvarez, J. A. and Fernández-López, J., "Tomato and tomato byproducts. Human health benefits of lycopene and its application to meat products: a review," Crit. Rev. Food Sci. Nutr. **54**(8), 1032–1049 (2014).

[183] Levy, J., Bosin, E., Feldman, B., Giat, Y., Miinster, A., Danilenko, M. and Sharoni, Y., "Lycopene is a more potent inhibitor of human cancer cell proliferation than either $α$-carotene or $β$-carotene" (1995).

[184] Stevenson, D. K., Dennery, P. A. and Hintz, S. R., "Understanding Newborn Jaundice<!----," J. Perinatol. **21**(S1), S21--S21 (2001).

[185] McDonagh, A. F. and Lightner, D. A., "Like a shrivelled blood orange'—bilirubin, jaundice, and phototherapy," Pediatrics **75**(3), 443–455 (1985).

[186] Wennberg, R., "Bilirubin transport and toxicity," Mead Johnson Symp. Perinat. Dev. Med.(19), 25–31 (1982).

[187] Wagener, F. A., Volk, H.-D., Willis, D., Abraham, N. G., Soares, M. P., Adema, G. J. and Figdor, C. G., "Different faces of the heme-heme oxygenase system in inflammation," Pharmacol. Rev. **55**(3), 551–571 (2003).

[188] Maines, M. D. and Cohn, J., "Bile pigment formation by skin heme oxygenase: studies on the response of the enzyme to heme compounds and tissue injury.," J. Exp. Med. **145**(4), 1054–1059 (1977).

[189] Pimstone, N. R., Tenhunen, R., Seitz, P. T., Marver, H. S. and Schmid, R., "The enzymatic degradation of hemoglobin to bile pigments by macrophages," J. Exp. Med. **133**(6), 1264–1281 (1971).

[190] Laiho, K. and Tenhunen, R., "Hemoglobin-degrading enzymes in experimental subcutaneous hematomas," Zeitschrift für Rechtsmedizin **93**(3), 193–198 (1984).

[191] Nachabé, R., Evers, D. J., Hendriks, B. H. W., Lucassen, G. W., van der Voort, M., Wesseling, J. and Ruers, T. J. M., "Effect of bile absorption coefficients on the estimation of liver tissue optical properties and related implications in discriminating healthy and tumorous samples," Biomed. Opt. Express **2**(3), 600–614 (2011).

[192] Schiff, E. R., Maddrey, W. C. and Reddy, K. R., [Schiff's diseases of the liver], John Wiley \& Sons (2017).

[193] Boyer, J. L., "Bile formation and secretion," Compr. Physiol. **3**(3), 1035 (2013).

[194] Hughes, V. K., Ellis, P. S., Burt, T. and Langlois, N. E. I., "The practical application of reflectance spectrophotometry for the demonstration of haemoglobin and its degradation in bruises," J. Clin. Pathol. **57**(4), 355–359 (2004).

[195] Kirkpatrick, N. D., Hoying, J. B., Botting, S. K., Weiss, J. A. and Utzinger, U., "In vitro model for endogenous optical signatures of collagen," J. Biomed. Opt. **11**(5), 54021 (2006).

[196] Eyre, D. R., Paz, M. A. and Gallop, P. M., "Cross-linking in collagen and elastin," Annu. Rev. Biochem. **53**(1), 717–748 (1984).

[197] Taroni, P., Comelli, D., Pifferi, A., Torricelli, A. and Cubeddu, R., "Absorption of collagen: effects on the estimate of breast composition and related diagnostic implications," J. Biomed. Opt. **12**(1), 14021 (2007).

[198] Taroni, P., Bassi, A., Comelli, D., Farina, A., Cubeddu, R. and Pifferi, A., "Diffuse optical spectroscopy of breast tissue extended to 1100 nm," J. Biomed. Opt. **14**(5), 54030 (2009).

[199] Taroni, P., Pifferi, A., Quarto, G., Spinelli, L., Torricelli, A., Abbate, F., Villa, A. M., Balestreri, N., Menna, S., Cassano, E. and others., "Noninvasive assessment of breast cancer risk using time-resolved diffuse optical spectroscopy," J. Biomed. Opt. **15**(6), 60501 (2010).

[200] Nachabé, R., Hendriks, B. H. W., Lucassen, G. W., van der Voort, M., Evers, D. J., Rutgers, E. J., Peeters, M.-J. V, der Hage, J. A., Oldenburg, H. S., Ruers, T. J. and others., "Diagnosis of breast cancer using diffuse optical spectroscopy from 500 to 1600 nm: comparison of classification methods," J. Biomed. Opt. **16**(8), 87010 (2011).

[201] Baldwin, A. K., Simpson, A., Steer, R., Cain, S. A. and Kielty, C. M., "Elastic fibres in health and disease," Expert Rev. Mol. Med. **15** (2013).

[202] Sinkus, R., Lorenzen, J., Schrader, D., Lorenzen, M., Dargatz, M. and Holz, D., "High-resolution tensor MR elastography for breast tumour detection," Phys. Med. \& Biol. **45**(6), 1649 (2000).

[203] Plewes, D. B., Bishop, J., Samani, A. and Sciarretta, J., "Visualization and quantification of breast cancer biomechanical properties with magnetic resonance elastography," Phys. Med. \& Biol. **45**(6), 1591 (2000).

[204] Barr, R. G., "Elastography in clinical practice," Radiol. Clin. **52**(6), 1145–1162 (2014).

[205] Bercoff, J., Tanter, M. and Fink, M., "Supersonic shear imaging: a new technique for soft tissue elasticity mapping," IEEE Trans. Ultrason. Ferroelectr. Freq. Control **51**(4), 396–409 (2004).

[206] Wang, Z. L., Sun, L., Li, Y. and Li, N., "Relationship between elasticity and collagen fiber content in breast disease: a preliminary report," Ultrasonics **57**, 44–49 (2015).

[207] Lindbergh, T., Larsson, M., Szabó, Z., Casimir-Ahn, H. and Strömberg, T., "Intramyocardial oxygen transport by quantitative diffuse reflectance spectroscopy in calves," J. Biomed. Opt. **15**(2), 27009 (2010).

[208] D'Alba, L. and Shawkey, M. D., "Melanosomes: biogenesis, properties, and evolution of an ancient organelle," Physiol. Rev. **99**(1), 1–19 (2019).

[209] Pacelli, C., Bryan, R. A., Onofri, S., Selbmann, L., Shuryak, I. and Dadachova, E., "Melanin is effective in protecting fast and slow growing fungi from various types of ionizing radiation," Environ. Microbiol. **19**(4), 1612–1624 (2017).

[210] Rogalla, S., D'Alba, L., Verdoodt, A. and Shawkey, M. D., "Hot wings: thermal impacts of wing coloration on surface temperature during bird flight," J. R. Soc. Interface **16**(156), 20190032 (2019).

[211] Riley, P. A., "A proposed selective mechanism based on metal chelation in industrial melanic moths," Biol. J. Linn. Soc. **109**(2), 298–301 (2013).

[212] Hong, L. and Simon, J. D., "Current understanding of the binding sites, capacity, affinity, and biological significance of metals in melanin" (2007).

[213] Stoddard, M. C. and Prum, R. O., "How colorful are birds? Evolution of the avian plumage color gamut," Behav. Ecol. **22**(5), 1042–1052 (2011).

[214] Agar, N. and Young, A. R., "Melanogenesis: a photoprotective response to DNA damage?," Mutat. Res. Mol. Mech. Mutagen. **571**(1–2), 121–132 (2005).

[215] Kollias, N. and Baqer, A. H., "Absorption mechanisms of human melanin in the visible, 400--720 nm," J. Invest. Dermatol. **89**(4), 384–388 (1987).

[216] Haining, R. L. and Achat-Mendes, C., "Neuromelanin, one of the most overlooked molecules in modern medicine, is not a spectator," Neural Regen. Res. **12**(3), 372 (2017).

[217] Anderson, R., "R., PARRISH, J., A," Opt. Hum. Ski., 13–19 (1981).

[218] Wolbarsht, M. L., Walsh, A. W. and George, G., "Melanin, a unique biological absorber," Appl. Opt. **20**(13), 2184–2186 (1981).

[219] Svaasand, L. O., Norvang, L. T., Fiskerstrand, E. J., Stopps, E. K. S., Berns, M. W. and Nelson, J. S., "Tissue parameters determining the visual appearance of normal skin and port-wine stains," Lasers Med. Sci. **10**(1), 55–65 (1995).

[220] Spott, T., "Characterization of layered tissue structures with diffusely propagating photon-density waves," Fac. Electr. Eng. Telecomunications. Dep. Phys. Electron. PhD thesis, Nor. Univ. Sci. Technol. Trondheim (1999).

[221] Peiris, A. N., Medlock, D. and Gavin, M., "Thyroglobulin for monitoring for thyroid cancer recurrence," Jama **321**(12), 1228 (2019).

[222] SMEDS, S., "A microgel electrophoretic analysis of the colloid proteins in single rat thyroid follicles. II. The protein concentration of the colloid in single rat thyroid follicles," Endocrinology **91**(5), 1300–1306 (1972).

[223] Troncone, L., Shapiro, B., Satta, M. A. and Monaco, F., [Thyroid diseases: basic science, pathology, clinical and

laboratory diagnoses], CRC Press (1993).

[224] Sekar, S. K. V., Farina, A., Dalla Mora, A., Lindner, C., Pagliazzi, M., Mora, M., Aranda, G., Dehghani, H., Durduran, T., Taroni, P. and others., "Broadband (550--1350 nm) diffuse optical characterization of thyroid chromophores," Sci. Rep. **8**(1), 1–8 (2018).

[225] Archibald, A. R., Fleming, I. D., Liddle, A. M., Manners, D. J., Mercer, G. A. and Wright, A., "232. α-1, 4-Glucosans. Part XI. The absorption spectra of glycogen--and amylopectin--iodine complexes," J. Chem. Soc., 1183–1190 (1961).

[226] Fyfe, J. C., Giger, U., Van Winkle, T. J., Haskins, M. E., Steinberg, S. A., Wang, P. and Patterson, D. F., "Glycogen storage disease type IV: inherited deficiency of branching enzyme activity in cats," Pediatr. Res. **32**(6), 719–725 (1992).

[227] Sidbury Jr, J. B., Mason, J., Burns Jr, W. B. and Ruebner, B. H., "Type IV glycogenosis. Report of a case proven by characterization of glycogen and studied at necropsy," Bull. Johns Hopkins Hosp. **111**, 157–181 (1962).

[228] Schochet Jr, S. S., McCormick, W. F. and Zellweger, H., "Type IV glycogenosis (amylopectinosis). Light and electron microscopic observations.," Arch. Pathol. **90**(4), 354–363 (1970).

[229] Hovenkamp-Hermelink, J. H. M., De Vries, J. N., Adamse, P., Jacobsen, E., Witholt, B. and Feenstra, W. J., "Rapid estimation of the amylose/amylopectin ratio in small amounts of tuber and leaf tissue of the potato," Potato Res. **31**(2), 241–246 (1988).

[230] Antosiewicz, J. M. and Shugar, D., "UV--Vis spectroscopy of tyrosine side-groups in studies of protein structure. Part 2: Selected applications," Biophys. Rev. **8**(2), 163–177 (2016).

[231] Antosiewicz, J. M. and Shugar, D., "UV--Vis spectroscopy of tyrosine side-groups in studies of protein structure. Part 1: basic principles and properties of tyrosine chromophore," Biophys. Rev. **8**(2), 151–161 (2016).

[232] Silberman, E. and Morgan, H. W., "Use of group theory in the interpretation of infrared and Raman spectra" (1977).

[233] Bunaciu, A. A., Aboul-Enein, H. Y. and Hoang, V. D., [Vibrational Spectroscopy Applications in Biomedical, Pharmaceutical and Food Sciences], Elsevier (2020).

[234] Larkin, P., [Infrared and Raman spectroscopy: principles and spectral interpretation], Elsevier (2017).

[235] Ellis, D. I., Harrigan, G. G. and Goodacre, R., "Metabolic fingerprinting with Fourier transform infrared spectroscopy," [Metabolic Profiling: Its role in biomarker discovery and gene function analysis], Springer, 111–124 (2003).

[236] Caine, S., Heraud, P., Tobin, M. J., McNaughton, D. and Bernard, C. C. A., "The application of Fourier transform infrared microspectroscopy for the study of diseased central nervous system tissue," Neuroimage **59**(4), 3624–3640 (2012).

[237] Lacombe, C., Untereiner, V., Gobinet, C., Zater, M., Sockalingum, G. D. and Garnotel, R., "Rapid screening of classic galactosemia patients: a proof-of-concept study using high-throughput FTIR analysis of plasma," Analyst **140**(7), 2280–2286 (2015).

[238] Yonar, D., Ocek, L., Tiftikcioglu, B. I., Zorlu, Y. and Severcan, F., "Relapsing-Remitting Multiple Sclerosis diagnosis from cerebrospinal fluids via Fourier transform infrared spectroscopy coupled with multivariate analysis," Sci. Rep. **8**(1), 1–13 (2018).

[239] Scott, D. A., Renaud, D. E., Krishnasamy, S., Meriç, P., Buduneli, N., Çetinkalp, \cSvetki and Liu, K.-Z., "Diabetes-related molecular signatures in infrared spectra of human saliva," Diabetol. \& Metab. Syndr. **2**(1), 1–9 (2010).

[240] Filik, J. and Stone, N., "Drop coating deposition Raman spectroscopy of protein mixtures," Analyst **132**(6), 544–550 (2007).

[241] Baker, M. J., Byrne, H. J., Chalmers, J., Gardner, P., Goodacre, R., Henderson, A., Kazarian, S. G., Martin, F. L., Moger, J., Stone, N. and Sulé-Suso, J., "Clinical applications of infrared and Raman spectroscopy: State of play and future challenges," Analyst **143**(8), 1735–1757 (2018).

[242] Bonnier, F., Blasco, H., Wasselet, C., Brachet, G., Respaud, R., Carvalho, L. F. C. S., Bertrand, D., Baker, M. J., Byrne, H. J. and Chourpa, I., "Ultra-filtration of human serum for improved quantitative analysis of low molecular weight biomarkers using ATR-IR spectroscopy," Analyst **142**(8), 1285–1298 (2017).

[243] Khoshmanesh, A., Dixon, M. W. A., Kenny, S., Tilley, L., McNaughton, D. and Wood, B. R., "Detection and quantification of early-stage malaria parasites in laboratory infected erythrocytes by attenuated total reflectance infrared spectroscopy and multivariate analysis," Anal. Chem. **86**(9), 4379–4386 (2014).

[244] Wood, B. R., Khoshmanesh, A., Dixon, M., Tilley, L. and McNAUGHTON, D., "Method and system for rapid malaria detection" (2018).

[245] Mwanga, E. P., Minja, E. G., Mrimi, E., Jiménez, M. G., Swai, J. K., Abbasi, S., Ngowo, H. S., Siria, D. J., Mapua, S., Stica, C. and others., "Detection of malaria parasites in dried human blood spots using mid-infrared spectroscopy and logistic regression analysis," Malar. J. **18**(1), 1–13 (2019).

[246] Pizarro, C., Esteban-Diez, I., Arenzana-Rámila, I. and González-Sáiz, J. M., "Discrimination of patients with different serological evolution of HIV and co-infection with HCV using metabolic fingerprinting based on Fourier transform infrared," J. Biophotonics **11**(3), e201700035 (2018).

[247] Sitole, L., Steffens, F., Krüger, T. P. J. and Meyer, D., "Mid-ATR-FTIR spectroscopic profiling of HIV/AIDS sera for novel systems diagnostics in global health," Omi. a J. Integr. Biol. **18**(8), 513–523 (2014).

[248] Santos, M. C. D., Nascimento, Y. M., Monteiro, J. D., Alves, B. E. B., Melo, M. F., Paiva, A. A. P., Pereira, H. W. B., Medeiros, L. G., Morais, I. C., Neto, J. C. F. and others., "ATR-FTIR spectroscopy with chemometric algorithms of multivariate classification in the discrimination between healthy vs. dengue vs. chikungunya vs. zika clinical samples," Anal. Methods **10**(10), 1280–1285 (2018).

[249] Naseer, K., Ali, S., Mubarik, S., Hussain, I., Mirza, B. and Qazi, J., "FTIR spectroscopy of freeze-dried human sera as a novel approach for dengue diagnosis," Infrared Phys. \& Technol. **102**, 102998 (2019).

[250] Hands, J. R., Dorling, K. M., Abel, P., Ashton, K. M., Brodbelt, A., Davis, C., Dawson, T., Jenkinson, M. D., Lea, R. W., Walker, C. and others., "Attenuated total reflection Fourier transform infrared (ATR-FTIR) spectral discrimination of brain tumour severity from serum samples," J. Biophotonics **7**(3–4), 189–199 (2014).

[251] Riça, L. B., Cassol, O. S., Rieger, A. and Corbellini, V. A., "Discrimination of healthy and colorectal cancer patients using FTIR and PLS-DA," Rev. Jovens Pesqui. **9**(2), 115–130 (2019).

[252] Khanmohammadi, M., Nasiri, R., Ghasemi, K., Samani, S. and Garmarudi, A. B., "Diagnosis of basal cell carcinoma by infrared spectroscopy of whole blood samples applying soft independent modeling class analogy," J. Cancer Res. Clin. Oncol. **133**(12), 1001–1010 (2007).

[253] Ildiz, G. O., Arslan, M., Unsalan, O., Araujo-Andrade, C., Kurt, E., Karatepe, H. T., Yilmaz, A., Yalcinkaya, O. B. and Herken, H., "FT-IR spectroscopy and multivariate analysis as an auxiliary tool for diagnosis of mental disorders: Bipolar and schizophrenia cases," Spectrochim. Acta Part A Mol. Biomol. Spectrosc. **152**, 551–556 (2016).

[254] Mordechai, S., Shufan, E., Katz, B. S. P. and Salman, A., "Early diagnosis of Alzheimer's disease using infrared spectroscopy of isolated blood samples followed by multivariate analyses," Analyst **142**(8), 1276–1284 (2017).

[255] Lechowicz, L., Chrapek, M., Gaweda, J., Urbaniak, M. and Konieczna, I., "Use of Fourier-transform infrared spectroscopy in the diagnosis of rheumatoid arthritis: a pilot study," Mol. Biol. Rep. **43**(12), 1321–1326 (2016).

[256] Khanmohammadi, M., Garmarudi, A. B., Ramin, M. and Ghasemi, K., "Diagnosis of renal failure by infrared spectrometric analysis of human serum samples and soft independent modeling of class analogy," Microchem. J.

106, 67–72 (2013).

[257] Gunasekaran, S. and Uthra, D., “FTIR and UV-Visible spectral study on normal and jaundice blood samples,” Asian J. Chem. **20**(7), 5695 (2008).

[258] Oleszko, A., Hartwich, J., Wójtowicz, A., G\kasior-Głogowska, M., Huras, H. and Komorowska, M., “Comparison of FTIR-ATR and Raman spectroscopy in determination of VLDL triglycerides in blood serum with PLS regression,” Spectrochim. Acta Part A Mol. Biomol. Spectrosc. **183**, 239–246 (2017).

[259] Li, Z., Lv, H., Li, T., Si, G., Wang, Q., Lv, J. and Hu, X., “Reagent-free simultaneous determination of glucose and cholesterol in whole blood by FTIR-ATR,” Spectrochim. Acta Part A Mol. Biomol. Spectrosc. **178**, 192–197 (2017).

[260] Spalding, K., Bonnier, F., Bruno, C., Blasco, H., Board, R., Benz-de Bretagne, I., Byrne, H. J., Butler, H. J., Chourpa, I., Radhakrishnan, P. and others., “Enabling quantification of protein concentration in human serum biopsies using attenuated total reflectance--Fourier transform infrared (ATR-FTIR) spectroscopy,” Vib. Spectrosc. **99**, 50–58 (2018).

[261] Perez-Guaita, D., Ventura-Gayete, J., Pérez-Rambla, C., Sancho-Andreu, M., Garrigues, S. and De La Guardia, M., “Protein determination in serum and whole blood by attenuated total reflectance infrared spectroscopy,” Anal. Bioanal. Chem. **404**(3), 649–656 (2012).

[262] Horosh, M., Feldman, H., Yablonovich, A., Firer, M. A. and Abookasis, D., “Broadband infrared spectroscopy for non-contact measurement of neurological disease biomarkers in cerebrospinal fluid,” Appl. Spectrosc. **71**(3), 496–506 (2017).

[263] Saranya, K. K. N., Maradi, A., Chithresan, K., Janakiram, S. H. and Krishna, P., “Molecular signatures in infrared spectra of saliva in healthy, chronic and aggressive periodontitis,” Vib. Spectrosc. **111**, 103179 (2020).

[264] Bottoni, U., Tiriolo, R., Pullano, S. A., Dastoli, S., Amoruso, G. F., Nisticò, S. P. and Fiorillo, A. S., “Infrared saliva analysis of psoriatic and diabetic patients: similarities in protein components,” IEEE Trans. Biomed. Eng. **63**(2), 379–384 (2015).

[265] Khaustova, S., Shkurnikov, M., Tonevitsky, E., Artyushenko, V. and Tonevitsky, A., “Noninvasive biochemical monitoring of physiological stress by Fourier transform infrared saliva spectroscopy,” Analyst **135**(12), 3183–3192 (2010).

[266] Mikkonen, J. J. W., Raittila, J., Rieppo, L., Lappalainen, R., Kullaa, A. M. and Myllymaa, S., “Fourier transform infrared spectroscopy and photoacoustic spectroscopy for saliva analysis,” Appl. Spectrosc. **70**(9), 1502–1510 (2016).

[267] Setti, G., Pezzi, M. E., Viani, M. V., Pertinhez, T. A., Cassi, D., Magnoni, C., Bellini, P., Musolino, A., Vescovi, P. and Meleti, M., “Salivary microRNA for diagnosis of cancer and systemic diseases: A systematic review,” Int. J. Mol. Sci. **21**(3), 907 (2020).

[268] Paschotto, D. R., Pupin, B., Bhattacharjee, T. T. and Soares, L. E. S., “Saliva preparation method exploration for ATR-FTIR spectroscopy: Towards bio-fluid based disease diagnosis,” Anal. Sci., 20P029 (2020).

[269] Rekha, P., Aruna, P., Brindha, E., Koteeswaran, D., Baludavid, M. and Ganesan, S., “Near-infrared Raman spectroscopic characterization of salivary metabolites in the discrimination of normal from oral premalignant and malignant conditions,” J. Raman Spectrosc. **47**(7), 763–772 (2016).

[270] Khurshid, Z., Asiri, F. Y. I. and Al Wadaani, H., “Human saliva: non-invasive fluid for detecting novel coronavirus (2019-nCoV),” Int. J. Environ. Res. Public Health **17**(7), 2225 (2020).

[271] Rodrigues, R. P. C. B., Aguiar, E. M. G., Cardoso-Sousa, L., Caixeta, D. C., Guedes, C. C. F. V, Siqueira, W. L., Maia, Y. C. P., Cardoso, S. V and Sabino-Silva, R., “Differential molecular signature of human saliva using ATR-FTIR spectroscopy for chronic kidney disease diagnosis,” Braz. Dent. J. **30**, 437–445 (2019).

[272] Bel’skaya, L. V, Sarf, E. A. and Solomatin, D. V., “Age and gender characteristics of the infrared spectra of normal

human saliva," Appl. Spectrosc. **74**(5), 536–543 (2020).

[273] Fujii, S., Sato, S., Fukuda, K., Okinaga, T., Ariyoshi, W., Usui, M., Nakashima, K., Nishihara, T. and Takenaka, S., "Diagnosis of periodontal disease from saliva samples using Fourier transform infrared microscopy coupled with partial least squares discriminant analysis," Anal. Sci. **32**(2), 225–231 (2016).

[274] Virkler, K. and Lednev, I. K., "Analysis of body fluids for forensic purposes: from laboratory testing to non-destructive rapid confirmatory identification at a crime scene," Forensic Sci. Int. **188**(1–3), 1–17 (2009).

[275] Oliver, K. V, Vilasi, A., Maréchal, A., Moochhala, S. H., Unwin, R. J. and Rich, P. R., "Infrared vibrational spectroscopy: a rapid and novel diagnostic and monitoring tool for cystinuria," Sci. Rep. **6**(1), 1–7 (2016).

[276] Oliver, K. V, Matjiu, F., Davey, C., Moochhala, S., Unwin, R. J. and Rich, P. R., "Attenuated total reflection Fourier transform infrared (ATR-FTIR) spectroscopy as a bedside diagnostic tool for detecting renal disease biomarkers in fresh urine samples," Opt. Diagnostics Sens. XV Towar. Point-of-Care Diagnostics **9332**, 933202 (2015).

[277] Paraskevaidi, M., Morais, C. L. M., Lima, K. M. G., Ashton, K. M., Stringfellow, H. F., Martin-Hirsch, P. L. and Martin, F. L., "Potential of mid-infrared spectroscopy as a non-invasive diagnostic test in urine for endometrial or ovarian cancer," Analyst **143**(13), 3156–3163 (2018).

[278] Lakowicz, J. R., "Fluorescence sensing," [Principles of fluorescence spectroscopy], Springer, 531–572 (1999).

[279] Stanley, W. C., Lopaschuk, G. D., Hall, J. L. and McCormack, J. G., "Regulation of myocardial carbohydrate metabolism under normal and ischaemic conditions: potential for pharmacological interventions," Cardiovasc. Res. **33**(2), 243–257 (1997).

[280] Marcu, L., French, P. M. W. and Elson, D. S., [Fluorescence lifetime spectroscopy and imaging: principles and applications in biomedical diagnostics], CRC Press (2014).

[281] Klaidman, L. K., Leung, A. C. and Adams, J. D., "High-performance liquid chromatography analysis of oxidized and reduced pyridine dinucleotides in specific brain regions," Anal. Biochem. **228**(2), 312–317 (1995).

[282] Avi-Dor, Y., Olson, J. M., Doherty, M. D. and Kaplan, N. O., "Fluorescence of pyridine nucleotides in mitochondria," J. Biol. Chem. **237**(7), 2377–2383 (1962).

[283] Lakowicz, J. R., "Principles of Fluorescence Spectroscopy, 29 Springer," Third Ed. **30** (2006).

[284] Zipfel, W. R., Williams, R. M., Christie, R., Nikitin, A. Y., Hyman, B. T. and Webb, W. W., "Live tissue intrinsic emission microscopy using multiphoton-excited native fluorescence and second harmonic generation," Proc. Natl. Acad. Sci. **100**(12), 7075–7080 (2003).

[285] Bird, D. K., Yan, L., Vrotsos, K. M., Eliceiri, K. W., Vaughan, E. M., Keely, P. J., White, J. G. and Ramanujam, N., "Metabolic mapping of MCF10A human breast cells via multiphoton fluorescence lifetime imaging of the coenzyme NADH," Cancer Res. **65**(19), 8766–8773 (2005).

[286] Niesner, R., Peker, B., Schlüsche, P. and Gericke, K.-H., "Noniterative biexponential fluorescence lifetime imaging in the investigation of cellular metabolism by means of NAD (P) H autofluorescence," ChemPhysChem **5**(8), 1141–1149 (2004).

[287] Chance, B. and Neilands, J. B., "STUDIES ON LACTIC DEHYDROGENASE OF HEART II. A COMPOUND OF LACTIC DEHYDROGENASE AND REDUCED PYRIDINE NUCLEOTIDE," J. Biol. Chem. **199**(1), 383–387 (1952).

[288] Chorvat Jr, D., Mateasik, A., Cheng, Y., Poirier, N., Miró, J., Dahdah, N. S. and Chorvatova, A., "Rejection of transplanted hearts in patients evaluated by the component analysis of multi-wavelength NAD (P) H fluorescence lifetime spectroscopy," J. Biophotonics **3**(10–11), 646–652 (2010).

[289] Chorvatova, A., Mateasik, A. and Chorvat Jr, D., "Spectral decomposition of NAD (P) H fluorescence components recorded by multi-wavelength fluorescence lifetime spectroscopy in living cardiac cells," Laser Phys. Lett. **10**(12),

125703 (2013).

[290] Vishwasrao, H. D., Heikal, A. A., Kasischke, K. A. and Webb, W. W., "Conformational Dependence of Intracellular NADH on Metabolic State Revealed by Associated Fluorescence Anisotropy*♦," J. Biol. Chem. **280**(26), 25119–25126 (2005).

[291] HÖNES, G., HöNES, J. and HAUSER, M., "Studies of enzyme-ligand complexes using dynamic fluorescence anisotropy. II. The coenzyme-binding site of malate dehydrogenase" (1986).

[292] Pires, L., Nogueira, M. S., Pratavieira, S., Moriyama, L. T. and Kurachi, C., "Time-resolved fluorescence lifetime for cutaneous melanoma detection," Biomed. Opt. Express **5**(9), 3080 (2014).

[293] Cosci, A., Nogueira, M. S., Pratavieira, S., Takahama, A., Azevedo, R. de S., Kurachi, C. and Kurachi, C., "Time-resolved fluorescence spectroscopy for clinical diagnosis of actinic cheilitis: erratum," Biomed. Opt. Express **7**(10), 4210–4219 (2016).

[294] Cosci, A., Nogueira, M. S., Prataviera, S., Takahama, A., de Souza Azevedo, R. and Kurachi, C., "Time-resolved fluorescence spectroscopy for clinical diagnosis of actinic cheilitis: erratum," Biomed. Opt. Express **9**(2), 648 (2018).

[295] Nogueira, M. S., Cosci, A., Pratavieira, S., Takahama Jr, A., Azevedo, R. S. and Kurachi, C., "Evaluation of actinic cheilitis using fluorescence lifetime spectroscopy," Proc. SPIE 9703 Opt. Biopsy XIV Towar. Real-Time Spectrosc. Imaging Diagnosis **9703**, 97031U (2016).

[296] Bastiaens, P. I., Van Hoek, A., Benen, J. A., Brochon, J.-C. and Visser, A. J., "Conformational dynamics and intersubunit energy transfer in wild-type and mutant lipoamide dehydrogenase from Azotobacter vinelandii. A multidimensional time-resolved polarized fluorescence study," Biophys. J. **63**(3), 839–853 (1992).

[297] van den Berg, P. A. W., van Hoek, A., Walentas, C. D., Perham, R. N. and Visser, A. J. W. G., "Flavin fluorescence dynamics and photoinduced electron transfer in Escherichia coli glutathione reductase," Biophys. J. **74**(4), 2046–2058 (1998).

[298] van den Berg, P. A. W., Widengren, J., Hink, M. A., Rigler, R. and Visser, A. J. W. G., "Fluorescence correlation spectroscopy of flavins and flavoenzymes: photochemical and photophysical aspects," Spectrochim. Acta Part A Mol. Biomol. Spectrosc. **57**(11), 2135–2144 (2001).

[299] Yang, H., Luo, G., Karnchanaphanurach, P., Louie, T.-M., Rech, I., Cova, S., Xun, L. and Xie, X. S., "Protein conformational dynamics probed by single-molecule electron transfer," Science (80-.). **302**(5643), 262–266 (2003).

[300] den Berg, P. A. W., Feenstra, K. A., Mark, A. E., Berendsen, H. J. C. and Visser, A. J. W. G., "Dynamic conformations of flavin adenine dinucleotide: simulated molecular dynamics of the flavin cofactor related to the time-resolved fluorescence characteristics," J. Phys. Chem. B **106**(34), 8858–8869 (2002).

[301] Berezin, M. Y. and Achilefu, S., "Fluorescence lifetime measurements and biological imaging," Chem. Rev. **110**(5), 2641–2684 (2010).

[302] Huerta, C., Borek, D., Machius, M., Grishin, N. V and Zhang, H., "Structure and mechanism of a eukaryotic FMN adenylyltransferase," J. Mol. Biol. **389**(2), 388–400 (2009).

[303] Billinton, N. and Knight, A. W., "Seeing the wood through the trees: a review of techniques for distinguishing green fluorescent protein from endogenous autofluorescence," Anal. Biochem. **291**(2), 175–197 (2001).

[304] Drössler, P., Holzer, W., Penzkofer, A. and Hegemann, P., "Fluoresence quenching of riboflavin in aqueous solution by methionin and cystein," Chem. Phys. **286**(2–3), 409–420 (2003).

[305] Singh, A. K. and Das, J., "Liposome encapsulated vitamin A compounds exhibit greater stability and diminished toxicity," Biophys. Chem. **73**(1–2), 155–162 (1998).

[306] Maeda, T., Taguchi, H., Minami, H., Sato, K., Shiga, T., Kosaka, H. and Yoshikawa, K., "Vitamin B6 phototoxicity

induced by UVA radiation," Arch. Dermatol. Res. **292**(11), 562–567 (2000).

[307] Coburn, S. P., Slominski, A., Mahuren, J. D., Wortsman, J., Hessle, L. and Millan, J. L., "Cutaneous metabolism of vitamin B-6," J. Invest. Dermatol. **120**(2), 292–300 (2003).

[308] Bueno, C., Pavez, P., Salazar, R. and Encinas, M. V., "Photophysics and photochemical studies of the vitamin B6 group and related derivatives," Photochem. Photobiol. **86**(1), 39–46 (2010).

[309] Richards-Kortum, R. and Sevick-Muraca, E., "Quantitative optical spectroscopy for tissue diagnosis," Annu. Rev. Phys. Chem. **47**(1), 555–606 (1996).

[310] Chen, R. F., "Fluorescence quantum yield measurements: vitamin B6 compounds," Science (80-.). **150**(3703), 1593–1595 (1965).

[311] National Institutes of Health (NIH)., "Folate - Fact Sheet for Health Professionals," 2021, <https://ods.od.nih.gov/factsheets/folate-HealthProfessional/> (20 July 2021).

[312] Wald, N. J., Morris, J. K. and Blakemore, C., "Public health failure in the prevention of neural tube defects: time to abandon the tolerable upper intake level of folate," Public Health Rev. **39**(1), 1–11 (2018).

[313] Wien, T. N., Pike, E., Wisløff, T., Staff, A., Smeland, S. and Klemp, M., "Cancer risk with folic acid supplements: a systematic review and meta-analysis," BMJ Open **2**(1), e000653 (2012).

[314] Herbert, V. and Bertino, J. R., "Folic acid. Gyorgy, P. Pearson, WN eds," Vitam. **7**, 243–276 (1967).

[315] Swarna, S., Lorente, C., Thomas, A. H. and Martin, C. B., "Rate constants of quenching of the fluorescence of pterins by the iodide anion in aqueous solution," Chem. Phys. Lett. **542**, 62–65 (2012).

[316] Thomas, A. H., Lorente, C., Capparelli, A. L., Pokhrel, M. R., Braun, A. M. and Oliveros, E., "Fluorescence of pterin, 6-formylpterin, 6-carboxypterin and folic acid in aqueous solution: pH effects," Photochem. \& Photobiol. Sci. **1**(6), 421–426 (2002).

[317] Lorente, C., Capparelli, A. L., Thomas, A. H., Braun, A. M. and Oliveros, E., "Quenching of the fluorescence of pterin derivatives by anions," Photochem. \& Photobiol. Sci. **3**(2), 167–173 (2004).

[318] Birn, H., "The kidney in vitamin B12 and folate homeostasis: characterization of receptors for tubular uptake of vitamins and carrier proteins," Am. J. Physiol. Physiol. **291**(1), F22--F36 (2006).

[319] Johns Hopkins Medicine., "Vitamin B12 Deficiency Anemia," 2021, <https://www.hopkinsmedicine.org/health/conditions-and-diseases/vitamin-b12-deficiency-anemia> (20 July 2021).

[320] National Institutes of Health (NIH)., "Vitamin B12 - Fact Sheet for Health Professionals," 2022, <https://ods.od.nih.gov/factsheets/VitaminB12-HealthProfessional/> (20 July 2022).

[321] Marriott, B. P., Birt, D. F., Stalling, V. A. and Yates, A. A., [Present Knowledge in Nutrition: Basic Nutrition and Metabolism], Academic Press (2020).

[322] Thiamin, R., "Dietary reference intakes for thiamin, riboflavin, niacin, vitamin B6, folate, vitamin B12, pantothenic acid, biotin, and choline1" (1998).

[323] Gordon, S., "Acid-Reflux Drugs & Lower Levels of Vitamin B-12," 2013, <https://www.webmd.com/heartburn-gerd/news/20131210/acid-reflux-drugs-tied-to-lower-levels-of-vitamin-b-12> (20 July 2021).

[324] Ohara, K., Mitsumori, R., Takebe, M., Kuzuhara, D., Yamada, H. and Nagaoka, S., "Vitamin K analogue as a new fluorescence probe for quantitative antioxidant assay," J. Photochem. Photobiol. A Chem. **215**(1), 52–58 (2010).

[325] Goldin, A., Beckman, J. A., Schmidt, A. M. and Creager, M. A., "Advanced glycation end products: sparking the development of diabetic vascular injury," Circulation **114**(6), 597–605 (2006).

[326] Haus, J. M., Carrithers, J. A., Trappe, S. W. and Trappe, T. A., "Collagen, cross-linking, and advanced glycation end products in aging human skeletal muscle," J. Appl. Physiol. **103**(6), 2068–2076 (2007).

[327] Sell, D. R., Nagaraj, R. H., Grandhee, S. K., Odetti, P., Lapolla, A., Fogarty, J. and Monnier, V. M., "Pentosidine: a molecular marker for the cumulative damage to proteins in diabetes, aging, and uremia.," Diabetes. Metab. Rev. **7**(4), 239–251 (1991).

[328] Lutz, V., Sattler, M., Gallinat, S., Wenck, H., Poertner, R. and Fischer, F., "Impact of collagen crosslinking on the second harmonic generation signal and the fluorescence lifetime of collagen autofluorescence," Ski. Res. Technol. **18**(2), 168–179 (2012).

[329] Ashwin, P. T. and McDonnell, P. J., "Collagen cross-linkage: a comprehensive review and directions for future research," Br. J. Ophthalmol. **94**(8), 965–970 (2010).

[330] Kollias, N., Gillies, R., Moran, M., Kochevar, I. E. and Anderson, R. R., "Endogenous skin fluorescence includes bands that may serve as quantitative markers of aging and photoaging," J. Invest. Dermatol. **111**(5), 776–780 (1998).

[331] Odetti, P. R., Borgoglio, A. and Rolandi, R., "Age-related increase of collagen fluorescence in human subcutaneous tissue," Metabolism **41**(6), 655–658 (1992).

[332] Provenzano, P. P., Eliceiri, K. W., Campbell, J. M., Inman, D. R., White, J. G. and Keely, P. J., "Collagen reorganization at the tumor-stromal interface facilitates local invasion," BMC Med. **4**(1), 1–15 (2006).

[333] Brown, E., McKee, T., Pluen, A., Seed, B., Boucher, Y., Jain, R. K. and others., "Dynamic imaging of collagen and its modulation in tumors in vivo using second-harmonic generation," Nat. Med. **9**(6), 796–800 (2003).

[334] Black, L. D., Allen, P. G., Morris, S. M., Stone, P. J. and Suki, B., "Mechanical and failure properties of extracellular matrix sheets as a function of structural protein composition," Biophys. J. **94**(5), 1916–1929 (2008).

[335] Knöbel, M., O'Toole, E. A. and Smith, F. J. D., "Keratins and skin disease," Cell Tissue Res. **360**(3), 583–589 (2015).

[336] Snider, N. T. and Omary, M. B., "Post-translational modifications of intermediate filament proteins: mechanisms and functions," Nat. Rev. Mol. cell Biol. **15**(3), 163–177 (2014).

[337] Karantza, V., "Keratins in health and cancer: more than mere epithelial cell markers," Oncogene **30**(2), 127–138 (2011).

[338] Singh, V., Wang, S. and Ng, K. W., "2.25 Keratin as a Biomaterial," [Comprehensive Biomaterials II], P. Ducheyne, Ed., Elsevier, Oxford, 542–557 (2017).

[339] Fois, G., Weimer, M., Busch, T., Felder, E. T., Oswald, F., von Wichert, G., Seufferlein, T., Dietl, P. and Felder, E., "Effects of keratin phosphorylation on the mechanical properties of keratin filaments in living cells," FASEB J. **27**(4), 1322–1329 (2013).

[340] Ku, N.-O., Toivola, D. M., Strnad, P. and Omary, M. B., "Cytoskeletal keratin glycosylation protects epithelial tissue from injury," Nat. Cell Biol. **12**(9), 876–885 (2010).

[341] Alam, H., Gangadaran, P., Bhate, A. V, Chaukar, D. A., Sawant, S. S., Tiwari, R., Bobade, J., Kannan, S., D'cruz, A. K., Kane, S. and others., "Loss of keratin 8 phosphorylation leads to increased tumor progression and correlates with clinico-pathological parameters of OSCC patients," PLoS One **6**(11), e27767 (2011).

[342] Busch, T., Armacki, M., Eiseler, T., Joodi, G., Temme, C., Jansen, J., von Wichert, G., Omary, M. B., Spatz, J. and Seufferlein, T., "Keratin 8 phosphorylation regulates keratin reorganization and migration of epithelial tumor cells," J. Cell Sci. **125**(9), 2148–2159 (2012).

[343] Chung, B.-M., Rotty, J. D. and Coulombe, P. A., "Networking galore: intermediate filaments and cell migration," Curr. Opin. Cell Biol. **25**(5), 600–612 (2013).

[344] Ehlers, A., Riemann, I., Stark, M. and König, K., "Multiphoton fluorescence lifetime imaging of human hair," Microsc. Res. Tech. **70**(2), 154–161 (2007).

[345] Wu, Y. and Qu, J. Y., "Autofluorescence spectroscopy of epithelial tissues," J. Biomed. Opt. **11**(5), 54023 (2006).

[346] Nogueira, M. S., Komolibus, K., Grygoryev, K., Gunther, J. E. and Andersson-Engels, S., "Fluorescence spectroscopy of mouse organs using ultraviolet excitation: towards assessment of organ viability for transplantation," Proc. SPIE 10876 Opt. Interact. with Tissue Cells XXX **10876**, 1087606 (2019).

[347] Nogueira, M. S. and Guimarães, F. E. G., "Photophysical processes on biological tissues and photodynamic therapy using steady-state and time-resolved fluorescence techniques: diagnosis applications, dosimetry and photodegradation kinetics," Livro de Resumos (2016).

[348] de Paula Campos, C., de Paula D'Almeida, C., Nogueira, M. S., Moriyama, L. T., Pratavieira, S. and Kurachi, C., "Fluorescence spectroscopy in the visible range for the assessment of UVB radiation effects in hairless mice skin," Photodiagnosis Photodyn. Ther. **20**(May), 21–27 (2017).

[349] Nogueira, M. S., D'Almeida, C. P., Pratavieira, S. and Kurachi, C., "Characterization of a fluorescence lifetime spectroscopy system for diagnostic purposes using an optic fiber probe," Livro de Resumos (2014).

[350] Pires, L., Nogueira, M. S., Moriyama, L. T. and Kurachi, C., "Fluorescence lifetime for melanoma murine detection," Tech. Summ. (2014).

[351] Silami, F. D. J., Pratavieira, S., Nogueira, M. S., Barrett, A. A., Sinhoreti, M. A. C., Geraldeli, S., Pires-de-Souza, F. de C. and others., "Quantitative image of fluorescence of ceramic and resin-cement veneers," Braz. Oral Res. **33** (2019).

[352] Nogueira, M. S., Panhóca, V. H. and Bagnato, V. S., "Fluorescence spectroscopy analysis of light-induced tooth whitening," Proc. SPIE 10876, Photonics West, 10876-45 (2019).

[353] Nogueira, M., D'Almeida, C. P., Cosci, A., Pratavieira, S., Kurachi, C. and Schimdt, P. A., "Montagem e caracterização de sistema de espectroscopia e tempo de vida de fluorescência utilizando fibra óptica," XXIV Congr. Bras. Eng. Biomédica--CBEB. Uberlandia, 2468–2471 (2014).

[354] Nogueira, M. S., "Fluorescence lifetime spectroscopy for diagnosis of clinically similar skin lesions" (2016).

[355] Nicolodelli, G., Tadini, A. M., Nogueira, M. S., Pratavieira, S., Mounier, S., Huaman, J. L. C., dos Santos, C. H., Montes, C. R. and Milori, D. M. B. P., "Fluorescence lifetime evaluation of whole soils from the Amazon rainforest," Appl. Opt. **56**(24), 6936–6941 (2017).

[356] Nogueira, M. S., D'Almeida, C. P., Pratavieira, S. and Kurachi, C., "Sistema de espectroscopia e tempo de vida de fluorescência para diagnóstico clinico," Anais/Resumos (2015).

[357] Kurachi, C., Pires, L., Nogueira, M. S. and Pratavieira, S., "Lifetime fluorescence for the detection of skin lesions," Biomed. Opt. 2014(April), BS4B.3 (2014).

[358] Nogueira, M. S., Pratavieira, S., Kurachi, C. and others., "Portable fluorescence microendoscope system for smartphones and imaging processing software," Tech. Summ. (2015).

[359] da Silva, A. P., Saito Nogueira, M., Jo, J. A., Salvador Bagnato, V. and Mayumi Inada, N., "Optical Based Diagnosis and Treatment of Onychomycosis," Biomed. Opt. 2016(January), JTu3A.37 (2016).

[360] de Andrade, C. T., Nogueira, M. S., Kanick, S. C., Marra, K., Gunn, J., Andreozzi, J., Samkoe, K. S., Kurachi, C. and Pogue, B. W., "Optical spectroscopy of radiotherapy and photodynamic therapy responses in normal rat skin shows vascular breakdown products," Proc. SPIE 9694 Opt. Methods Tumor Treat. Detect. Mech. Tech. Photodyn. Ther. XXV **9694**, 969410 (2016).

[361] Ono, B. A., Nogueira, M., Pires, L., Pratavieira, S. and Kurachi, C., "Subcellular localization and photodynamic activity

of Photodithazine (glucosamine salt of chlorin e6) in murine melanoma B16-F10: an in vitro and in vivo study," Proc. SPIE 10476 Opt. Methods Tumor Treat. Detect. Mech. Tech. Photodyn. Ther. XXVII **10476**(February), 44 (2018).

[362] Carvalho, L. F. C. S., Nogueira, M. S., Bhattacharjee, T., Neto, L. P. M., Daun, L., Mendes, T. O., Rajasekaran, R., Chagas, M., Martin, A. A. and Soares, L. E. S., "In vivo Raman spectroscopic characteristics of different sites of the oral mucosa in healthy volunteers," Clin. Oral Investig. **23**(7), 3021–3031 (2019).

[363] Carvalho, L. F. C. S., Nogueira, M. S., Neto, L. P. M., Bhattacharjee, T. T. and Martin, A. A., "Raman spectral post-processing for oral tissue discrimination – a step for an automatized diagnostic system," Biomed. Opt. Express **8**(11), 5218 (2017).

[364] Nogueira, M. S., Pratavieira, S., Júnior, A. T., Azevedo, R. S. and Kurachi, C., "Diagnóstico de queilite actinica por espectroscopia de tempo de vida de fluorescência," Anais/Resumos (2015).

[365] Salvio, A. G., Ramirez, D. P., Inada, N. M., Stringasci, M. D., Nogueira, M. S. and Bagnato, V. S., "Fractionated illumination in a single visit photodynamic therapy for basal cell carcinoma," B. Abstr. (2017).

[366] Salvio, A. G., Ramirez, D. P., Nogueira, M. S., Stringasci, M. D., Oliveira, E. R., Inada, N. M. and Bagnato, V. S., "Evaluation of pain and treatment effect during large area photodynamic therapy in 140 patients with widespread actinic keratosis of upper limbs," B. Abstr. (2017).

[367] Nogueira, M. S., Rosa, R. G. T., Pratavieira, S., de Paula, D. and Kurachi, C., "Assembly and characterization of a fluorescence lifetime spectroscopy system for skin lesions diagnostic," Proc. SPIE 9531 Biophotonics South Am. **9531**, 95313D (2015).

[368] Nogueira, M. S., Junior, F. F. P., Caface, R. A., Oliveira, K. T. de, Bagnato, V. S. and Guimarães, F. E. G., "Characterization of photophysical properties of curcumin for theranostics of neurodegenerative diseases," Proc. SPIE 10876, Photonics West, 10876-37 (2019).

[369] Nogueira, M. S., Bagnato, V. S. and Panhoca, V. H., "Characterization of teeth fluorescence properties due to coffee pigmentation: towards optimization of quantitative light-induced fluorescence for tooth color assessment," Proc. SPIE 11238, Photonics West, 11238-51 (2020).

[370] Nogueira, M. S., Pinto Junior, F. F., Caface, R. A., Oliveira, K. T. de and Guimarães, F. E. G., "Optimization of curcumin formulations for fluorescence-based applications," Proc. SPIE 11238, Photonics West, 11238-50 (2020).

[371] Nogueira, M. S., Bagnato, V. S. and Panhoca, V. H., "Calculation of whiteness and yellowness indexes using colorimetric and photographic methods for tooth shade evaluation," Proc. SPIE 11238, Photonics West, 11238-52 (2020).

[372] Nogueira, M. S., Brugnera Junior, A., Bagnato, V. S., Panhóca, V. H. and Panhoca, V. H., "Evaluation of the whitening effectiveness of violet illumination alone or combined with hydrogen peroxide gel," Photobiomodulation, Photomedicine, Laser Surg. (2021).

[373] Nogueira, M. S., Cosci, A. and Kurachi, C., "Assessment of oxidative stress and metabolic rates in liver grafts using time-resolved fluorescence spectroscopy," Proc. SPIE 10685 Biophotonics Photonic Solut. Better Heal. Care VI **10685**, 106853Z (2018).

[374] Nogueira, M. S. and Kurachi, C., "Assessing the photoaging process at sun exposed and non-exposed skin using fluorescence lifetime spectroscopy," Proc. SPIE 9703 Opt. Biopsy XIV Towar. Real-Time Spectrosc. Imaging Diagnosis **9703**, 97031W (2016).

[375] Pires, L., Nogueira, M. S., Pratavieira, S., Moriyama, L. T. and Kurachi, C., "Time-resolved fluorescence lifetime for cutaneous melanoma detection," Biomed. Opt. Express **5**(9), 3080 (2014).

[376] Nogueira, M. S., Raju, M., Gunther, J., Maryam, S., Amissah, M., Lu, H., Killeen, S., O'Riordain, M. and Andersson-

Engels, S., “Tissue biomolecular and microstructure profiles in optical colorectal cancer delineation,” J. Phys. D. Appl. Phys. (2021).

[377] Leal, L. B., Nogueira, M. S., Mageski, J. G. A., Martini, T. P., Barauna, V. G., Dos Santos, L., e Silva, L. F. das C. and others., “Diagnosis of Systemic Diseases Using Infrared Spectroscopy: Detection of Iron Overload in Plasma—Preliminary Study,” Biol. Trace Elem. Res., 1–15.

[378] Panhóca, V. H., Nogueira, M. S. and Bagnato, V. S., “Treatment of facial nerve palsies with laser and endermotherapy: a report of two cases,” Laser Phys. Lett. **18**(1), 15601 (2020).

[379] Nogueira, M. S., Gunther, J. E., Komolibus, K. and Andersson-Engels, S., “User-friendly graphical user interface for simulating tissue optical properties and fluence rates: improving students learning in tissue optics,” Opt. Interact. with Tissue Cells XXXI **11238**, 112380B (2020).

[380] Nogueira, M. S., Gunther, J. E., Komolibus, K., Ryan, S. M., Murray, B., Jezzini, M. A., Kennedy, D. and Andersson-Engels, S., “Method of continuous improvement of multidisciplinary programs and outreach activities,” Educ. Train. Opt. Photonics, 11143_41 (2019).

[381] Nogueira, M. S., Gunther, J., Komolibus, K. and Andersson-Engels, S., “Teaching light-tissue interactions: using technology for education,” Opt. Interact. with Tissue Cells XXX **10876**, 108761H (2019).

[382] Nogueira, M. S., Leal, L. B., Marcarini, W. D., Pimentel, R. L., Muller, M., Vassallo, P. F., Campos, L. C. G., Dos Santos, L., Luiz, W. B., Mill, J. G. and others., “Rapid diagnosis of COVID-19 using FT-IR ATR spectroscopy and machine learning,” Sci. Rep. **11**(1), 1–13 (2021).

[383] Nogueira, M. S., Leal, L. B., Marcarini, W. D., Pimentel, R. L., Muller, M., Vassallo, P. F., Campos, L. C. G., Dos Santos, L., Luiz, W. B., Mill, J. G. and others., “Author Correction: Rapid diagnosis of COVID-19 using FT-IR ATR spectroscopy and machine learning,” Sci. Rep. **11**(1), 1 (2021).

[384] Nogueira, M. S., Komolibus, K., Tobo, A. L. P., Jayet, B., Sekar, S. K. V., Sorensen, S., Tyndall, C. and Andersson-Engels, S., “Biophotonics box: educational kit for multidisciplinary outreach activities in optics and photonics,” Educ. Train. Opt. Photonics, W4B--5 (2021).

[385] “BIOPHOTONICS BOX | Marcelo Saito Nogueira | Research Project.”, <https://www.researchgate.net/project/Biophotonics-box> (2 November 2021).

[386] Bunaciu, A. A., Hoang, V. D. and Aboul-Enein, H. Y., “Applications of FT-IR spectrophotometry in cancer diagnostics,” Crit. Rev. Anal. Chem. **45**(2), 156–165 (2015).

[387] Nogueira, M. S., Komolibus, K., Gunther, J. E., Sekar, S. K. V., Jayet, B., Tobo, A. L. P., Li, C. L., Maryam, S., Tyndall, C., Kennedy, D. and others., “Online learning combining virtual lectures, at-home experiments and computer simulations: a multidisciplinary teaching and learning approach,” Educ. Train. Opt. Photonics, F2B--6 (2021).

[388] Saito Nogueira, M., Gunther, J. E., Jayet, B., Souza Matias, J., Tyndall, C. and Andersson-Engels, S., “Biophotonics computer app: fostering multidisciplinary distance self-paced learning with a user-friendly interface,” OSA Tech. Dig., 1–2 (2021).

[389] Nogueira, M. S., Amissah, M., Maryam, S., Lynch, N., Killeen, S., O’Riordain, M. and Andersson-Engels, S., “Optimization of tissue classification for colorectal cancer detection using support vector machines and diffuse reflectance spectroscopy,” Eur. Conf. Biomed. Opt., EW4A--17 (2021).

[390] Nogueira, M. S., Raju, M., Gunther, J., Maryam, S., Amissah, M., Killeen, S., O’Riordain, M. and Andersson-Engels, S., “Optical determination of superficial and deeper tissue biochemistry and microstructure for delineation and early detection of colorectal cancer,” Eur. Conf. Biomed. Opt., ETu3A--1 (2021).

[391] Nogueira, M. S., Maryam, S., Amissah, M., Lynch, N., Killeen, S., O’Riordain, M. and Andersson-Engels, S., “Benefit of extending near-infrared wavelength range of diffuse reflectance spectroscopy for colorectal cancer detection

using machine learning," Eur. Conf. Biomed. Opt., EW4A--16 (2021).

[392] Saito Nogueira, M., Ribeiro, V., Pires, M., Peralta, F. and others., "Biochemical Profiles of In Vivo Oral Mucosa by Using a Portable Raman Spectroscopy System," Optics **2**(3), 134–147 (2021).

[393] Nogueira, M. S., Maryam, S., Amissah, M., Lu, H., Manning, E., Killeen, S., O'Riordain, M. and Andersson-Engels, S., "Broadband diffuse reflectance spectroscopy for colorectal surgical guidance (Conference Presentation)," Opt. Interact. with Tissue Cells XXXI **11238**, 1123802 (2020).

[394] Marcelo, S. N., "Biophotonics for pandemic control: large-area infection monitoring and microbial inactivation of COVID-19," Photodiagnosis Photodyn. Ther. (2020).

[395] Nogueira, M. S., "Espectroscopia de tempo de vida de fluorescência para o diagnóstico de lesões de pele clinicamente semelhantes" (2016).

[396] Nogueira, M. S., Raju, M., Gunther, J., Maryam, S., Amissah, M., Lu, H., Killeen, S., O'Riordain, M. and Andersson-Engels, S., "Accurate colorectal cancer detection and delineation by probing superficial and deeper tissue biochemistry and microstructure using diffuse reflectance spectroscopy," Proc. SPIE 11943, Photonics West, 11943-4 (2022).

[397] Carvalho, L. F. C. S., Nogueira, M. S., Neto, L. P. M., Bhattacharjee, T. T. and Martin, A. A., "Raman spectral post-processing for oral tissue discrimination--a step for an automatized diagnostic system: erratum," Biomed. Opt. Express **9**(2), 649 (2018).

[398] Panhoca, V. H., Nogueira, M. S. and Bagnato, V. S., "Laser and vacuum therapy for treatment of facial nerve palsies," Proc. SPIE 11935, Photonics West, 11935-21 (2022).

[399] Nogueira, M. S., Bagnato, V. S. and Panhoca, V. H., "Effectiveness of whitening treatments employing violet illumination alone or combined with bleaching agents," Proc. SPIE 11942, Photonics West, 11942-6 (2022).

[400] Nogueira, M. S., Maryam, S., Amissah, M., Lynch, N., Killeen, S., Lu, H., O'Riordain, M. and Andersson-Engels, S., "Improving colorectal cancer detection by extending the near-infrared wavelength range and tissue probed depth of diffuse reflectance spectroscopy: a support vector machine approach," Proc. SPIE 11954, Photonics West, 11954-15 (2022).

[401] Ferreira, M. C. de M. S. C., Leal, L. B., Nogueira, M. S., Castro, P. A. A., Peralta, F., Zezell, D. M. and Carvalho, L. F. C. S., "Biochemical characterization of saliva of smoking and non-smoking patients by using Fourier-transform infrared spectroscopy," Proc. SPIE 11957, Photonics West, 11957-49 (2022).

[402] Nogueira, M. S., Jayet, B., Matias, J. S., Gunther, J. E., Tyndall, C. and Andersson-Engels, S., "Biophotonics web application for computer simulations in diffuse optics: fostering multidisciplinary education and research," Proc. SPIE 11958, Photonics West, 11958-18 (2022).

[403] Nogueira, M. S., Li, C. L., Maryam, S., Tyndall, C., Donovan, S., Komolibus, K., Gunther, J. E., Sekar, S. K. V., Jayet, B., Fisher, C., Kennedy, D. and Andersson-Engels, S., "Multidisciplinary teaching and learning biophotonics: assessing the effectiveness of fully online outreach events," Proc. SPIE 11958, Photonics West, 11958-39 (2022).

[404] e Silva, L. F. das C., Nogueira, M. S. and others., "New insights of Raman spectroscopy for oral clinical applications," Analyst **143**(24), 6037–6048 (2018).

[405] Carvalho, L. F. C. S., Nogueira, M. S., Bhattacharjee, T., Neto, L. P. M., Daun, L., Mendes, T. O., Rajasekaran, R., Chagas, M., Martin, A. A. and Soares, L. E. S., "In vivo Raman spectroscopic characteristics of different sites of the oral mucosa in healthy volunteers," Clin. Oral Investig., 1–11 (2018).

[406] e Silva, L. F. das C. and de Carvalho, M. S. N., "Optical techniques for fast screening--towards prevention of the coronavirus COVID-19 outbreak," Photodiagnosis Photodyn. Ther. (2020).

[407] Nogueira, M. S., "Optical theranostics and treatment dosimetry for COVID-19 lung complications: towards

increasing the survival rate of vulnerable populations," Photodiagnosis Photodyn. Ther. (2020).

[408] Carnevalli, A. C., Leal, L., Scherma, A., Morais, C., Martin, F., Bonnier, F., Baker, M., Byrne, H. J., Nogueira, M. S. and others., "Identification of diabetic patients via urine analysis by FTIR: preliminary study (Conference Presentation)," Photonic Diagnosis Treat. Infect. Inflamm. Dis. II **10863**, 108630E (2019).

[409] Nogueira, M. S., "Ultraviolet-based biophotonic technologies for control and prevention of COVID-19, SARS and related disorders," Photodiagnosis Photodyn. Ther. (2020).

[410] Nogueira, M. S., "Biophotonic telemedicine for disease diagnosis and monitoring during pandemics: overcoming COVID-19 and shaping the future of healthcare," Photodiagnosis Photodyn. Ther. (2020).

[411] Nogueira, M. S., Maryam, S., Amissah, M., Lu, H., Lynch, N., Killeen, S., O'Riordain, M. and Andersson-Engels, S., "Evaluation of wavelength ranges and tissue depth probed by diffuse reflectance spectroscopy for colorectal cancer detection," Sci. Rep. **11**(1), 1–17 (2021).

[412] Nogueira, M. S., Lacerenza, M., Sekar, S. K. V., Buttafava, M., Pifferi, A., Tosi, A., Contini, D. and Andersson-Engels, S., "Broadband extraction of tissue optical properties using a portable hybrid time-resolved continuous wave instrumentation: characterization of ex vivo organs," Clin. Transl. Biophotonics, TM2B--3 (2020).

[413] Lacerenza, M., Pacheco, A., Sekar, S. K. V., Nogueira, M. S., Buttafava, M., Tosi, A., Pifferi, A., Contini, D. and Andersson-Engels, S., "Functional monitoring of lung tissue using a hybrid hyperspectral Time-Resolved GASMAS system: a systematic study on ex vivo sample.," Opt. Tomogr. Spectrosc., SW1D--2 (2020).

[414] Nogueira, M. S., Barreto, A. L., Furukawa, M., Rovai, E. S., Bastos, A., Bertoncello, G., e Silva, L. F. das C. and others., "FTIR spectroscopy as a point of care diagnostic tool for diabetes and periodontitis: A saliva analysis approach," Photodiagnosis Photodyn. Ther. **40**, 103036 (2022).

[415] Nogueira, M. S., Brugnera Junior, A., Bagnato, V. S. and Panhóca, V. H., "Evaluation of the whitening effectiveness of violet illumination alone or combined with hydrogen peroxide gel," Photobiomodulation, Photomedicine, Laser Surg. (2021).

[416] Panhóca, V. H., Nogueira, M. S. and Bagnato, V. S., "Laser and vacuum therapy for treatment of facial nerve palsies," Imaging, Ther. Adv. Technol. Head Neck Surg. Otolaryngol. 2022 **11935**, 39–48 (2022).

[417] Nogueira, M. S., "Biophotonics for pandemic control: large-area infection monitoring and microbial inactivation of COVID-19," Photodiagnosis Photodyn. Ther. **31**, 101823 (2020).

[418] Carvalho, L. F. das C. e S. and Saito Nogueira, M., "Optical techniques for fast screening--towards prevention of the coronavirus COVID-19 outbreak," Photodiagnosis Photodyn. Ther. (2020).

[419] Cosci, A., Nogueira, M. S., Pratavieira, S., Takahama, A., Azevedo, R. de S., Kurachi, C. and Kurachi, C., "Time-resolved fluorescence spectroscopy for clinical diagnosis of actinic cheilitis," Biomed. Opt. Express **7**(10), 4210–4219 (2016).

[420] Mousavi, M., Moriyama, L. T. T., Grecco, C., Nogueira, M. S., Svanberg, K., Kurachi, C. and Andersson-Engels, S., "Photodynamic therapy dosimetry using multiexcitation multiemission wavelength: toward real-time prediction of treatment outcome," J. Biomed. Opt. **25**(6), 63812 (2020).

[421] Ferreira, M. C. C., Monteiro, G. R., Peralta, F., Castro, P. A. A., Zezell, D., Nogueira, M. S. and Carvalho, L. F. C. S., "Assessment of bound water of saliva samples by using FT-IR spectroscopy," Lat. Am. Opt. Photonics Conf., M4B--1 (2022).

[422] Bomfin, L. S., Kitakawa, D., Nogueira, M. S., e Silva, L. F. das C. and others., "Low Level Laser Therapy as adjuvant treatment for lower lip lesion," Lat. Am. Opt. Photonics Conf., M2B--6 (2022).

[423] Nogueira, M. S., Matthews, R., Killeen, S., O'Riordain, M. and Andersson-Engels, S., "Colorectal cancer detection based on the extraction of scattering properties and biochemical concentrations from fluorescence spectroscopy

measurements," Clin. Transl. Biophotonics, TS2B--5 (2022).

[424] Maryam, S., Nogueira, M. S., Krishnamoorthy, S., Sekar, S. K. V., Lu, H., Gautam, R., Burke, R., Andersson-Engels, S., Riordain, R. N. and Sheahan, P., "Multi-configuration Raman spectrometer for early stage diagnosis of oral cancer," Biomed. Vib. Spectrosc. 2022 Adv. Res. Ind. **11957**, 20–26 (2022).

[425] Maryam, S., Sekar, S. K. V., Gautam, R., Kho, K. W., Ghauri, D., Nogueira, M. S., Beffara, F., Fahy, E., Riordain, R. N., Burke, R., Sheahan, P., Feeley, L. and Andersson-Engels, S., "Portable multi-configuration clinical translational Raman system for oral cancer application," Analyst (2022).

[426] Nogueira, M. S., Ferreira, M. C. M. S. C., Leal, L. B., Castro, P. A. A., Peralta, F., Zezell, D. M. and Carvalho, L. F. C. S., "A validation step for point of care diagnostics through saliva characterization of smoking patients by using FTIR spectroscopy," Exp. Mol. Pathol. (2023).

[427] Coelho, M. C. M. S., Leal, L. B., Nogueira, M. S., Castro, P. A. A., Peralta, F., Zezell, D. M. and others., "Biochemical characterization of saliva of smoking and non-smoking patients by using Fourier-transform infrared spectroscopy," Biomed. Vib. Spectrosc. 2022 Adv. Res. Ind. **11957**, 86–97 (2022).

[428] Saito Nogueira, M., Maryam, S., Amissah, M., McGuire, A., Spillane, C., Killeen, S., Andersson-Engels, S. and O'Riordain, M., "Insights into Biochemical Sources and Diffuse Reflectance Spectral Features for Colorectal Cancer Detection and Localization," Cancers (Basel). **14**(22), 5715 (2022).

[429] Panhóca, V. H., Nogueira, M. S., Zanin, F. A. A., Brugnera, A. P., Brugnera Jr, A. and Bagnato, V. S., "Dental sensitivity and color change in patients undergoing dental bleaching with application of violet light," Oral Health Dent. Manag. **21**(6), 1–14 (2022).

[430] de Paula, D., Campos, C., Nogueira, M. S., Pratavieira, S. and Kurachi, C., "Time-resolved and steady-state fluorescence spectroscopy for the assessment of skin photoaging process," Proc. SPIE 9531 Biophotonics South Am. **9531**, 953146 (2015).

[431] Panhóca, V. H., Aquino Junior, A. E., Souza, V. B., Ferreira, S. A., Ferreira, L. T., Souza, K. J. O., Tamae, P. E., Saito Nogueira, M. and Bagnato, V. S., "Effects of red and infrared laser therapy in patients with tinnitus: a double-blind, clinical, randomized controlled study combining light with ultrasound, drugs and vacuum therapy," J. Pers. Med. (2023).